THE WERNECKE IGNEOUS CLASTS IN YUKON, CANADA: EVIDENCE FOR A PALEOPROTEROZOIC VOLCANIC ARC TERRANE AT 1.7 GA AND ITS OBDUCTION ONTO ANCESTRAL NORTH AMERICA

by

Alexander Bøndrup Nielsen
B.Sc. (Hons.), Queen's University, 2005

THESIS SUBMITTED IN PARTIAL FULFILLMENT OF
THE REQUIREMENTS FOR THE DEGREE OF

Master of Science

In the
Department of Earth Sciences
Faculty of Science

Simon Fraser University

Fall 2011

Approval

Name: **Alexander Bøndrup Nielsen**

Degree: Master of Science

Title of Thesis: The Wernecke Igneous Clasts in Yukon, Canada: evidence for a Paleoproterozoic volcanic arc terrane at 1.7 Ga and its obduction onto ancestral North America

Examining Committee:

Chair: **Dr. Andrew Calvert**
Professor – Department of Earth Sciences

_____

Dr. Derek Thorkelson
Senior Supervisor
Professor – Department of Earth Sciences

_____

Dr. Dan Gibson
Supervisor
Professor – Department of Earth Sciences

_____

Dr. Dan Marshall
Supervisor
Professor – Department of Earth Sciences

_____

Dr. Jim Mortensen
External Examiner
Professor – EOS, University of British Columbia

Date Defended/Approved: December 15th 2011

Declaration of
Partial Copyright Licence

Abstract

All observed Wernecke igneous clasts (WIC) occur within the 1.60 Ga Wernecke Breccias of Yukon, Canada. The clasts range up to 5.4 million m^3 in volume, and comprise the 1.71 Ga Bonnet Plume River Intrusions (BPRI), the Slab volcanics, the Devil volcanics, and the Blackstone River megaclast. The WIC were not emplaced through the <1.64 Ga Wernecke Supergroup (WSG). The BPRI and Devil volcanics have a geochemical affinity with volcanic arcs. The Slab volcanics are more alkaline, like mantle plume or slab-window derived volcanoes. Sm-Nd isotopes indicate that magmas of the BPRI and Devil volcanics assimilated older basement rock. The WIC originated in a terrane that was obducted onto the WSG. Hydrothermal fluids brecciated these units, forming the Wernecke Breccias. WICs derived from the terrane foundered into these breccias to the level of the WSG and were metasomatized. The obducted terrane eroded entirely prior to deposition of the Pinguicula Group.

Keywords: geochemistry; metasomatism; tectonic environments; samarium neodymium isotopes; Proterozoic; Yukon;

To those that have helped,

and those that, in hindering, have helped nonetheless.

Acknowledgements

I would like to thank everyone who contributed in the completion of this thesis. D. Thorkelson provided input and feedback throughout the entire project from fieldwork to final drafting. D. Marshall assisted with work on the scanning electron microscope (SEM), contributed in defining temperatures and pressures of metamorphic assemblages and gave helpful feedback and suggestions during the review process. T. Peters provided insight into the Blackstone River megaclast at the Yukon Olympic mineral occurrence. D. Gibson provided direction for heavy mineral extraction and gave helpful feedback and suggestions during the review process. J Mortensen provided helpful feedback and suggested edits that substantially improved the final draft of this work. K. Medig helped by keeping it fun while still talking geology, as did R. Staples. Finally, I would like to thank my parents, and my wonderful partner, Kate for all of their support.

Table of Contents

List of Figures

List of Tables

1: Introduction

This thesis investigates the field relations, geochemistry, origin, and tectonic significance of the Wernecke igneous clasts (herein defined as the Bonnet Plume River Intrusions, the Slab volcanics, the Devil volcanics, and the Blackstone River megaclast). These aspects of the Wernecke igneous clasts have a significant bearing on the tectonic environment of the northwestern (current co-ordinates) Laurentian craton in the late Paleo- to Mesoproterozoic. By determining the tectonic environment of these clasts, constraints are placed on models for the nature of the Wernecke Supergroup, Racklan orogeny, and the purported Precambrian supercontinent Columbia (Rogers and Santosh, 2002). Initially, the scope of the thesis was intended to include new U-Pb age determinations of the Bonnet Plume River Intrusions (Thorkelson, 2000). New dating was not carried out, however, as no zircon or baddeleyite crystals, which would have permitted new U-Pb age determinations, were found in the samples collected. Accordingly, greater emphasis was placed on geochemical characterization including Nd isotope analysis. The results have been integrated to provide a thorough depiction of the source region of the Wernecke igneous clasts and add detail to a recent tectonic model of northwestern Laurentia (ancestral North America) in the Paleo- to Mesoproterozoic (Furlanetto et al., 2009a).

Field work for this project was undertaken between the 19th of June and the 24th of July 2009 at numerous localities in central to northern Yukon (see Appendix A), and chiefly involved mapping, sampling and recording detailed observations of the Bonnet Plume River Intrusions and Devil volcanics. With the exception of the Yukon Olympic mineral occurrence (see Fig. 1),

all locations are remote and accessible only by helicopter. The Yukon Olympic location is most easily accessed by crossing the Blackstone River by small watercraft. The terrain is rugged and mountainous and the weather is variable in the summer with temperatures fluctuating between above 25^0C and below 0^0C from day to day and with elevation.

This thesis is in journal paper style. It consists of one paper, intended for publication in an international journal, and supporting appendices of data and analytical methods. It is part of ongoing research into the Proterozoic history of Yukon Territory directed by Dr. D. Thorkelson at Simon Fraser University.

The paper presented herein, "The Wernecke igneous clasts in Yukon, Canada: evidence for a Paleoproterozoic volcanic arc terrane at 1.7 Ga and its obduction onto ancestral North America," presents the most current information on the Wernecke igneous clasts and hypotheses pertaining to their geochemical evolution, tectonic environment of formation, and mode of emplacement in the Wernecke breccias. It builds on a substantial body of previous work, notably Laznicka and Edwards (1979), Bell (1986), Lane (1990), Thorkelson (2000), Thorkelson et al. (2001a; 2001b; 2005), Brideau et al. (2002), Laughton (2004), Hunt and Thorkelson (2006), and Furlanetto et al. (2009a; 2009b).

2: THE WERNECKE IGNEOUS CLASTS IN YUKON CANADA: EVIDENCE FOR A PALEOPROTEROZOIC VOLCANIC ARC TERRANE AT 1.7 GA AND ITS OBDUCTION ONTO ANCESTRAL NORTH AMERICA

Abstract

The origin of the Wernecke igneous clasts is an enigma that bears on the Proterozoic evolution of the northwestern margin of Laurentia. Wernecke igneous clasts are found exclusively within the Wernecke Breccias of central and northern Yukon, which are developed within the Wernecke Supergroup. The field relations and ages of the observed Wernecke igneous clasts (1714-1706 Ma) relative to the Wernecke Supergroup (<1640 Ma), indicate that they did not intrude the Wernecke Supergroup. The Wernecke igneous clasts comprise clasts up to 900 m x 200 m x 30 m in size of mafic to intermediate subalkaline and alkaline plutonic and volcanic rocks, as well as fragments of volcaniclastic sediments. Geochemical characteristics of the Wernecke igneous clasts suggest that they were derived from a volcanic arc with a component of within-plate magmatism. Neodymium isotope analysis suggests that they magmatically assimilated older continental crust. We suggest that the Wernecke igneous clasts were formed as part of a volcanic arc built on a continental fragment (possibly a rifted fragment of Laurentia) or the leading edge of another continent, which was obducted onto the northwestern margin of Laurentia. The Wernecke Breccias may have developed in response to this tectonic loading of the crust. The breccias fragmented the obducted arc and clasts of volcanic and plutonic rock foundered into the Wernecke Breccias, some reaching the level of the Wernecke Supergroup. Subsequent erosion removed the arc terrane entirely, prior to Pinguicula Group sedimentation.

2.1 Introduction

Accretion of volcanic arc terranes to continental margins is a key process in the growth of cratons (e.g., Windley, 1993; Rudnick, 1995; Kusky et al., 2007). During the late Paleoproterozoic, arc terranes accreted to the southern and eastern margins of Laurentia (current coordinates) during the Makkovikian, Yavapai, Mazatzal, and Labradorian orogenies (e.g., Condie, 1982; Windley, 1992; Karlstrom et al., 2001; Gower and Krogh, 2002; Ketchum et al., 2002; Whitmeyer and Karlstrom, 2007). The arc terranes are isotopically juvenile and appear to have formed in an intra-oceanic environment shortly before accretion (Bowering and Karlstrom, 1990; Condie, 1992; Shaw and Karlstrom, 1999). Their addition substantially broadened the Laurentian craton in advance of the younger Grenville orogeny.

The northwestern margin of Laurentia underwent a deformational event that was broadly contemporaneous with, and analogous to, the Yavapai and Mazatzal orogenies. The deformational event, termed the Racklan orogeny, is evident in Proterozoic inliers in Yukon Territory, Canada (Figure 1; Mitchelmore and Cook, 1994; Thorkelson, 2000; Thorkelson et al., 2001a; Brideau et al., 2002; Laughton et al., 2005; Thorkelson et al., 2005). The Racklan orogeny is expressed by east and south-verging structures and localized lower to middle greenschist facies metamorphism (Brideau et al., 2002) in the Wernecke Supergroup, a younger than 1640 Ma metasedimentary succession (Fig. 2) (Furlanetto et al., 2009b). A pronounced angular unconformity and metamorphic break separates the Wernecke Supergroup from overlying Proterozoic and Phanerozoic strata (Eisbacher, 1978). This orogenic event occurred in the late Paleoproterozoic, between the formation of the Wernecke Supergroup later than 1640 Ma (Furlanetto et al., 2009b) and the surges of voluminous hydrothermal fluids that formed the widespread Wernecke Breccias at approximately 1.60 Ga (Thorkelson et al., 2001b).

Despite the temporal correlation between the Racklan orogeny and the Yavapai-Mazatzal orogenic events, the tectonic framework of the Racklan orogeny remains an outstanding problem. Indeed, it remains uncertain whether the Wernecke Supergroup, which hosted the deformation, was deposited on a continental margin or in a deep intracratonic basin (Thorkelson et al., 2001b). In the continental margin option (Furlanetto et al., 2009a), the Racklan orogeny could be regarded as craton-directed transport of continental margin strata in response to a nearby collision between Laurentia and another landmass such as Australia. In the intracratonic basin model, the Racklan orogeny could represent contraction of a rift or aulacogen in response to far-field stresses from the Yavapai-Mazatzal belt (Thorkelson et al., 2001b), in a manner similar to the tectonic model of Alkmim et al. (2006).

Constraining the nature and significance of the Racklan orogeny hinges on the interpretation of igneous megaclasts hosted by the hydrothermal Wernecke Breccias, which crosscut Racklan fabrics and metamorphic assemblages (Thorkelson et al., 2005). The igneous clasts include the Slab volcanics (Laughton et al., 2005), the Bonnet Plume River Intrusions (Thorkelson et al., 2001a), and newly discovered volcanic and volcaniclastic rocks (Peters and Thorkelson, 2011; Nielsen et al., 2011) termed the Blackstone River megaclast. The Bonnet Plume River Intrusions have been dated at approximately 1710 Ma (Thorkelson et al., 2001a), and therefore pre-date the deposition of the Wernecke Supergroup by approximately70 m.y. and the development of Wernecke Breccia by approximately 110 m.y. (Fig. 2). In order to accommodate the relationship of older clasts hosted by younger rocks, Furlanetto et al. (2009a) outlined a new hypothesis calling for the Proterozoic obduction of a volcano-plutonic terrane onto the Wernecke Supergroup after deformation and exhumation. In that model, the obduction

was followed by hydrothermal brecciation and foundering of volcano-plutonic clasts into zones of Wernecke Breccia.

In order to evaluate this hypothesis, we undertook a comprehensive field and laboratory study of the igneous clasts hosted by Wernecke Breccia (Fig. 1). Using the results from new geological mapping, petrography, major and trace element geochemistry, and Nd isotope geochemistry, we provide a detailed physical and chemical description of the igneous clasts and an assessment of their origin. Our results shed new light on the obducted terrane model and clarify the tectonic environment of northwestern Laurentia and its configuration within the supercontinent Columbia (Rogers and Santosh, 2002) during the Racklan orogeny.

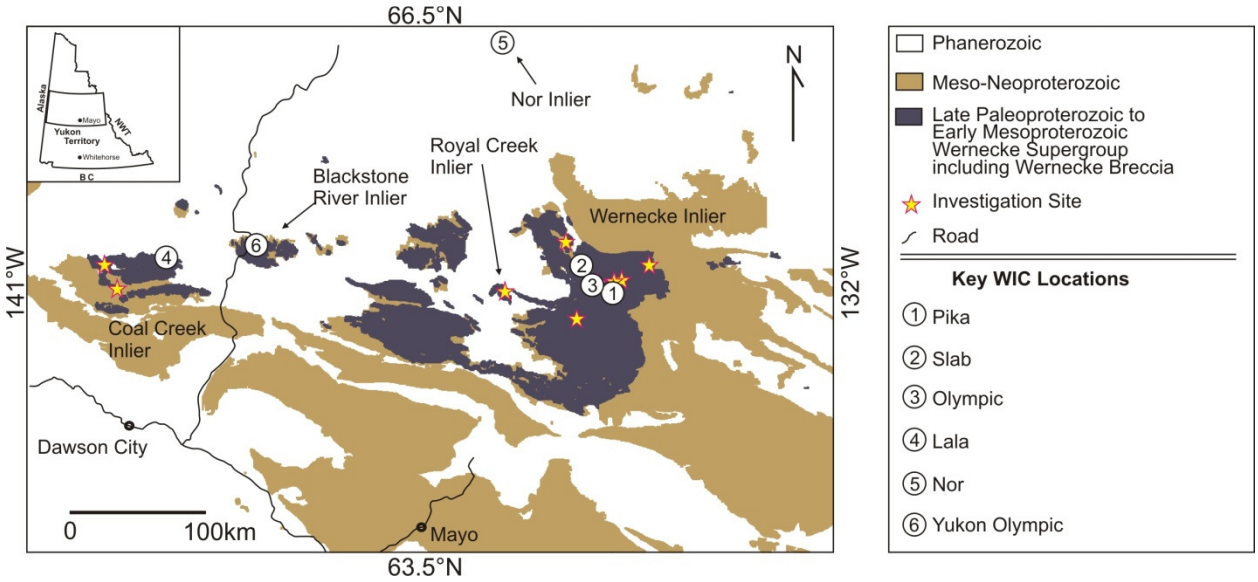

Fig. 1: Location map of central Yukon showing the extent of the Wernecke Supergroup and Proterozoic inliers, key locations where the Wernecke igneous clasts are exposed (numbered circles), and locations which were investigated as part of this study (red and yellow stars and numbered circles).

2.2 Geological context

In the late Paleoproterozoic and Mesoproterozoic, northwestern Laurentia underwent a series of geological events that involved both continental growth and destruction (Fig. 2)

(Thorkelson et al., 2005). The most obvious of these involved extensional basin formation and the deposition of three temporally distinct sedimentary successions: the Wernecke Supergroup, the Pinguicula Group, and the Mackenzie Mountains Supergroup. These "rift" events would have thinned and weakened the existing Laurentian lithosphere, and one or more of them may have led to continental separation between Laurentia and another landmass (Thorkelson et al., 2005). However, these basin forming events were interspersed with orogenesis, metamorphism, magmatism, and hydrothermal activity (Fig. 2) (Thorkelson et al., 2005; Hunt et al., 2007; Milidragovic et al., 2011). By the Neoproterozoic, northwestern Laurentia was a complexly deformed and locally metamorphosed continental margin which may have had tectonic interactions with oceanic terranes and/or continents such as Australia, Cathaysia, and Siberia (e.g., Hoffman, 1988; Sears and Price, 2000; Karlstrom et al., 2001; Thorkelson et al., 2001a; Betts et al., 2008; Li et al., 2008a; Li et al., 2008b; Milidragovic et al., 2011).

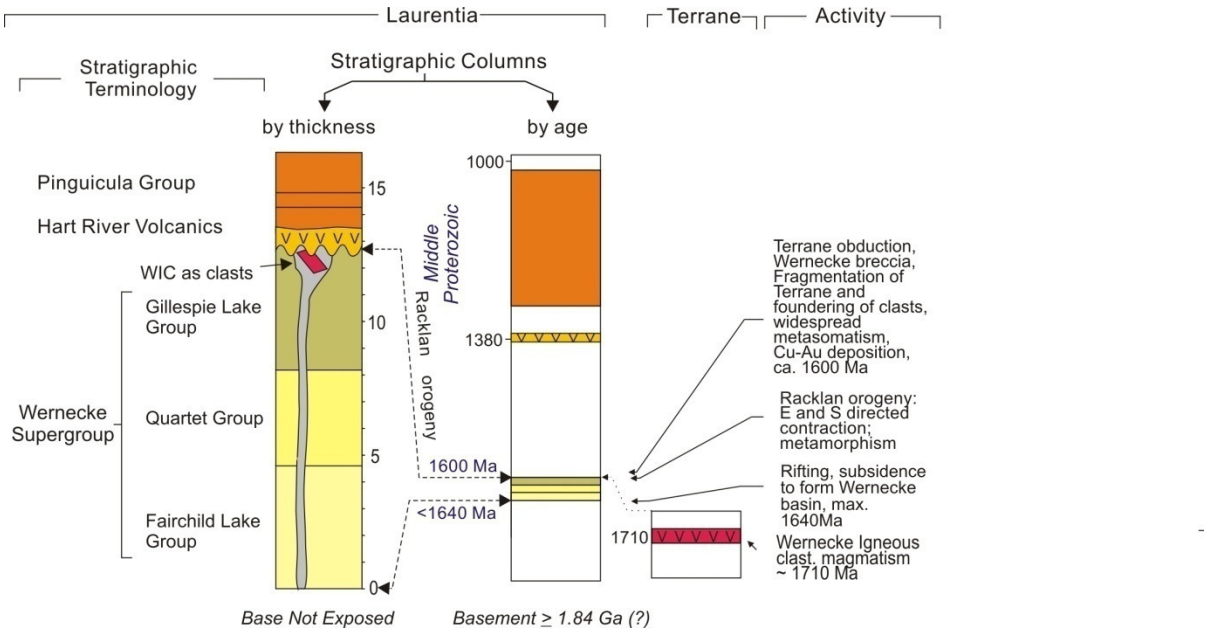

Fig. 2: Time and thickness for stratigraphy of the late Paleoproterozoic to Neoproterozoic Yukon, showing key events in the development of Yukon geology, modified after Thorkelson et al. (2005).

2.2.1 Basement

The basement to the Wernecke Supergroup is not exposed and its age and nature are unknown (Fig. 2). It must be older than about 1640 Ma, the approximate maximum age of the Wernecke Supergroup (Furlanetto et al., 2009b), but parts could be as old as Archean. Whether it is part of the Nahanni or Fort Simpson aeromagnetic domains, as identified by Hoffman (1988), remains unresolved. Most likely it is Paleoproterozoic in age and broadly coeval with the Fort Simpson domain and Wopmay orogen (Thorkelson et al., 2005).

2.2.2 The Wernecke Supergroup

The Wernecke Supergroup is a late Paleoproterozoic sedimentary succession with a minimum thickness of approximately 13 km (Fig. 2) (Delaney, 1981; Norris, 1997; Thorkelson, 2000), comprising two clastic-carbonate grand cycles. There is no known lower limit to the Wernecke Supergroup, because the crystalline basement is not exposed. The Wernecke Supergroup consists of three conformable groups: the Fairchild Lake Group (lowest unit, >4.8 km thick), which consists primarily of siltstone and fine sandstone with minor dolostone and marble; the Quartet Group (approximately 3.4 km thick), which consists of weakly pyritic shale, siltstone, and very fine sandstone with fine quartz arenite near the top; and the Gillespie Lake Group (>4.7 km thick), which consists of orange weathering dolostone with interbeds of shale and siltstone (Delaney, 1981; Thorkelson, 2000). Locally, the Wernecke Supergroup, especially the Fairchild Lake Group, is metamorphosed to phyllite and fine-grained schist.

2.2.3 Racklan orogeny

The Racklan orogeny, as used by Thorkelson (2000) and Laughton et al. (2005), applies to deformational events affecting the Wernecke Supergroup prior to the emplacement of

Wernecke Breccia at approximately 1.60 Ga (Fig. 2). Three phases of deformation have been identified within the Racklan orogeny (Brideau et al., 2002; Thorkelson et al., 2005). The first produced east-verging folds and a fabric ranging from slaty cleavage to schistose foliation. The second produced upright to overturned, south-verging folds, and likely caused the tightening and overturning of the older fold set (Fig. 3). This phase of deformation may have been associated with the formation of tight, asymmetric crenulations and crenulation cleavage. The third phase produced kink bands with inconsistent orientation. The metamorphic effects of the Racklan are most notable in the Fairchild Lake Group, which was locally metamorphosed to chloritoid-garnet-biotite-bearing quartz-muscovite schist, with peak conditions estimated at 450-550 ºC and 3-6 kbar (Brideau et al., 2002). The Racklan orogeny appears to be the thin-skinned equivalent of the ca. 1.66 Ga thick-skinned Forward orogeny to the east within the Northwest Territories, which is characterized by Laramide-style reverse faulting (Cook and MacLean, 1995; Thorkelson et al., 2003; MacLean and Cook, 2004).

Fig. 3: White, recrystallized limestone marker bed within the Fairchild Lake Group showing folds from the Racklan orogeny.

2.2.4 Wernecke Breccia

The early Mesoproterozoic Wernecke Breccias were dated at 1595 ±5 Ma by U-Pb dating of hydrothermal titanite crystals from the matrix of the Slab mountain Wernecke Breccia occurrence (Thorkelson et al., 2001b). The breccias occur within the Wernecke Supergroup (Fig. 2) (Bell, 1986; Thorkelson, 2000) as numerous zones up to several kilometres long and hundreds of metres wide, scattered throughout much of the area of the Proterozoic inliers (Fig. 1). The breccias crosscut the metamorphic foliations that developed during the Racklan orogeny (Thorkelson, 2000). Many Wernecke Breccia occurrences host iron-oxide copper gold mineral occurrences (Hunt et al., 2007).

Most of the breccia clasts are pebble to cobble-sized (Fig. 4), but some are much larger, with the largest being volcanic and plutonic clasts with areas of exposure up to 900 m x 200 m (Fig. 5, Fig. 11) (Thorkelson et al., 2001b). The majority of clasts in the Wernecke Breccias are sedimentary in character and appear to be derived from the Paleoproterozoic Wernecke Supergroup. Igneous clasts are also present and form a less abundant, but critically important population. They are derived from rock units other than the Wernecke Supergroup. Clasts such as peridotite or gneiss, which would suggest the entrainment of clasts derived from the underlying crustal basement or mantle, are absent in the Wernecke Breccias (Thorkelson et al., 2001b).

The clasts are set in a matrix composed of microclasts and minerals precipitated from the brecciating fluid. The breccia fluids precipitated primarily hematite, magnetite, dolomite, siderite, chlorite, biotite, albite, microcline, rutile, titanite, apatite, and muscovite, with localized pyrite, chalcopyrite, cobaltite, pitchblende, brannerite, and gold (Thorkelson et al., 2001b; Hunt et al., 2007). It is highly improbable that the fluids which formed the Wernecke Breccias had any

magmatic component; it was probably a mixture of crustal brines and metamorphic waters (Hunt et al., 2005; Gillen, 2010; Hunt et al., 2011).

Fig. 4: Typical, potassic-hematitic Wernecke breccia with variably metasomatized, cm-dm scale clasts, predominantly from the Wernecke Supergroup.

2.2.5 Igneous clasts in Wernecke Breccia

Various types of plutonic rock, plus volcanic and minor intercalated sedimentary rock, constitute what we herein name the *Wernecke igneous clasts,* based on their common field relations. This assemblage consists of four types of clasts. Two clast types have been previously named: the *Slab volcanics* (Thorkelson, 2000; Laughton et al., 2005); and the *Bonnet Plume River Intrusions* (Thorkelson, 2000; Thorkelson et al., 2001a). The other two clast types, the *Devil volcanics* (defined herein), and volcanic and related sedimentary rocks of the *Blackstone River megaclast* (Peters and Thorkelson, 2011), were previously unnamed. None of these clast types correlate with known stratigraphic units and, as discussed in this paper, are considered exotic with reference to the Laurentian continental margin.

2.2.5.1 Bonnet Plume River Intrusions

The Bonnet Plume River Intrusions are a group of late Paleoproterozoic clasts and megaclasts that occur within the Wernecke Breccias (Thorkelson et al., 2001a). Megaclasts of the Bonnet Plume River Intrusions range up to 900 m x 200 m x 30 m (Fig. 5). Only four samples of Bonnet Plume River Intrusions have been dated (ca. 1714-1706 Ma) and these are all from the Wernecke inlier (Fig. 1) (Thorkelson et al., 2001a). Further attempts to date the Bonnet Plume River Intrusions have proven unsuccessful. The majority of Bonnet Plume River Intrusions are fine- to medium-grained, dioritic-gabbroic clasts (Fig. 6). Clasts of fine grained albite-alkali feldspar syenite at the Olympic occurrence (location 3 in Fig. 1; Fig. 11C), and a megaclast of fine grained quartz-albite syenite at the porphyry occurrence constitute the remainder of the Bonnet Plume River Intrusions (Thorkelson et al., 2001a). All the Bonnet Plume River Intrusions have been altered to some degree. Chlorite, epidote, sericite, Na-Ca zeolites, and iron oxides are all common alteration minerals within the Bonnet Plume River Intrusions. Potassium feldspar is common in clasts affected by potassic-alteration whereas albite is common in clasts affected by sodic alteration. Veins that are composed primarily of calcite, commonly with quartz, epidote, hematite, and other minor phases commonly crosscut the Bonnet Plume River Intrusions. The Bonnet Plume River Intrusions were originally identified as breccia clasts in the Wernecke inlier (Fig. 1) by Thorkelson (2000). Subsequently, they were discovered in other localities including the Nor and Hart River inliers (Fig. 1) (Hunt and Thorkelson, 2006) and the Coal Creek inlier (Fig. 1) (this study, Lane, 1990), with an aerial distribution comparable to that of the Wernecke Breccias: approximately 50,000 km^2 (Fig. 1). Although attempts to date the Bonnet Plume River intrusive clasts both inside and outside the Wernecke inlier as part of this study were unsuccessful, previous work yielded dates of 1705.9 ± 0.7 Ma, 1709.4 ±1.4 Ma, 1711.1 ±5.1 Ma, and 1713.6 ± 12.7 Ma (Thorkelson et al., 2001a). The lithological and broad

geochemical characteristics of this clast type are common throughout, giving the impression that the clasts were derived from a common source (Hunt and Thorkelson, 2006; this study) .

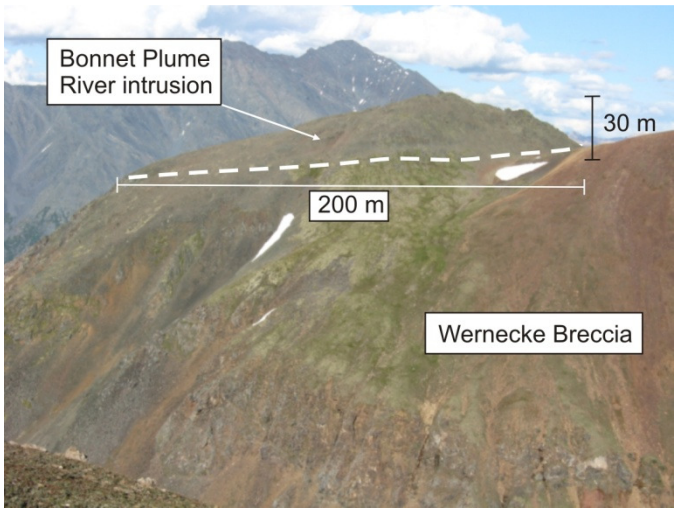

Fig. 5: 900 m x 200 m x 30m megaclast of Bonnet Plume River Intrusion (short axis view), near the Olympic mineral occurrence, (Fig. 1, Fig. 11C)

Fig. 6: Medium-grained dioritic Bonnet Plume River Intrusion showing pervasive chlorite alteration and fracture-controlled potassic (red) and epidote (yellowish green) alteration, near the Pika mineral occurrence (Fig. 1, Fig. 11A).

Fig. 7: Fine-grained clasts of albite syenite Bonnet Plume River Intrusion near the Olympic mineral occurrence, Wernecke Inlier (Fig. 1, Fig. 11C)

2.2.5.2 Slab volcanics

The Slab volcanics comprise a set of mafic volcanic clasts from within Wernecke Breccia zones at or near the Slab mineral occurrence (location 2 in Fig. 1; Fig. 11B). The largest consists of 31 thin (average 5m) basaltic to andesitic lava flows, with well-preserved pahoehoe flows and scoreaceous flow tops. These flows are amygdaloidal at the bottoms (Fig. 8), grading to massive in the middle. Intercalated between these flows there are two sandstone beds and one round-pebble diamictite (Laughton et al., 2002; Laughton, 2004). The Slab volcanics are composed of albite, phlogopite, scapolite, hematite, and magnetite, with minor secondary phases indicating that the volcanics have been affected by metasomatism. A 1380 Ma rutile date on the Slab volcanics is interpreted as a product of renewed hydrothermal activity within the Slab breccia zone forming new rutile. The renewed hydrothermal activity is believed to be related to the nearby Hart River sills (Abbott, 1997; Thorkelson et al., 2001b; Laughton, 2004).

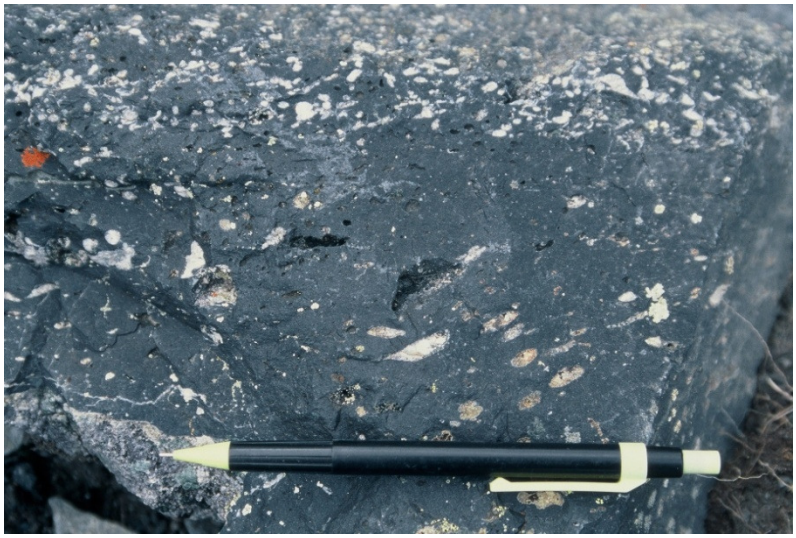

Fig. 8: Amygdaloidal basalt from the Slab volcanics, near the Slab mineral occurrence, Wernecke Inlier (location 2 in Fig. 1, Fig. 11B).

2.2.5.3 Devil volcanics

The Devil volcanics are located in the Hart River inlier, within Wernecke Breccia of the Yukon Olympic mineral occurrence (Fig. 1, Location 5; Fig. 11F). Three megaclasts (>100 m^2) and numerous smaller clasts were identified during field investigations. The clasts consist of massive, amygdaloidal basalt and andesite (Fig. 9). They have been altered to chlorite and sericite and their vesicles have been filled by quartz and hematite and are crosscut by veins of epidote, quartz, carbonate, and hematite. Their generally massive character suggests a possible origin as a submarine volcanic unit, and contrasts with the relatively thin and subaerially deposited flows of the Slab volcanics.

Fig. 9: Amygdaloidal basalt from the Devil volcanics, near the Yukon Olympic mineral occurrence, Blackstone River inlier (location 6 in Fig. 1, Fig. 11F).

2.2.5.4 Blackstone River megaclast

The Blackstone River megaclast (Peters and Thorkelson, 2011) is a 125 x 25 m block of volcanic and sedimentary rock that lies within a Wernecke Breccia zone near the breccia zone that hosts the Devil volcanic clasts (location 6 in Fig. 1; Fig. 11F). It is a unique clast type in that it consists mainly of felsic lapillistone and intercalated quartz-bearing volcaniclastic wacke (Fig. 10). The lapillistone contains a penecontemporaneous (volcanic) flattening fabric, which implies subaerial deposition. The quartz-rich composition of some of the sedimentary interbeds suggests derivation from an evolved crustal source (Peters and Thorkelson, 2011).

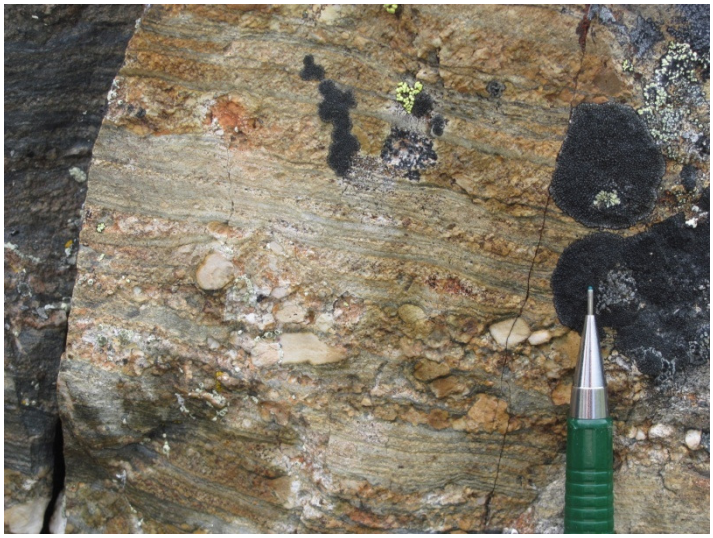

Fig. 10: Lithic wacke from the Blackstone River megaclast, prominent white clasts are composed of fine quartz arenite, near the Yukon Olympic mineral occurrence, Blackstone River inlier (location 6 in Fig. 1, Fig. 11F).

2.3 Descriptions of key field localities

2.3.1 Pika

Near the Pika mineral occurrence (Fig. 1, Fig. 11A), megaclasts of the Bonnet Plume River Intrusions are hosted by a large zone (1.5 km^2) of Wernecke Breccia that is hosted by the Quartet and Gillespie Lake groups. Some of the megaclasts are exposed along stream valleys, with the largest clast likely exceeding 30 m in width and 320 m in length (Fig. 10). The surrounding breccia consists mainly of sedimentary rock fragments, most likely derived from the surrounding Wernecke Supergroup. The igneous megaclasts are fine- to medium-grained diorite with pervasive chlorite-sericite alteration, and disseminations of hematite and magnetite. Veins of epidote and alkali feldspar are common. Pyrite and chalcopyrite veins and lenses are locally present on or near some of the edges of the igneous megaclasts. The topographic distance between the Wernecke igneous clasts at the bottom of the stream valleys and the local unconformity with the Pinguicula Group suggests that these clasts foundered at least 600 m.

2.3.2 Slab

At the Slab mineral occurrence, igneous and sedimentary megaclasts are contained within a large zone of Wernecke Breccia (1.9 km^2) that is hosted by the Fairchild Lake Group in the Wernecke inlier (Fig. 1; Fig. 11B) (Hunt et al., 2002; Laughton et al., 2002). The breccia zone hosts both sedimentary and igneous megaclasts, including a giant block of the Slab volcanics and megaclasts of the Bonnet Plume River Intrusions. The block of the Slab volcanics is 380 m long and 160 m wide, and consists of 31 flows of amygdaloidal pahoehoe lava (Fig. 8) with minor interbeds of sandstone (Laughton, 2004). Hydrothermal titanite from the matrix of the breccia zone has been dated at ca. 1.60 Ga (Thorkelson et al., 2001b). The surrounding Fairchild Lake Group has been locally metamorphosed to chloritoid +/- garnet bearing quartz-chlorite-muscovite schist with calculated peak temperatures of approximately 450-550 ˚C (Brideau et al., 2002). The schistose fabric is crosscut by the breccia zone, indicating that deformation and metamorphism (Racklan orogeny) preceded the surges of hydrothermal fluids that produced Wernecke Breccia. Mineralization at the Slab occurrence is primarily found as disseminated chalcopyrite in quartz-carbonate veins (Hunt et al., 2002).

2.3.3 Olympic

At the Olympic mineral occurrence, megaclasts of Bonnet Plume River Intrusions sit within a Wernecke Breccia body (1.6 km^2) hosted by the Gillespie Lake Group (Fig. 1; Fig. 11C). The clasts are exposed in the steep walls of a cirque and on hilltops. This breccia body hosts the largest known Wernecke igneous clast, a clast of medium-grained diorite 900 m by 200 m with a thickness of 30 m, as well as several clasts of fine-grained albite syenite (Fig. 7). The diorite clasts have been altered to chlorite and scapolite, with disseminated hematite.

Mineralization is primarily located in proximity to the margins of Wernecke igneous clasts, in veins and pods of chalcopyrite.

2.3.4 Lala

Near the Lala mineral occurrence in the Coal Creek inlier (Fig. 1; Fig. 11D), megaclasts of the Bonnet Plume River Intrusions and sedimentary rock are hosted by a large hydrothermal breccia (6 km^2) (Lane, 1990) composed of smaller clasts and a hydrothermally precipitated matrix of hematite, carbonate, and chlorite (Butler and Gill, 1997) within the Quartet and Gillespie Lake Groups. The megaclasts are exposed on steep slopes and bedrock knobs. The largest clast has an apparent length of 700 m and a width of 100 m. The igneous clasts consist of fine to medium-grained diorite that have been pervasively altered to chlorite and sericite, and host veins of epidote, alkali feldspar, and hematite. Chalcopyrite mineralization occurs at Lala both in the breccia and in fragments (Lane, 1990).

2.3.5 Nor

The breccia zone at the Nor mineral occurrence (Fig. 1; Fig. 11E) is hosted by the schist of the Fairchild Lake Group. Field relations from a combination of surface exposures and drill core, indicate a large breccia zone (1.5 km^2) (Templeman-Kluit, 1981) with a hematite-rich core and localized chalcopyrite stringers in the wall rock. Clasts of altered diorite, ranging from 1 cm to tens of metres wide, are scattered within the breccia (Terry et al., 2006). The alteration of the clasts ranges from chlorite-biotite to potassic.

2.3.6 Yukon Olympic

Two large zones of Wernecke Breccia are located near the Yukon Olympic mineral occurrence in the Blackstone River inlier (Fig. 1; Fig. 11F). The first breccia zone (3.6 km^2) lies

to the east of the Blackstone River within the Quartet Group and hosts clasts and megaclasts of the Bonnet Plume River Intrusions and the Devil volcanics that are exposed in stream valleys. The largest observed clast likely exceeds 30 m wide by 100 m long. The Devil volcanics are massive to locally amygdaloidal basalt (Fig. 9), and have been pervasively chlorite altered and host veins of epidote, alkali feldspar and hematite. The Bonnet Plume River intrusive clasts consist of fine- to medium-grained diorite, and are similarly altered and veined. The second breccia zone (0.15 km^2) lies to the west of the Blackstone river, also within the Quartet Group, and hosts the 125 m by 15 m volcaniclastic Blackstone River megaclast (Fig. 10) (Peters and Thorkelson, 2011).

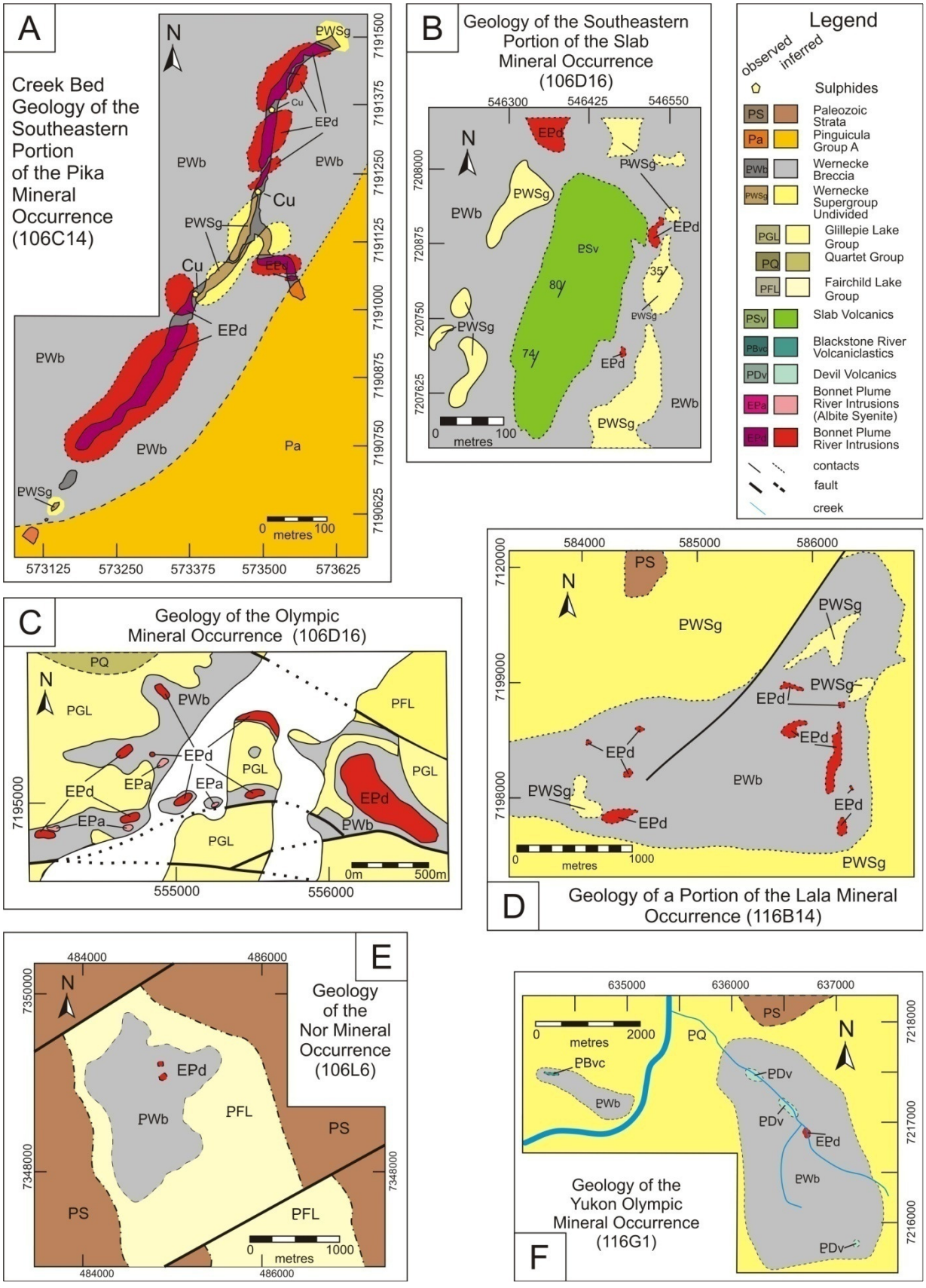
A
Creek Bed Geology of the Southeastern Portion of the Pika Mineral Occurrence (106C14)
N
PWSg
Cu
EPd
PWb
Pa
0 metres 100
573125
573250
573375
573500
573625
7191500
7191375
7191250
7191125
7191000
7190875
7190750
7190625
B
Geology of the Southeastern Portion of the Slab Mineral Occurrence (106D16)
546300
546425
546550
7208000
720875
720750
7207625
PSv
80
35
74
0 metres 100
Legend
observed
inferred
Sulphides
PS Paleozoic Strata
Pa Pinguicula Group A
PWb Wernecke Breccia
PWSg Wernecke Supergroup Undivided
PGL Glillepie Lake Group
PQ Quartet Group
PFL Fairchild Lake Group
PSv Slab Volcanics
PBvc Blackstone River Volcaniclastics
PDv Devil Volcanics
EPa Bonnet Plume River Intrusions (Albite Syenite)
EPd Bonnet Plume River Intrusions
contacts
fault
creek
C
Geology of the Olympic Mineral Occurrence (106D16)
N
PQ
PGL
PWb
PFL
EPd
EPa
0m 500m
555000
556000
7195000
D
Geology of a Portion of the Lala Mineral Occurrence (116B14)
584000
585000
586000
7120000
7199000
7198000
PS
PWSg
PWb
0 metres 1000
E
Geology of the Nor Mineral Occurrence (106L6)
484000
486000
7350000
7348000
0 metres 1000
F
Geology of the Yukon Olympic Mineral Occurrence (116G1)
635000
636000
637000
7218000
7217000
7216000
0 metres 2000
PBvc
PDv

Fig. 11: Maps of key field localities, discussed in text. A: Pika, this study. B: Slab, modified after Laughton et al. (2005). C: Olympic, modified after Thorkelson (2000). D: Lala, modified after Butler and Gill (1997), Lane (1990). E: Nor, modified after Terry et al. (2006). F: Yukon Olympic, modified after Peters and Thorkelson (2011), Gordey and Makepeace (2000). All co-ordinates are in the North American Datum 83 (NAD 83).

2.3.7 Summary of field relations

The Wernecke igneous clasts are located within zones of Wernecke Breccia that crop out in a vast area of central to northern Yukon, 320 km in the east-west direction and 200 km north-south (Fig. 1). The breccias occur at a wide range of stratigraphic levels within the Wernecke Supergroup, from the locally schistose Fairchild Lake Group to the carbonate-rich Gillespie Lake Group, representing a difference in stratigraphic height of approximately 10 km (Fig. 2) (Delaney, 1981; Norris, 1997; Thorkelson, 2000). Clast sizes range from pebble-size to giant blocks hundreds of metres long and millions of cubic metres in volume (Fig. 4; Fig. 5, Fig. 11). The largest megaclast is a block of diorite that is 900 m long, 200 m wide and at least 30 m thick (Fig. 5, Fig. 11C) (Thorkelson and Wallace, 1998) with a volume likely greater than 5.4 million cubic metres. The clasts are typically altered to lower greenschist mineral assemblages, with abundant chlorite, epidote, biotite sericite, scapolite, and secondary K-feldspar, and are commonly crosscut by veins and stringers of carbonate, quartz, K-feldspar and hematite. Unlike the sedimentary clasts, which appear to have been derived from wall rock of the Wernecke Supergroup, none of the Wernecke igneous clasts can be correlated with any known stratigraphic unit or intrusions. This relationship requires transport of the clasts to their present positions within zones of Wernecke Breccia from a source located either above or below the Wernecke Supergroup, a subject explored in more detail below.

2.4 Petrography

2.4.1 Bonnet Plume River Intrusions

The Bonnet Plume River Intrusions are predominantly diorite and gabbro with minor albite-alkali feldspar syenite and quartz-albite syenite. The diorite and gabbro were most likely originally composed of plagioclase, one or more pyroxenes, and minor amounts of magnetite or ilmenite. However, metasomatism has since altered these minerals leaving rare relicts, pseudomorphs, and secondary overgrowths.

Sericite, scapolite and Na-Ca zeolites form partial to complete replacements of lath shaped grains that display relict twinning, most likely after plagioclase. Chlorite is present primarily as overgrowing mats; however, it also forms pseudomorphs of euhedral-subhedral phenocrysts and interstitial mafic minerals bounded by plagioclase pseudomorphs (former pyroxene or olivine crystals). Commonly, the chlorite pseudomorphs include grains of hematite. Hematite also forms pseudomorphs after magnetite and possibly ilmenite as well as newly formed metasomatic porphyroblasts.

The albite syenite is composed of ragged-edged, well-twinned plagioclase, minor tartan-twinned potassium feldspar, overgrowths of polycrystalline carbonate, and hematite and pyrite metasomatic porphyroblasts. The plagioclase as determined by the Michel-Lévy method (Michel-Lévy, 1894; Nesse, 2003) is end member albite and likely the product of metasomatism. The well-defined carlsbad twinning suggests that the primary mineral was also plagioclase, though of a more anorthitic composition (Turner, 1951).

2.4.2 Slab volcanics

The Slab volcanics are intermediate in composition and moderately alkalic, and plot mainly in the tephriphonolite to trachyandesite fields on a total alkalis and silica diagram (see Fig. 13) (LeMaitre, 2002). Their primary mineralogy may have been predominantly plagioclase of an intermediate composition with one or more pyroxenes and other mafic silicates (Laughton, 2004). Plagioclase was likely replaced by end member albite and scapolite, and the mafic silicates were likely replaced by biotite. Scapolite, phlogopite, magnetite, hematite, and minor actinolite, titanite, apatite, carbonate, microcline, chlorite, epidote, and rutile form the fine-grained groundmass of the Slab volcanics (Laughton, 2004).

2.4.3 Devil volcanics

The Devil volcanics are composed of amygdaloidal basalt and andesite. Their primary mineralogy was most likely predominantly pyroxene and olivine, with or without visible plagioclase phenocrysts. The amygdules are filled by quartz. The metasomatizing fluids of the Wernecke Breccias have altered the primary minerals. The mafic silicates have been replaced by chlorite and hematite, commonly grouped together in well-formed pseudomorphs. Where present, plagioclase has been altered to sericite. The fine-grained groundmass is composed primarily of chlorite and hematite with minor alkali feldspar, plagioclase, and scapolite.

2.4.4 Blackstone River megaclast

The Blackstone River megaclast consists of layers of lapillistone, lapilli tuff, lithic wacke and volcaniclastic breccias (Peters and Thorkelson, 2011). Though the lithologies of the Blackstone river megaclast are less altered than other clasts in Wernecke Breccia, chlorite alteration is common, including chlorite precipitation in lapilli amygdules.

2.5 Geochemistry

This paper integrates the results of previous studies on the Wernecke igneous clasts with new geochemical and isotopic information to provide a more comprehensive investigation of their primary composition, tectonic affinity and metasomatic alteration. Previous studies examined the Bonnet Plume River Intrusions (Thorkelson, 2000; Thorkelson et al., 2001a; Hunt and Thorkelson, 2006) and the Slab volcanics (Laughton, 2004), but the recently discovered Blackstone River megaclast (Peters and Thorkelson, 2011) has not been studied geochemically. The studies on the Bonnet Plume River Intrusions, which were focused mainly on the Wernecke inlier, concluded that they are tholeiitic diorites and gabbros which were emplaced in a continental extensional environment and subsequently metasomatized by the fluids of the Wernecke Breccias (Thorkelson et al., 2001a). The Slab volcanics were described as tholeiitic, mafic to intermediate sub-alkaline to alkaline basalts, andesites, and trachyandesites emplaced in a within-plate tectonic environment (Laughton, 2004). This paper re-evaluates these previous findings and clarifies the geochemical composition and tectonic affinity of the Wernecke igneous clasts.

Thirty new samples of Wernecke igneous clasts were collected from locations in all of the major inliers and analyzed for major and trace elements; a subset was analyzed for Nd isotopes. Analytical techniques are detailed in Appendix C2. Results are presented in Appendix C3. The results of this study along with a reinterpretation of the results of the previous studies indicate that the analyzed Wernecke igneous clasts are predominantly subalkaline, transitional to calc-alkaline basalts and andesites.

2.5.1 Major and minor oxides

The Bonnet Plume River Intrusions display a wide range of compositions. SiO_2 ranges from 45-68 wt% with the majority of samples between 47 and 57 wt%. The alkali elements vary widely: CaO from 0.2-12 wt%, Na from 0.01-8.5 wt%, K_2O from 0.12-9.76 wt%. FeO* (all Fe as Fe^{2+}) ranges from 6.3-23 wt%, TiO_2 from -0.6-3.1 wt%, and Mg-number (all Fe as Fe^{2+}) ranges from 21.4-68.2 (Fig. 12).

The Slab volcanics are more restricted in their geochemical range. This is expected because nearly all samples of the Slab volcanic come from one megaclast. SiO_2 ranges from 47-59 wt%, with most samples between 50-55 wt%. The alkalis vary widely within the Slab volcanics, but overall have a higher concentration than in the Bonnet Plume River Intrusions: CaO from 2-10 wt%, Na from 0.9-10 wt%, K_2O from 0.45-8.0 wt%. FeO* ranges from 9-18 wt%, TiO_2 from -1.4-2.5 wt% and Mg-number from 19-55 (Fig. 12). The Devil volcanics have not been sufficiently sampled to permit an analysis of their geochemical patterns; however, their compositional range overlaps that of the Bonnet Plume River Intrusions.

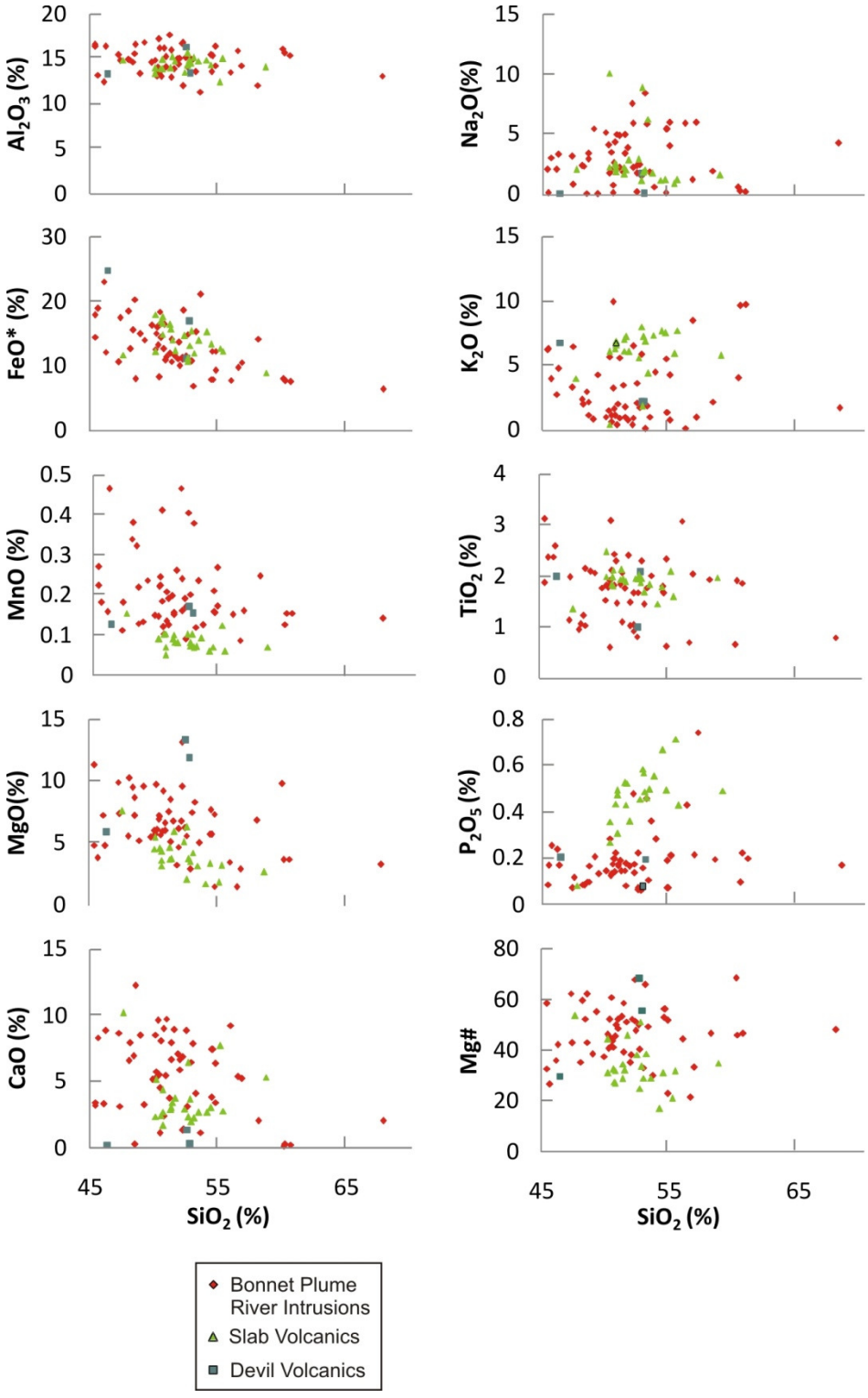

Fig. 12: Harker geochemical variation diagram showing how the weight percent of the major and minor oxides and the whole-rock Mg number of the samples vary with respect to weight percent silica.

The total alkali-silica (TAS) plot (LeMaitre, 2002) shows a large scatter in putative rock types within the Wernecke igneous clasts. The Bonnet Plume River Intrusions plot mainly in the fields of basalt, trachybasalt, and basaltic trachyandesite, and to a lesser degree in the fields of basaltic andesite, andesite, dacite, trachyandesite, trachyte, tephrite-basanite, tephriphonolite, and phonotephrite (Fig. 13). The Slab volcanics are generally more alkalic than the Bonnet Plume River Intrusions and plot in the fields of trachybasalt, basaltic trachyandesite, trachyandesite, trachyte, tephrite-basanite, tephriphonolite, and phonotephrite (Fig. 13). Devil volcanic samples plot in the fields of basaltic andesite and tephrite-phonolite. This wide range of rock types does not reflect the predominantly dioritic mineralogy of the Bonnet Plume River Intrusions that was apparent in hand sample and thin section. The scatter likely reflects the mobility of the alkali elements and silica during Wernecke Breccia metasomatism, a topic explored in detail, below.

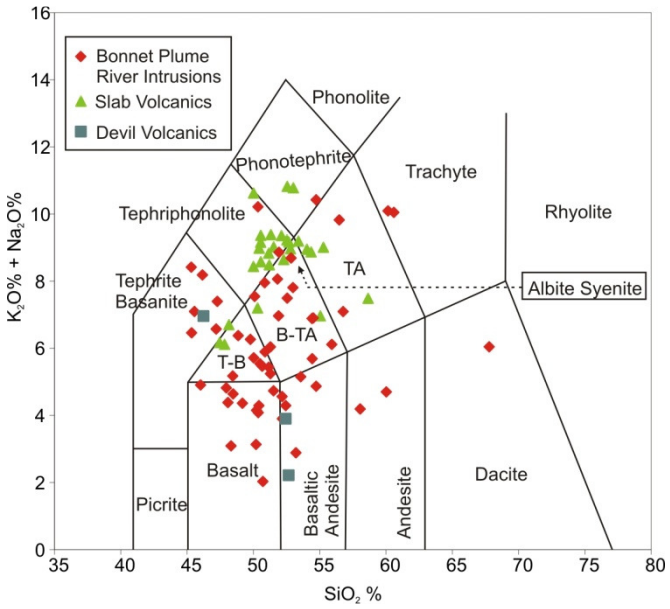

Fig. 13: Total alkali-silica diagram after LeMaitre (2002), field T-B is trachybasalt, field B-TA is basaltic trachyandesite, field TA is trachyandesite.

The minor oxides MnO, P_2O_5 and TiO_2 further distinguish the Slab volcanics from the Bonnet Plume River Intrusions and Devil volcanics, with notably higher TiO_2/MnO ratios in the

Slab volcanics. Consequently, on the tectonic affinity plot of Mullen (1983), the Slab volcanics plot almost entirely within the ocean island - alkalic basalt field whereas the Bonnet Plume River Intrusions and Devil volcanics plot predominantly in volcanic arc and mid-ocean ridge basalt fields (Fig. 14).

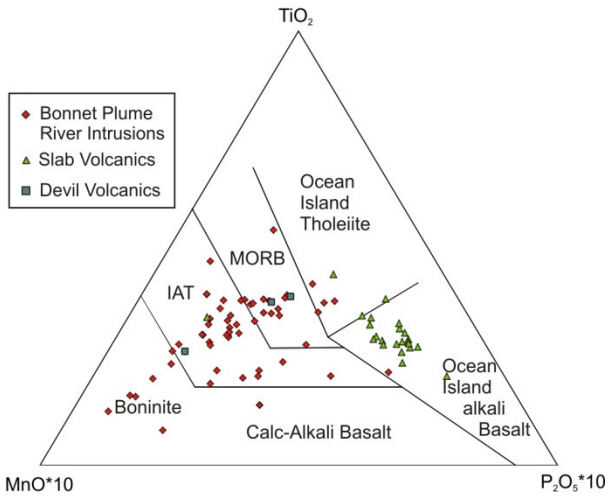

Fig. 14: Minor element tectonic discrimination diagram, after Mullen (1983), IAT field is island arc tholeiite; MORB field is mid-ocean ridge basalt.

2.5.2 Trace elements

The trace element distributions of the Bonnet Plume River Intrusions vary markedly. The large ion lithophile elements (LILE) are scattered chaotically and have large ranges; for example, Ba ranges from 30-3159 ppm. The high field strength elements (HFSE) are less scattered than the LILE. Some elements display a wide range of concentration; for example, Y varies from 8-43 ppm whereas Zr ranges from 18-516 ppm. Abundances of the transition metals are also fairly scattered; for example Cr ranges from less than 0.5- 490 ppm and Ni ranges from 10-255 ppm (Fig. 15).

The Slab volcanics are more restricted in their trace element concentration ranges than the Bonnet Plume River Intrusions. The LILE also display chaotic concentrations, but they are

not as wide ranging as in the Bonnet Plume River Intrusions; for example, Ba ranges from 97-1120 ppm. The HFSE are generally more enriched in the Slab volcanics than in the Bonnet Plume River Intrusions, for example, Zr ranges from 204-482 ppm whereas Y ranges from 34-88 ppm. In contrast, transition metal abundances in the Slab volcanics are generally depleted relative to the Bonnet Plume River Intrusions; for example, Cr ranges from 1.2-7.5 ppm and Ni ranges from 3.5-43 ppm. The Slab volcanics are enriched in the REE, Nb, and Ta relative to the Bonnet Plume River Intrusions (Fig. 15). The Devil volcanics have trace element concentrations that lie within the range of the Bonnet Plume River Intrusions.

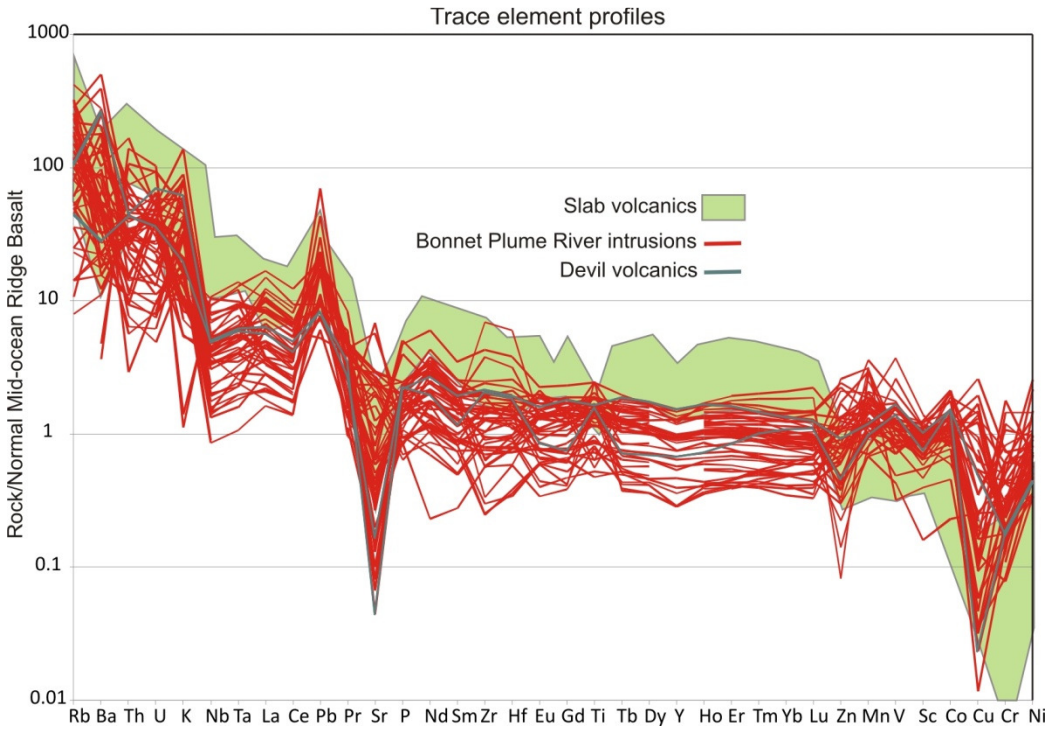

Fig. 15: N-MORB normalized spider diagram. Data for the Slab volcanics from Laughton (2004). Normalizing values Cs-Lu after Sun and McDonough (1989); Gd-Ti order reversed, Co to Ni except Cu and Zn, after Pearce and Parkinson (1993), Zn, Cu estimated by D.J. Thorkelson (unpublished) from Basaltic Volcanism Study Group (1981).

An N-MORB normalized rare-earth element plot shows LREE concentration increasing toward La, a flat HREE pattern, and slight Eu enrichments and depletions for the Bonnet Plume

River Intrusions and Devil volcanics (Fig. 16). Their La_N/Lu_N (NMORB normalized) ratio ranges from 1.5-19. The Slab volcanics are enriched in REE over almost all the Bonnet Plume River Intrusions, especially in the HREE, however, their LREE slope is not as steep as that of the Bonnet Plume River Intrusions (Fig. 16), with La_N/Lu_N ranging from 1.7-13.

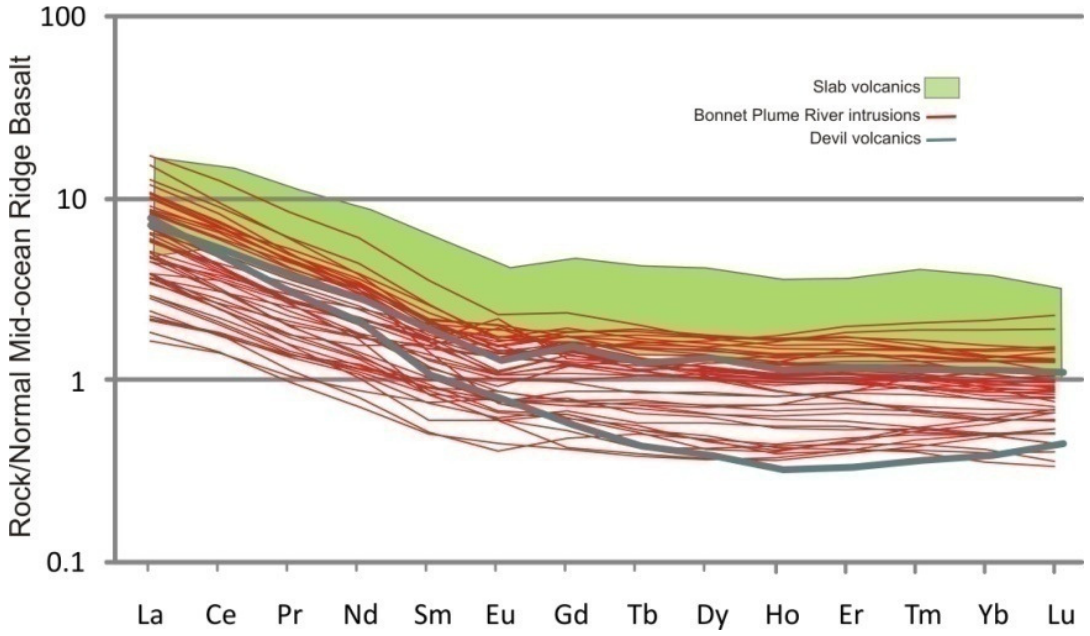

Fig. 16: N-MORB normalized rare earth element plot, normalizing values after Sun and McDonough (1989)

The Wernecke igneous clasts are classified as mafic to intermediate basalt, andesite, and trachyandesite; therefore, the scatter in the LILE and the wide range of abundances in the other elements in the Wernecke igneous clasts is unlikely to be the product of primary igneous processes alone. The bulk of the variation is more likely to be the product of significant metasomatism by the fluids of the Wernecke Breccias. This elemental mobility is characterized below so that the Wernecke igneous clasts may be meaningfully classified.

2.5.3 Element mobility

The Wernecke igneous clasts were exposed to the hydrothermal fluids that formed Wernecke Breccia. These fluids ranged in temperature from 110^0C-400^0C (Hunt et al., 2007; Gillen, 2010; Hunt et al., 2011), and have metasomatized clasts and wall rocks in a range of ways including potassic, sodic, carbonic and iron oxide metasomatism (Hitzman et al., 1992; Thorkelson et al., 2001b; Laughton et al., 2005). Characterizing geochemical mobility was therefore a major concern in analyzing the geochemical data.

In order to examine elemental mobility in Wernecke Breccia metasomatism, we built on the concepts of potassic and sodic metasomatism, which are widely recognized as common alteration types, especially in iron ore copper gold and porphyry type deposits (e.g., Laznicka and Edwards, 1979; Carten, 1986; Hitzman, 2000; Williams et al., 2005; Sillitoe, 2010). This approach has been used extensively with regards to the Wernecke Breccias (Laznicka and Edwards, 1979; Hitzman et al., 1992; Thorkelson et al., 2001b; Hunt et al., 2005; Laughton et al., 2005; Gillen, 2010; Hunt et al., 2011). The K/Na values of the rocks affected by the Wernecke Breccias have been altered by the brecciating fluids; therefore, the K/Na of the analyzed samples were used to discern the degree of metasomatism. Wernecke igneous clasts with "extreme" potassium-sodium ratios (K/Na greater than 10 or less than 0.1) are likely to have been metasomatized, whereas clasts with "normal" igneous K/Na values ranging between 0.5 and 2 are less likely to have been extensively metasomatized.

The effects of sodic and potassic metasomatism can be seen in Fig. 17. The LILE show chaotic enrichments and depletions with sodic and potassic alteration. The HFSE (except Y), show enrichments with both sodic and potassic alteration, whereas Y shows a slight depletion with strong potassic alteration. Sodic alteration shows increased concentration of the REE

overall, whereas weak potassic alteration shows depleted concentrations of the REE, and strong potassic alteration shows increased concentration in the LREE up to Nd and decreased concentration in the REE heavier than Nd. Among the transition metals, Cu, Cr, Zn, and Sc are depleted with both sodic and potassic alteration, though Sc only weakly so. Ni and Co show depletions only with sodic alteration. Tl and V show enrichment by potassic alteration and depletion by sodic alteration. Viewed as a whole, this pattern indicates that the fluids of the Wernecke breccia have imparted an "evolved continental" geochemical signature on the Wernecke igneous clasts that they have metasomatized.

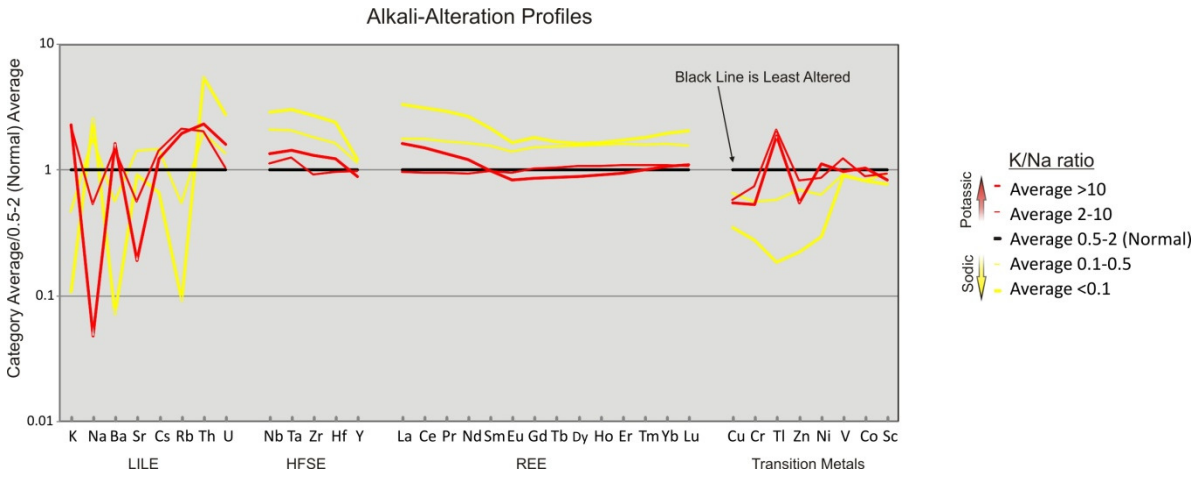

Fig. 17: Selected elements showing enrichments and depletions due to alkali metasomatism, normalized to the average elemental concentration of samples with "normal" K/Na values (0.5-2). LILE – large ion lithophile elements, HFSE – high field strength elements, REE – rare earth elements.

The idea that the dioritic Bonnet Plume River Intrusions may represent a significant source of mineralization in the Wernecke Breccias was first proposed by Laznicka and Edwards (1979) and supported by Thorkelson (2000). Gillen (2010) further indicated that the main sources of Cu-mineralization in the Wernecke Breccias were clasts of the Bonnet Plume River Intrusions. Our study found that with increasing sodic and potassic metasomatism, the Bonnet Plume River Intrusions and Devil volcanics are progressively depleted in copper contents (Fig.

18). This relationship suggests that Wernecke Breccia metasomatism has played a role in scavenging copper from the igneous clasts. There are no other copper-rich lithologies in the immediate wall rock from which the hydrothermal fluids could have sourced significant amounts of Cu (Gillen, 2010); therefore, the Bonnet Plume River Intrusions and Devil volcanics represent a key part of the copper budget of Wernecke Breccia iron oxide copper gold deposits.

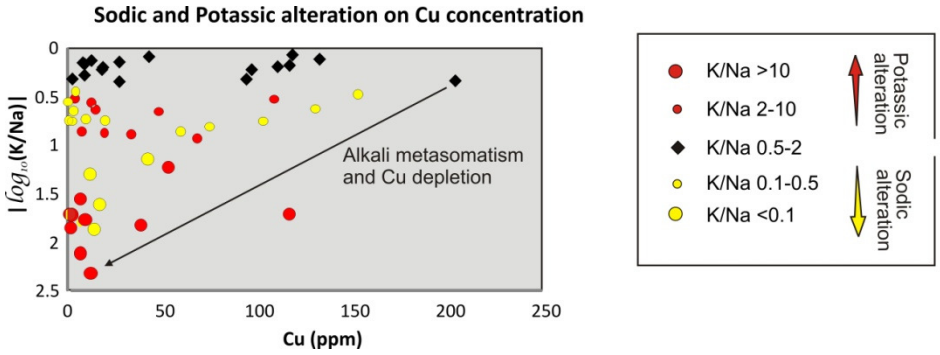

Fig. 18: Cu variation compared to the absolute value of the base ten logarithm of K/Na. Copper is depleted with "extreme" K/Na values. The y-axis scale |log(K/Na)| was used so that both sodic and potassic metasomatism are equally treated (e.g., a K/Na value of 1/10 plots equivalently on the y-axis to a K/Na value of 10/1).

2.5.3.1 Rock classification

Geochemical classification systems that are appropriate for the Bonnet Plume River Intrusions must be relatively insensitive to Wernecke Breccia metasomatism and they must display the effects of metasomatism on the plotted points. Both of these approaches are used in this analysis. The most suitable system for determining the rock type of the Bonnet Plume River Intrusions and Devil volcanics is Zr/Ti vs. Nb/Y (Winchester and Floyd, 1977), which shows that the they are primarily subalkaline basalt and andesite (Fig. 19A). Some samples plot in the fields of alkali basalt and rhyolite; however, these samples display strong sodic and potassic alteration; therefore, this is unlikely to represent their original igneous composition. Using

equivalent names for phaneritic rocks, the Bonnet Plume River Intrusions are geochemically classified as diorite and gabbro. The Slab volcanics plot in the fields of subalkaline basalt, andesite-basalt, andesite, rhyodacite-dacite, alkaline basalt, and trachyandesite.

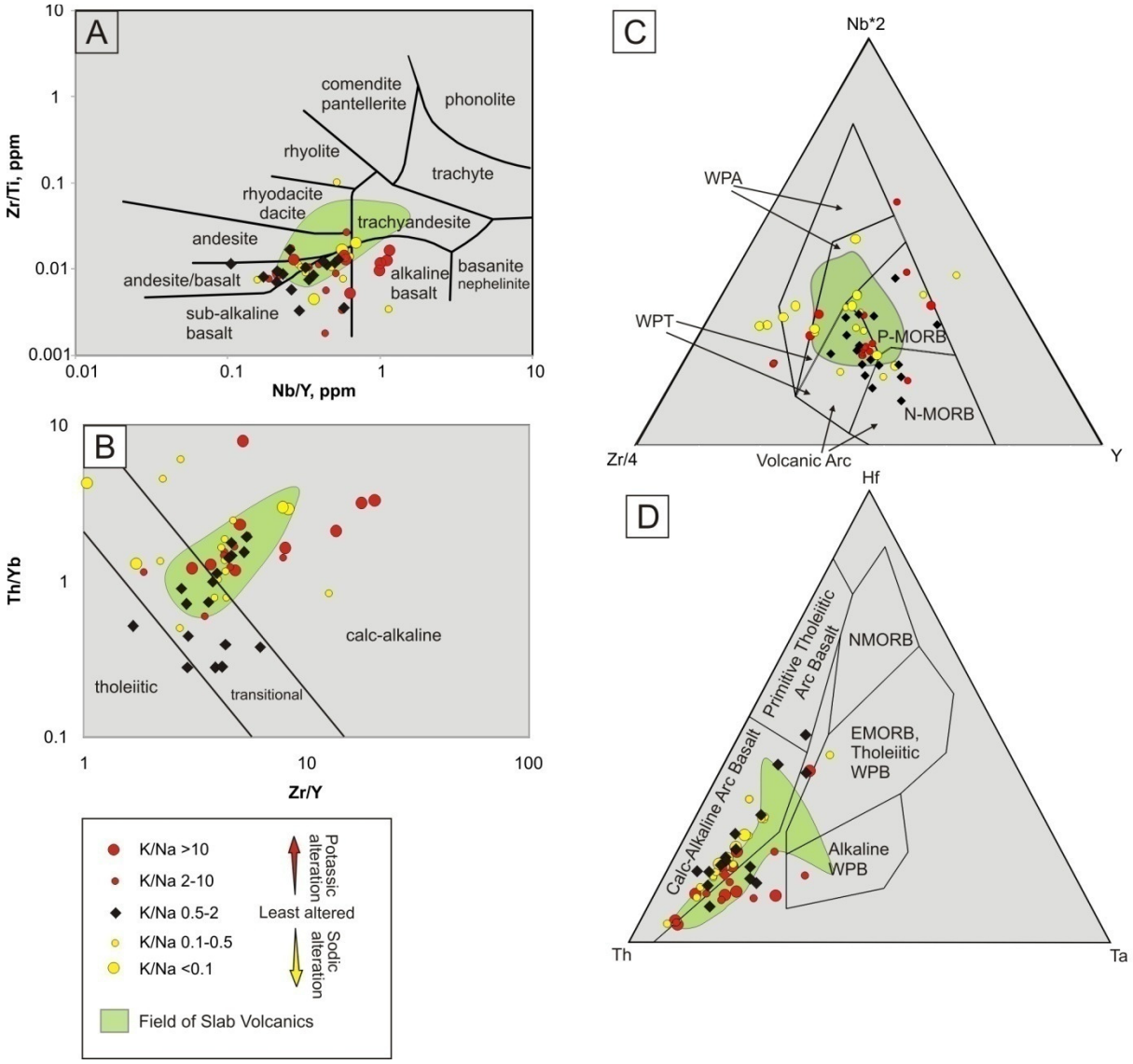

Fig. 19: Geochemical characterization plots for Bonnet Plume River Intrusions, Devil volcanics, and Slab volcanics: A) Rock Classification plot after Winchester and Floyd (1977) B) Rock series determination plot after Ross and Bédard (2009) C) Tectonic affinity plot after Meschede (1986) D) Tectonic affinity plot after Wood (1980). WPB – within plate basalt; WPT – within plate tholeiite; WPA – within plate alkali basalt; NMORB – normal mid-ocean ridge basalt; EMORB – enriched mid-ocean ridge basalt; PMORB – plume-influenced mid-ocean ridge basalt

In order to further describe the nature of the Bonnet Plume River Intrusions and Devil volcanics, the method of determining rock series based on immobile elements developed by Ross and Bédard (2009) was applied because it is less susceptible to metasomatic alteration than the standard methods of differentiating the magma series of rocks (e.g., Irvine and Baragar, 1971; Miyashiro, 1974; Pecerillo and Taylor, 1976). This method indicates that the Bonnet Plume River Intrusions and Devil volcanics follow the transitional to mildly calc-alkaline series trend, as opposed to a tholeiitic one (Fig. 19B). Some samples show strong calc-alkaline affinity; however, these samples have been strongly affected by Wernecke Breccia metasomatism. The Slab volcanics also plot in the transitional and calc-alkaline fields, although overall they are more calc-alkaline than the Bonnet Plume River Intrusions and the Devil volcanics.

2.5.3.2 Arc affinity of the Bonnet Plume River Intrusions and Devil volcanics, within-plate affinity of the Slab volcanics

Two discriminant plots were used in order to determine the tectonic affinity of the Bonnet Plume River Intrusions and Devil volcanics. Nb, Zr, Y, Th, Hf, Ta were used because they are relatively immobile, especially with potassic alteration. The Zr/4-Y-Nb*2 plot of Meschede (1986) (Fig. 19C) shows the Bonnet Plume River Intrusions and Devil volcanics plotting in the fields of volcanic arcs. Strongly altered samples are scattered with no distinct pattern. The field of Slab volcanics lies in the fields of mantle plume-influenced mid-ocean ridge basalt (P-MORB), within-plate tholeiites (WPT), and within-plate alkaline basalt (WPA).

The Ta-Th-Hf ternary of Wood (1980a) (Fig. 19D) shows the Bonnet Plume River Intrusions and Devil volcanics plotting mainly in the field of calc-alkaline arc basalt. Several samples, particularly those with potassic alteration, lie adjacent to this field in an undefined part of the diagram. The alteration in these elements has biased the position of the samples away from

the Hf maximum with a slight bias towards the Th maximum; however, this has not changed the outcome of the plot significantly. The field of Slab volcanics plots on the margin of calc-alkaline arc basalts and overlaps the fields of E-MORB/tholeiitic within plate basalts and alkaline within-plate basalts.

The dominant geochemical signal among the Bonnet Plume River Intrusions and the Devil volcanics indicates that they were derived from hydrous mantle above a subducting slab and emplaced or erupted in a volcanic arc. The Slab volcanics have a distinct intraplate geochemical signal that indicates involvement of enriched mantle. Such an involvement could have occurred from the subduction of a spreading ridge and formation of a slab window, which are known to cause intraplate-style magmatism in volcanic arc environments (e.g., Marshak and Karig, 1977; Hole et al., 1991; Thorkelson et al., 2011). Alternatively, the geochemical characteristics of the Slab volcanics could have been produced by a mantle plume that contaminated the source region of the volcanic arc (Johnston and Thorkelson, 1997; Wyman and Kerrich, 2010; Gazel et al., 2011).

2.6 Samarium-Neodymium Isotope Analysis

Neodymium isotope analysis was performed on nine samples selected from the Bonnet Plume River Intrusions and one of the Devil volcanics by the Pacific Centre for Isotopic and Geochemical Research at the University of British Columbia. The results show that the Bonnet Plume River Intrusions assimilated older crust during their ascent and that Wernecke Breccia metasomatism altered the εNd evolution path of the Bonnet Plume River Intrusions and Devil volcanics by changing their Sm/Nd ratio.

εNd values for the Bonnet Plume River Intrusions and Devil volcanics range from 0.0 to -18.5 and T_{DM}^{NK98} values of 2.07-2.76 Ga (Table 1; Fig. 20) (Nägler and Kramers, 1998). The wide range of isotopic compositions among the Bonnet Plume River Intrusions and Devil volcanics is most likely an effect of Wernecke Breccia metasomatism. The samples can be grouped into two distinct categories: relatively unaltered samples with high Sm/Nd , high ^{143}Nd values and moderate εNd values; and altered samples with low Sm/Nd, low ^{143}Nd values and low εNd values (DePaolo and Wasserburg, 1976).

Table 1: Sm-Nd analyses for the Bonnet Plume River Intrusions and one Devil volcanic (ABN 09 19-02-02). OAE – older than the age of the earth

	K/Na	Sample	Sm (ppm)	Nd (ppm)	Sm/Nd	$^{147}Sm/^{144}Nd$	$^{143}Nd/^{144}Nd$	uncert.[a]	T_{DM}^{NK98}[b]	T Ma	εNd_0	εNd_{1710}	εNd_{1595}
Potassic	127	ABN09 04-11-01b	3	13	0.23	0.139495060	0.511801	0.00000724	2.54	1710	-16.3	-3.9	-4.7
	55.6	ABN09 12-04-01b	2.28	9.9	0.23	0.139209505	0.511688	0.00000702	2.76	1710	-18.5	-6.0	-6.8
	49.6	ABN09 17-02-01b	1.56	7.4	0.21	0.127430043	0.511782	0.00000676	2.23	1710	-16.7	-1.6	-2.6
	49.0	ABN-09 19-02-02b	5.11	19.7	0.26	0.156808680	0.512135	0.00000664	2.43	1710	-9.8	-1.1	-1.7
	6.96	ABN-09 20-02-01b	1.33	5.74	0.23	0.140067123	0.511951	0.00000732	2.27	1710	-13.4	-1.1	-1.8
	6.60	DT-93-163-1b	1.27	3.97	0.32	0.193200000	0.512249	0.00001900	OAE	1714	-7.6	-6.9	-6.9
	1.86	ABN09 06-01-01b	2.35	8.24	0.29	0.172418536	0.512405	0.00000690	2.36	1710	-4.6	0.7	0.4
	0.70	ABN09 12.5-01-01	1.96	6.31	0.31	0.187799410	0.512639	0.00000618	2.39	1710	0.0	1.9	1.8
	0.52	ABN09 14-02-01b	2.18	8.02	0.27	0.164324241	0.512174	0.00000658	2.67	1710	-9.0	-2.0	-2.5
	0.34	ABN09 18-03-01b	3.85	12.9	0.30	0.180421095	0.512143	0.00000628	OAE	1710	-9.6	-6.1	-6.4
	0.31	DT-94-20-1b	5.63	24.89	0.23	0.136700000	0.512003	0.00000600	2.08	1706	-12.4	-4.0	-5.3
Sodic	0.16	DT-94-22-1b	16.73	81.51	0.21	0.124100000	0.511736	0.00000900	2.23	1709	-17.6	-6.5	-8.0
	0.02	ABN09 11-02-01b	4.92	22.4	0.22	0.132768023	0.511757	0.00000774	2.42	1710	-17.2	-3.3	-4.1
	0.01	ABN09 12-01-01b	9.15	43.4	0.21	0.127441930	0.511802	0.00000910	2.20	1710	-16.3	-1.2	-2.2
	0.01	DT-93-52-1b	19.02	79.3	0.24	0.145000000	0.511997	0.00000900	2.32	1711	-12.5	-6.0	-7.1

a Uncertainty is epressed as 2σ
b Depleted mantle model of Nägler and Kramers (1998)

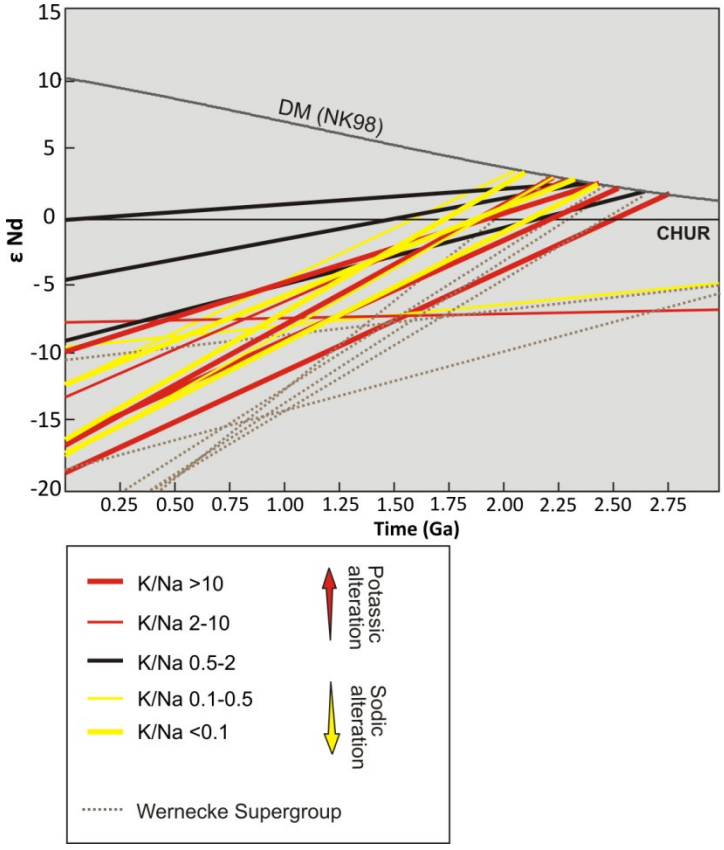

Fig. 20: εNd plot after DePaolo (1981a) showing the depleted mantle (DM) (model of Nägler and Kramers, 1998), CHUR (chondritic uniform reservoir), Wernecke Supergroup (Thorkelson

et al, 2005), and Bonnet Plume River Intrusions and Devil volcanics ((Thorkelson et. al., 2001; this study)

The first group (black lines in Fig. 20) is dissimilar in isotopic composition to the Wernecke Supergroup. In thin section, this group shows the least amount of secondary mineral growth and commonly displays primary textures. Geochemically, this group belongs to the set of samples with "normal" K/Na values, and thus, are considered the least altered samples and the most likely to represent the primary isotopic composition of the Bonnet Plume River Intrusions and Devil volcanics. The T_{DM}^{NK98} model ages (DePaolo, 1981a; Nägler and Kramers, 1998) for these samples are 2.36 Ga, 2.39 Ga and 2.67 Ga. The Bonnet Plume River Intrusions are considered to be approximately 1710 Ma based on four U-Pb zircon dates (Thorkelson et al., 2001b), although these ages were obtained from only four samples from a restricted area. Given the similar compositions and field relations of the Bonnet Plume River Intrusions and Devil volcanics throughout the study area, an age of 1.71 Ga is considered broadly representative of all of the Bonnet Plume River Intrusions and Devil volcanics.

Sm-Nd systems of mantle melts may be altered by magmatic assimilation of older basement rock, making the Nd model age appear older than the U-Pb crystallization age (DePaolo, 1981b). This process is a reasonable explanation for the difference between the Nd model age of the unaltered samples and the U-Pb crystallization age of the Bonnet Plume River Intrusions.

The second group (red and yellow lines in Fig. 20) has similar Sm/Nd and ^{143}Nd values to the Wernecke Supergroup. When viewed in thin section, the samples in this group show abundant secondary mineral growth, indicating significant metasomatism. The samples in this group belong to the sodic or potassic metasomatized geochemical series. Their compositions

likely represent a trend towards rare earth element and isotopic equilibration with the Wernecke Supergroup host rocks.

Depleted mantle model ages T_{DM}^{NK98} (DePaolo, 1981a; Nägler and Kramers, 1998) for the altered Bonnet Plume River Intrusions and Devil volcanics range from 2.07 Ga to 2.76 Ga (depleted mantle model of Nägler and Kramers (1998)). It is probable that the altered samples have also assimilated basement material; however, the subsequent Wernecke Breccia metasomatism has obscured any Nd isotope signal of basement assimilation. This metasomatism has predominantly decreased the εNd value of the altered samples and increased their projected T_{DM}. LREE slopes (La/Gd) in the Bonnet Plume River Intrusions and Devil volcanics are predominantly increased by Wernecke Breccia metasomatism (Fig. 21); therefore, their Sm/Nd values are decreased, though some altered samples have had their Sm/Nd value increased. If Sm/Nd values are increased or decreased by metasomatism, their rate of evolution away from the chondritic uniform reservoir (CHUR) is affected, which in turn affects their T_{DM} (Rosing, 1990; Gruau et al., 1996). If the Sm/Nd of a rock derived from the depleted mantle is decreased, its T_{DM} decreases and its εNd increases and conversely, when the Sm/Nd of a rock derived from the depleted mantle is increased, its T_{DM} also increases and its εNd decreases (Rosing, 1990). The samples in Fig. 21 with steep slopes have had their Sm/Nd ratio decreased whereas the sample in Fig. 21 with a very shallow slope has had its Sm/Nd ratio increased. It is also possible that Wernecke Breccia metasomatism affected the $^{143}Nd/^{144}Nd$ ratio of the altered Bonnet Plume River Intrusions and Devil volcanics. The cause of the steep or very shallow slopes of the altered Bonnet Plume River Intrusions and Devil volcanics is interpreted as Wernecke Breccia metasomatism.

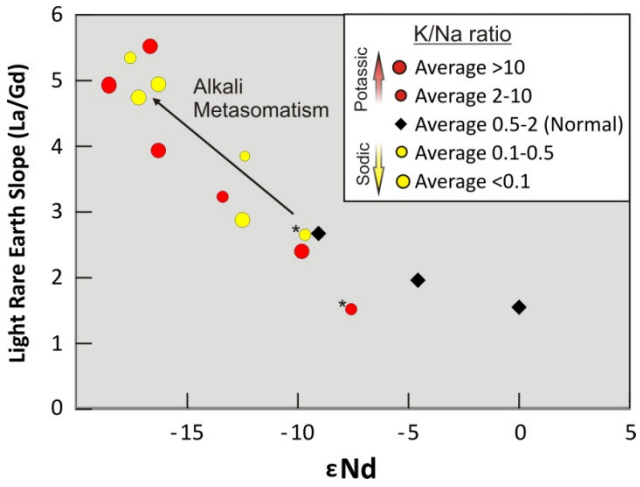

Fig. 21: Epsilon Neodymium related to the La/Gd ratio, showing how Wernecke Breccia metasomatism increased LREE slopes, thereby decreasing εNd. Asterisks indicate altered samples that have high Sm/Nd, relatively low epsilon neodymium values and T_{DM} older than the age of the earth.

Most of the Bonnet Plume River Intrusions and Devil volcanics have been altered, masking their primary isotopic composition. By identifying the least altered samples, we have been able to make meaningful determinations of the original isotopic characteristics of the Bonnet Plume River Intrusions and Devil volcanics. These characteristics indicate that the Bonnet Plume River Intrusion and Devil volcanics are not juvenile, but are significantly less evolved than indicated by the more altered samples. The εNd values of the least altered Bonnet Plume River Intrusion and Devil volcanics at 1710 Ma (the time of igneous crystallization) indicate that they either magmatically assimilated older crust or that their source region in the mantle had an εNd value more enriched than the depleted mantle (model of Nägler and Kramers, 1998), likely due to an isotopic input from subducted sediment.

2.7 Origin and emplacement of the Wernecke igneous clasts

Our results, in conjunction with the newly constrained age of the Wernecke Supergroup and the recently proposed model for the evolution of the northwestern margin of Laurentia in the

late Paleoproterozoic and early Mesoproterozoic (Furlanetto et al., 2009a; Furlanetto et al., 2009b), require a new interpretation of the origins of the Wernecke igneous clasts. This interpretation must account for the tectonic environments in which the Wernecke igneous clasts were formed and explain how the clasts came to be emplaced within the Wernecke Breccias, with no known remnants of their source rocks.

2.7.1 Evolution of constraints and ideas

The Bonnet Plume River Intrusions and the Slab volcanics were previously regarded as products of continental extensional magmatism within Laurentia (Thorkelson et al., 2001a; Laughton, 2004). However, as noted by Furlanetto et al. (2009a), this interpretation cannot account for the approximately 70 m.y. age difference between the older (1.71 Ga) Bonnet Plume River Intrusions and younger (less than 1.64 Ga) Wernecke Supergroup that they were previously thought to have intruded (Thorkelson et al., 2001a). It also (a) fails to account for the lack of igneous bodies of adequate age and size within the Wernecke Supergroup to have been the parent body to the megaclast of the Bonnet Plume River Intrusions and Slab volcanics, and (b) has difficulty explaining the absence of volcanism anywhere within the Wernecke Supergroup, despite excellent exposure over tens of thousands of km^2. In order to explain the absence of volcanism within the Wernecke Supergroup, Laughton et al. (2005) suggested that Slab volcanics were erupted above the Wernecke Supergroup; however, the complete absence of dykes that could have been feeders to the Slab volcanics remained an unresolved problem. Hence, the Wernecke Supergroup has no adequate record of volcanism, dyking or plutonism within it to support a model in which either the Wernecke igneous clasts were sourced from plutons emplaced into the Wernecke Supergroup or volcanic units erupted at higher stratigraphic levels.

The foregoing review of information indicates that the Wernecke igneous clasts cannot have been derived from within the Wernecke Supergroup; therefore, transport from above or below the Wernecke Supergroup must have taken place. If the source of the igneous clasts lay below the level of the Wernecke Supergroup, then the clasts would have been transported to their present positions by processes involved in the development of the Wernecke breccia zones. The Wernecke breccias were produced by the flow of hydrothermal fluids (Hitzman et al., 1992; Thorkelson, 2000; Laughton et al., 2005; Hunt et al., 2007; Gillen, 2010), which would be their sole transporting force. Importantly, some of the breccias were emplaced within the Gillespie Lake Group approximately 10 km above the lowest strata of the Wernecke Supergroup, requiring at least 10 km of upward transport. It is implausible that the Wernecke igneous clasts, particularly those that are hundreds of metres long (millions of cubic metres in volume) could have been moved intact upward through the crust for several kilometres solely by the force of hydrothermal activity within the breccia zones. Another observation that is contradictory to upward transport is the absence of gneiss or peridotite clasts in the Wernecke breccias. Such compositions could be regarded as evidence for the entrainment of clasts from a source in the basement to the Wernecke Supergroup; however, no such clasts have been found. Furthermore, the metamorphic grade of the clasts themselves argues against the idea of a clast source located beneath the Wernecke Supergroup. The Bonnet Plume River Intrusions, Devil volcanics and Slab volcanics show metamorphism to greenschist facies, which could apply to conditions beneath the Wernecke Supergroup (i.e., >500 ˚C). However, the Blackstone River megaclast is virtually unmetamorphosed (Peters and Thorkelson, 2011), and cannot have been part of the substrate to the Wernecke Supergroup.

If the Wernecke igneous clasts were not derived from beneath, nor within the Wernecke Supergroup, then they must have been derived from above the Wernecke Supergroup. This hypothesis is tenable if the issue of age relations is adequately addressed and if appropriate mechanisms are identified. Laughton et al. (2005) recognized that downward transport of the megaclasts of the Slab volcanics was reasonable only if the distances travelled were modest, and yet these authors were faced with the observation that these megaclasts were located in a breccia zone that was hosted by the Fairchild Lake Group, the lowest unit in the Wernecke Supergroup. If the clasts were required to travel downward through the overlying Gillespie Lake and Quartet Groups, then the distance of transport would have been on the order of10 km, an unreasonable amount, given the high lithostatic pressures that would have existed at 10 km below the depth of formation of the Wernecke Breccias and the size of intact clasts. To address this problem, Laughton et al. (2005) noted that the Wernecke breccias formed after metamorphism and deformation of Racklan orogeny (Thorkelson, 2000), and appealed to this event as a mechanism by which the Fairchild Lake, Quartet and Gillespie Lake strata were locally brought to the same crustal levels by folding and faulting. Their hypothesis also required erosion following or during Racklan orogeny to expose all of these units at the surface, much as they are at the present day, followed by eruption of lava flows that subsequently became the sources of the Slab volcanics megaclasts. In this way, lava flows that were erupted above the Wernecke Supergroup would, in some locations, lie directly above the exhumed Fairchild Lake Group, and would require minimal foundering to become engulfed in breccia zones hosted by the Fairchild Lake Group. In some cases, such as at the Pika occurrence, the topographic distance between the Wernecke igneous clasts and the present top of the Wernecke Supergroup (unconformity with Pinguicula Group) required more than 600m of downward transport.

Despite the apparent success of the Laughton model to explain the origin of the Slab volcanics megaclasts, it cannot apply without modification to the origin of the Bonnet Plume River Intrusions megaclasts, which are older than the Wernecke Supergroup by about 70 m.y. To account for the age differential and observed field relations, Furlanetto et al. (2009a) suggested that downward-travelling clasts of the Bonnet Plume River Intrusions were derived from an older volcano-plutonic terrane that was obducted onto the Laurentian continental margin after or during the final phase of Racklan orogeny. This hypothesis affirmed the need for the clast sources to overlie deformed and exhumed strata of the Wernecke Supergroup, but differed from the Laughton model by invoking tectonic emplacement rather than volcanic eruption and deposition.

The geochemical and Sm-Nd results of this study and the petrologic results of Peters and Thorkelson (2011) provide additional constraints for the terrane obduction model of Furlanetto et al. (2009a). Our analyses indicate that the terrane which was obducted over the Wernecke Supergroup predominantly had the geochemical characteristics of calc-alkaline volcanic arcs (Wood, 1980b; Gill, 1981), based on the composition of the widespread Bonnet Plume River intrusive clasts. However, it also contained the Slab volcanics with compositions that are intermediate between those of volcanic arcs and alkalic ocean-islands. The neodymium signature of the Wernecke igneous clasts has a component of older, evolved continental crust (DePaolo, 1981b), suggesting that the magmas that formed the Wernecke igneous clasts were either emplaced through an older continental basement or derived from mantle with an εNd value enriched relative to depleted mantle (Nägler and Kramers, 1998). The Blackstone River megaclast contains quartz-rich sediments that suggest the likelihood of some evolved crust in the sediment source region, possibly from an older geological unit within the terrane. We propose

that the obducted terrane of Furlanetto et al. (2009a) in this model was a volcanic arc built upon a continent or continental fragment with some contribution from a plume (e.g., Thompson et al., 1983) or slab window source (Thorkelson et al., 2011).

2.7.2 A model of terrane obduction, brecciation, and foundering

The proposed model (Fig. 22) depicts the genesis, emplacement, and exhumation of the Wernecke igneous clasts. The source rocks to the Wernecke igneous clasts were formed in an offshore arc above a subducting slab of oceanic crust at 1.71 Ga (Fig. 22A). The arc was mainly a volcanic arc complex, but included rocks with plume or slab window character. This combination may have occurred by separate formation of these components followed by tectonic amalgamation, such as collision between the volcanic arc and an ocean island or oceanic plateau. Alternatively, the pairing of arc and intraplate compositions may have occurred by variations in the source of the magmas through time. In one scenario, subduction of a mid-ocean spreading ridge occurred beneath the arc, forming a slab window and allowing drier, more enriched mantle to upwell beneath the arc, leading to intraplate magma compositions (e.g., Hole et al., 1991; Gorring and Kay, 2001). In another, a mantle plume impinged on the region, temporarily contaminating the source of the arc magmas with more enriched peridotite (e.g., Johnston and Thorkelson, 1997; Wyman and Kerrich, 2010; Gazel et al., 2011).

Formation of the Wernecke basin at or after 1.64 Ga (Furlanetto et al., 2009a) was likely related to rifting of a continental block away from Laurentia (which may have existed within Columbia (Rogers and Santosh, 2002). The Wernecke Supergroup began to be deposited into this basin on the rifted margin of Laurentia (Fig. 22B). After sedimentation, the region was affected by contractional deformation of Racklan orogeny, causing cratonward directed transport of the passive margin sediments and sedimentary rock. The Wernecke Supergroup was locally

metamorphosed to lower greenschist facies. Following metamorphism, the deformed Wernecke Supergroup was exhumed, exposing all units of the Wernecke Supergroup at a single erosional surface (Fig. 22C) (Laughton et al., 2005).

At some time between 1.64 and 1.60 Ga, part of the volcanic arc collided with and overrode the continental margin (cf. Shervais, 2001; Whitmeyer and Karlstrom, 2007; Windley et al., 2007). The obduction was followed by voluminous surges of hydrothermal fluids and the formation of numerous zones of Wernecke Breccia. The process of obduction may have caused the hydrothermal activity through overpressuring of crustal brines (Kendrick et al., 2008; Gillen, 2010; Hunt et al., 2011) trapped within the Wernecke Supergroup beneath the obducted terrane. A second fluid source could be metamorphic waters (Kendrick et al., 2008; Gillen, 2010; Hunt et al., 2011) released due to the increased temperature (e.g., Walther and Orville, 1982; Connolly, 1997) of the Wernecke Supergroup as a consequence of the added thickness of the overlying terrane. Both of these scenarios are consistent with the near-absence of evidence for a contemporaneous magmatic source for the breccia-forming fluids, as indicated by fluid inclusion, stable isotope and noble gas studies (Hunt et al., 2005; Kendrick et al., 2008; Gillen, 2010; Hunt et al., 2011). In the model, the brecciating fluids affected both the Wernecke Supergroup and the overthrust arc complex, leading to metasomatism and iron oxide copper gold mineralization. During the process of brecciation, clasts and megaclasts of the Wernecke igneous clasts foundered and travelled downward in the breccia zones, some coming to rest at the level of the Wernecke Supergroup (Fig. 22D). To allow for the foundering of large blocks in the Wernecke Breccias, these hydrothermal brecciation episodes must have opened sufficient space in the crust. The open space may have been generated by violent expansion of the hydrothermal

fluids coupled with the possible ejection of clasts at the surface (Thorkelson et al. 2005; cf. Browne and Lawless, 2001)).

Hunt et al. (2011) estimated the range of depths of the presently exposed parts of the Wernecke breccias, at the time of their formation, to be from 5.7-11.3 km. This estimate, in the model of terrane obduction, would equal the sum of the thickness of the obducted terrane plus the depth to which the Wernecke igneous clasts travelled downward beneath the decollement of the terrane and into the Wernecke Supergroup. As noted earlier, it is likely that the megaclasts moved rather short distances within the crust – probably no more than approximately 1 km (but more than 600 m in some cases). Consequently, the range of thickness of the terrane could be estimated as approximately 1 km less than the depth values provided by Hunt et al. (2011), i.e., approximately 5-10 km. The absence of ultramafic clasts within Wernecke Breccia (Thorkelson, 2000) suggests that the underlying mantle substrate of the colliding volcanic arc complex was not obducted as part of the terrane (and was presumably subducted), and that the entire 5-10 km-thick nappe consisted of crustal material.

Following the formation of the Wernecke Breccias (1595 Ma; Thorkelson et al., 2001b), but before the deposition of the Pinguicula Group, at some point between 1380 and approximately 1000 Ma (Thorkelson, 2000; Medig et al., 2010), erosion denuded the obducted terrane and exposed the Wernecke igneous clasts within breccia zones hosted by the Wernecke Supergroup (Fig. 22E). The interval available for erosion of the terrane and re-exhumation of Wernecke Supergroup is therefore at least 215 m.y., and possibly as long as 562 m.y. – ample time for complete removal of the terrane.

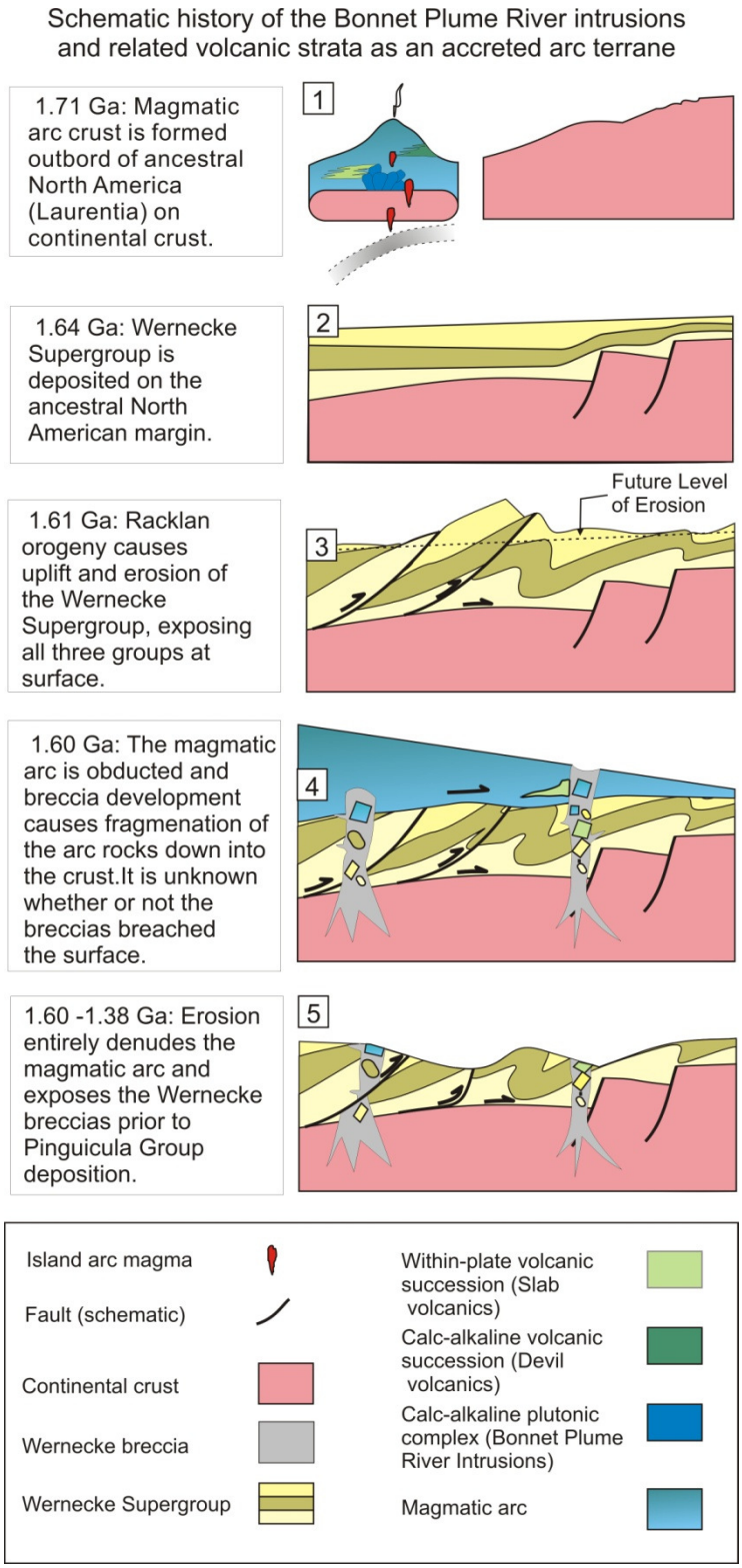

Fig. 22: Schematic history of the Wernecke igneous clasts, the Wernecke Breccia, and the Wernecke Supergroup.

2.8 Conclusions

1. The Wernecke igneous clasts comprise the Bonnet Plume River Intrusions, the Slab volcanics, the Devil volcanics, and the Blackstone River megaclast and range from less than one centimetre to hundreds of metres in size. All observed Wernecke igneous clasts occur within the Wernecke Breccias. The Bonnet Plume River Intrusions comprise mainly diorite and gabbro, the Slab volcanics and Devil volcanics comprise mafic to intermediate lavas, and the Blackstone river megaclast comprises volcaniclastic sedimentary rock.
2. The geochemical signature of the Bonnet Plume River Intrusions and Devil volcanics indicates that they were derived from a calc-alkaline to weakly tholeiitic volcanic arc built on continental crust that was active at approximately 1.71 Ga. The geochemical signature of the Slab volcanics is distinct from the other Wernecke igneous clasts and indicates that an alkalic intraplate source such as a mantle plume or a slab window was involved in their formation.
3. The Wernecke igneous clasts were not derived from the Wernecke Supergroup. Instead, they were derived from the crustal portion of a volcanic arc complex that was obducted onto the Laurentian continental margin. The thickness of the terrane is estimated at 5-10 km.
4. The obduction the volcanic arc terrane occurred after (or during the final phase of) the Racklan orogeny, during which the Wernecke Supergroup was folded, metamorphosed, exhumed and exposed at the crustal surface.
5. Following the obduction, surges of hydrothermal fluids burst through the crust, brecciating the Wernecke Supergroup and the overlying terrane and producing widespread zones of Wernecke Breccia. Fragments of rock, including igneous megaclasts of the terrane, foundered into the open spaces within the breccia zones, many coming to rest at the level of the Wernecke Supergroup (Fig. 22).
6. The Wernecke igneous clasts were affected by hydrothermal fluid-induced elemental mobility and the development of iron oxide copper gold (IOCG) occurrences. Leaching of Cu from the igneous clasts into the breccia fluids occurred during alkali metasomatism (both sodic and potassic). The IOCG occurrences are products of localized metal redistribution and concentration within the breccia systems.

7. Prior to the deposition of the Pinguicula Group, which occurred between ca. 1.38 and 1.0 Ga, erosion denuded the obducted terrane, exposing the Wernecke Supergroup, Wernecke Breccias, and the Wernecke igneous clasts.

3: Recommendations for further work

Further attempts to date the Wernecke igneous clasts should be made. This would significantly advance the present understanding of Wernecke igneous clast evolution and would test the assumption that the Wernecke igneous clasts are broadly related.

A study involving detrital zircon geochronology and clast provenance should be performed on the various sedimentary units that are contained within Wernecke igneous clast bodies. The Blackstone River megaclast volcanosedimentary rock at the Yukon Olympic mineral occurrence, the mudstone clasts at the Yukon Olympic mineral occurrence (Peters and Thorkelson, 2011), the two sandstone beds within the Slab volcanics (Laughton, 2004), the pebble diamictite within the Slab volcanics (Laughton, 2004), and the central mudstone megaclast at the Bel mineral occurrence (see Fig. 24) would likely prove fruitful lithologies for the study.

4: Conclusions

The Bonnet Plume River Intrusions, the Slab volcanics, the Devil volcanics, and the Blackstone River megaclast, together termed the Wernecke igneous clasts, sit as clasts within the Wernecke Breccias throughout much of central and northern Yukon. The Bonnet Plume River Intrusions were most likely diorites and gabbros originally. The Slab volcanics were most likely originally sub-alkaline basalts to trachyandesites. The Devil volcanics were most likely basalts and basaltic andesites. The Blackstone river megaclast is weakly altered volcaniclastic rock. Most of the Wernecke igneous clasts bear the signal of metasomatism by the Wernecke Breccias, including "extreme" K/Na values and elemental enrichments and depletions relative to less altered clasts.

The age of the Wernecke igneous clasts precludes their emplacement in the Wernecke Supergroup. Additionally, field investigations have discovered no evidence for intrusions of sufficient size or appropriate age to represent the source rocks of the Wernecke igneous clasts therefore; they were not derived from within the Wernecke Supergroup. It is geologically unreasonable for them to have been part of the basement to the Wernecke Supergroup; therefore, they must have been part of a nappe that was thrust over the Wernecke Supergroup. During Wernecke Brecciation, this nappe was fragmented and the resulting clasts and megaclasts foundered into the Wernecke Breccia to the level of the Wernecke Supergroup.

The geochemical and isotopic signature of the Bonnet Plume River Intrusions and Devil volcanics indicates that they were derived from suprasubduction zone mantle, and emplaced in a

calc-alkaline volcanic arc built on continental crust. The geochemical signature of the Slab volcanics indicates that they were derived from enriched mantle (either plume or slab window).

We propose that the volcanic arc was obducted over the Wernecke Supergroup after the Racklan orogeny, forming a nappe overlying the Wernecke Supergroup. During the hydrothermal activity of the Wernecke Breccia event, the volcanic arc fragmented and many clasts were dropped down to the level of the Wernecke Supergroup within zones of Wernecke Breccia Fig. 22

References

Abbott, J.G., 1997. Geology of the Upper Hart River Area, Eastern Ogilvie Mountains, Yukon Territory (116A/10, 116A/11). Exploration and Geological Services Division, Yukon, Indian and Northern Affairs Canada, Bulletin 9, 92 p.

Amelin, Y., Rotenberg, E., 2004. Sm-Nd systemtics of chorndrites. Earth and Planetary Science Letters 233, 267-282

Baker, D.R., 1987. Depths and water content of magma chambers in the Aleutian and Mariana island arcs. Geology 15, 496-499.10.1130/0091-7613(1987)15<496:dawcom>2.0.co;2

Baker, D.R., Eggler, D.H., 1987. Compositions of anhydrous and hydrous melts coexisting with plagioclase, augite, and olivine or low-Ca pyroxene from 1 atm to 8 kbar; application to the Aleutian volcanic center of Atka. American Mineralogist 72, 12-28

Bell, R.T., 1986. Megabreccias in northeastern Wernecke Mountains, Yukon Territory, Paper 1986-1A. Geological Survey of Canada, pp. 375 - 384.

Betts, P.G., Giles, D., Schaefer, B.F., 2008. Comparing 1800-1600 Ma accretionary and basin processes in Australia and Laurentia: Possible geographic connections in Columbia. Precambrian Research 166, 81-92

Bowering, S.A., Karlstrom, K.E., 1990. Growth, stabilization, and reactivation of Proterozoic lithosphere in the southwestern United States. Geology 18, 1203-1206.10.1130/0091-7613(1990)018<1203:GSAROP>2.3.CO;2.

Brideau, M.A., Thorkelson, D.J., Godin, L., Laughton, J.R., 2002. Paleoproterozoic deformation of the Racklan Orogeny, Slats Creek (106D/16) and Fairchild Lake (106C/13) map areas, Wernecke Mountains, Yukon, in: Edmond, D.S., Weston, L.H., Lewis, L.L. (Eds.), Yukon Exploration and Geology 2001. Exploration and Geological Services Division, Yukon Region, Indian and Northern Affairs Canada.

Browne, P.R.L., Lawless, J.V., 2001. Characteristics of hydrothermal eruptions, with examples from New Zealand and elsewhere. Earth-Science Reviews 52, 299-331.10.1016/s0012-8252(00)00030-1

Burton, K.W., O'Nions, R.K., 1988. Isotope systematics and chronology of granulite genesis in SRI lanka. Chemical Geology 70, 5-5.Doi: 10.1016/0009-2541(88)90181-7

Butler, S.G., Gill, D.G., 1997. Olympic Property 1997 Report 093700. Major General Resources Ltd., Vancouver.

Carten, R.B., 1986. Sodium-calcium metasomatism; chemical, temporal, and spatial relationships at the Yerington, Nevada, porphyry copper deposit. Economic Geology 81, 1495-1519.10.2113/gsecongeo.81.6.1495

Condie, K.C., 1982. Plate-tectonics model for Proterozoic continental accretion in the southwestern United States. Geology 10, 37-42

Condie, K.C., 1992. Chapter 12 Proterozoic Terranes and Continental Accretion in Southwestern North America, in: Condie, K.C. (Ed.), Developments in Precambrian Geology. Elsevier, pp. 447-480.

Connolly, J.A.D., 1997. Devolatilization-generated fluid pressure and deformation-propagated fluid flow during prograde regional metamorphism. J. Geophys. Res. 102, 18149-18173.10.1029/97jb00731

Cook, D.G., MacLean, B.C., 1995. The intracratonic Paleoproterozoic Forward orogeny, and implications for regional correlations, Northwest Territories, Canada. Canadian Journal of Earth Sciences 32, 1991-2008.10.1139/e95-152

Cross, W., Iddings, J.P., Pirsson, L.V., Washington, H.S., 1903. Quantitative classification of igneous rocks. University of Chicago Press, Chicago.

Cullers, R.L., Medaris, L.G., Haskin, L.A., 1973. Experimental studies of the distribution of rare earths as trace elements among silicate minerals and liquids and water. Geochimica et Cosmochimica Acta 37, 1499-1512.Doi: 10.1016/0016-7037(73)90086-0

Delaney, G.D., 1981. The mid-Proterozoic Wernecke Supergroup, Wernecke Mountains, Yukon Territory, in: Campbell, F.H.A. (Ed.), Geological Survey of Canada Paper. Geological Survey of Canada, pp. 1-23.

DePaolo, D.J., 1981a. Neodymium isotopes in the Colorado Front Range and crust-mantle evolution in the Proterozoic. Nature 291, 193-196

DePaolo, D.J., 1981b. Trace element and isotopic effects of combined wallrock assimilation and fractional crystallization. Earth and Planetary Science Letters 53, 189-202

DePaolo, D.J., Wasserburg, G.J., 1976. Nd isotopic variations and pertogenetic models. Geophysical Research Letters 3, 249-252

Eisbacher, G.D., 1978. Two Major Proterozoic Unconformities, Northern Cordillera, Current Research. Geological Survey of Canada, pp. 53-58.

Fliedner, M.M., Klemperer, S.L., 1999. Structure of an island-arc: Wide-angle seismic studies in the eastern Aleutian Islands, Alaska. J. Geophys. Res. 104, 10667-10694.10.1029/98jb01499

Floyd, P.A., Winchester, J.A., 1978. Identification and discrimination of altered and metamorphosed volcanic rocks using immobile elements. Chemical Geology 21, 291-306

Furlanetto, F., Thorkelson, D.J., Davis, W.J., Gibson, H.D., Rainbird, R.H., Marshall, D.D., 2009a. A New Model of Terrane Accretion in Northwestern Laurentia required by U-Pb SHRIMP Analysis of Detrital Zircons from the Paleoproterozoic Wernecke Supergroup, Wernecke Mountains, Yukon. [Abstract U74A-04], Geological Association of Canada, Joint Assembly, Toronto, Canada.

Furlanetto, F., Thorkelson, D.J., Davis, W.J., Gibson, H.D., Rainbird, R.H., Marshall, D.D., 2009b. Preliminary results of detrital zircon geochronology, Wernecke Supergroup, Yukon in: Weston, L.H., Blackburn, L.R., Lewis, L.L. (Eds.), Yukon Exploration and Geology 2008. Yukon Geological Survey, pp. 125 - 135.

Gazel, E., Hoernle, K., Carr, M.J., Herzberg, C., Saginor, I., den Bogaard, P.v., Hauff, F., Feigenson, M., Swisher Iii, C., 2011. Plume–subduction interaction in southern Central America: Mantle upwelling and slab melting. Lithos 121, 117-134.10.1016/j.lithos.2010.10.008

Gifkins, C., Herrmann, W., Large, R., 2005. Altered Volcanic Rocks; a guide to description and interpretation. Centre for Ore Deposits Research, University of Tasmania, Hobart.

Gill, J.B., 1981. Orogenic Andesites and Plate Tectonics. Springer-Verlag, Berlin.

Gillen, D., 2010. A study of IOCG-related hydrothermal fluids in the Wernecke Mountains, Yukon Territory, Canada, School of Earth and Environmental Sciences. James Cook University, Townsville.

Goldstein, S.L., O'Nions, R.K., Hamilton, P.J., 1984. A Sm-Nd isotopic study of atmospheric dusts and particulates from major river systems. Earth and Planetary Science Letters 70, 221-236.Doi: 10.1016/0012-821x(84)90007-4

Gordey, S.P., Makepeace, A.J., 2000. Yukon Digital Geology. Geological Survey of Canada.

Gorring, M.L., Kay, S.M., 2001. Mantle Processes and Sources of Neogene Slab Window Magmas from Southern Patagonia, Argentina. Journal of Petrology 42, 1067-1094.10.1093/petrology/42.6.1067

Govindaraju, K., 1994. 1994 COMPILATION OF WORKING VALUES AND SAMPLE DESCRIPTION FOR 383 GEOSTANDARDS. Geostandards Newsletter 18, 1-158.10.1046/j.1365-2494.1998.53202081.x-i1

Gower, C.F., Krogh, T.E., 2002. A U-Pb geochronological review of the Proterozoic history of the eastern Grenville Province. Canadian Journal of Earth Sciences 39, 795-829

Grant, J.A., 1986. The isocon diagram: A simple solution to Gresen's equation for metasomatic alteration. Economic Geology 81, 1976-1982

Gruau, G., Rosing, M., Bridgwater, D., Gill, R.C.O., 1996. Resetting of Sm-Nd systematics during metamorphism of >3.7-Ga rocks: implications for isotopic models of early Earth differentiation. Chemical Geology 133, 225-240.10.1016/s0009-2541(96)00092-7

Halama, R., John, T., Herms, P., Hauff, F., Schenk, V., 2011. A stable (Li, O) and radiogenic (Sr, Nd) isotope perspective on metasomatic processes in a subducting slab. Chemical Geology 281, 151-166.DOI: 10.1016/j.chemgeo.2010.12.001

Hitzman, M.W., 2000. Iron oxide-Cu-Au deposits:what, where, when, and why?, in: Porter, T.M. (Ed.), Hydrothermal Iron Oxide Copper-Gold and Related Deposits: A Global Perspective. PGC Publishing, Adelaide, Australia, pp. 9-25.

Hitzman, M.W., Oreskes, N., Einaudi, M.T., 1992. Geological characteristics and tectonic setting of proterozoic iron oxide (Cu---U---Au---REE) deposits. Precambrian Research 58, 241-287.Doi: 10.1016/0301-9268(92)90121-4

Hoffman, P.F., 1988. United Plates of America, The Birth of a Craton: Early Proterozoic Assembly and Growth of Laurentia. Annual Review of Earth and Planetary Sciences 16, 543-603.doi:10.1146/annurev.ea.16.050188.002551

Holbrook, W.S., Lizarralde, D., McGeary, S., Bangs, N., Diebold, J., 1999. Structure and composition of the Aleutian Island arc and implication for continental crustal growth. Geology 27, 31-34

Hole, M.J., Rogers, G., Saunders, A.D., Storey, M., 1991. Relation between alkalic volcanism and slab-window formation. Geology 19, 657-660.10.1130/0091-7613(1991)019<0657:rbavas>2.3.co;2

Hunt, J., Baker, T., Thorkelson, D., 2005. Regional-scale Proterozoic IOCG-mineralized breccia systems: examples from the Wernecke Mountains, Yukon, Canada. Mineralium Deposita 40, 492-514.10.1007/s00126-005-0019-5

Hunt, J.A., Baker, T., Cleverley, J., Davidson, G.J., Fallick, A.E., Thorkelson, D.J., 2011. Fluid inclusion and stable isotope constraints on the origin of Wernecke Breccia and associated iron oxide – copper – gold mineralization, Yukon. Canadian Journal of Earth Sciences 48, 1425-1445.10.1139/e11-044

Hunt, J.A., Baker, T., Thorkelson, D.J., 2007. A Review of Iron Oxide Copper-Gold Deposits, with Focus on the Wernecke Breccias, Yukon,Canada, as an Example of a Non-Magmatic End Member and Implications for IOCG Genesis and Classification. Canadian Institute of Mining, Metallurgy, and Petroleum 16, 209-232

Hunt, J.A., Laughton, J.R., Brideau, M.A., Thorkelson, D.J., Brookes, M.L., Baker, T., 2002. New mapping around the Slab iron oxide-copper-gold occurrence, Wernecke Mountains (parts of NTS 106C/13, 106D/16, 106E/1 and 106F/4), Yukon, in: Emond, D.S., Weston, L.H., Lewis, L.L. (Eds.), Yukon Exploration and Geology 2001. Exploration and Geological Services Division, Yukon Region, Indian and Northern Affairs Canada, pp. 125-138.

Hunt, J.A., Thorkelson, D.J., 2006. Are mafic dykes in the Nor and Hart River areas of the Yukon correlative to the Bonnet Plume River Intrusions? Constraints from geochemistry, in: Esmond, D.S., Lewis, L.L., Weston, L.H. (Eds.), Yukon Exploration and Geology 2006. Yukon Geological Survey.

Irvine, G.J., Baragar, W., 1971. A guide to the chemical classification of the common volcanic rocks. Canadian Journal of Earth Sciences 8, 523-584

Jacobsen, S.B., Wasserburg, G.J., 1980. Sm-Nd isotopic evolution of chondrites. Earth and Planetary Science Letters 50, 139-155

Johnston, S.T., Thorkelson, D.J., 1997. Cocos-Nazca slab window beneath Central America. Earth and Planetary Science Letters 146, 465-474.10.1016/s0012-821x(96)00242-7

Karlstrom, K.E., Åhäll, K.-I., Harlan, S.S., Williams, M.L., McLelland, J., Geissman, J.W., 2001. Long-lived (1.8-1.0 Ga) convergent orogen in southern Laurentia, its extensions to Australia and Baltica, and implications for refining Rodinia. Precambrian Research 111, 5-30.10.1016/s0301-9268(01)00154-1

Kendrick, M.A., Honda, M., Gillen, D., Baker, T., Phillips, D., 2008. New constraints on regional brecciation in the Wernecke Mountains, Canada, from He, Ne, Ar, Kr, Xe, Cl, Br and I in fluid inclusions. Chemical Geology 255, 33-46.10.1016/j.chemgeo.2008.05.021

Ketchum, J.W.F., Culshaw, N.G., Barr, S.M., 2002. Anatomy and orogenic history of a Paleoproterozoic accretionary belt: the Makkovik Province, Labrador, Canada. Canadian Journal of Earth Sciences 39, 711-730.10.1139/e01-099

Kikawada, Y., Ossaka, T., Oi, T., Honda, T., 2001. Experimental studies on the mobility of lanthanides accompanying alteration of andesite by acidic hot spring water. Chemical Geology 176, 137-149.Doi: 10.1016/s0009-2541(00)00375-2

Kusky, T.M., Glass, A., Tucker, R., 2007. Structure, Cr-chemistry, and age of the Border Ranges Ultramafic-Mafic Complex: A suprasubduction zone ophiolite complex, in: Ridgway, K.D., Trop, J.M., Glen, J.M.G., O'Niell, J.M. (Eds.), Tectonic Growth of a Collisional Continental Margin: Crustal Evolution of Southern Alaska: Geological Society of America Special Paper 431, pp. 207-225.

Lane, R.A., 1990. Geologic setting and petrology of the Proterozoic Ogilvie Mountains Breccia of the Coal Creek inlier, southern Ogilvie Mountains, Yukon Territory. University of British Columbia, Vancouver.

Laughton, J.R., 2004. The Proterozoic Slab Volcanics of Northern Yukon, Canada: Megaclasts of a Volcanic Succession in Proterozoic Wernecke Breccia, and Implications for the Evolution of Northwestern Laurentia, Earth Sciences. Simon Fraser University, Burnaby, p. 81.

Laughton, J.R., Thorkelson, D.J., Brideau, M.A., Hunt, J.A., 2002. Paleoproterozoic volcanism and plutonism in the Wernecke Mountains, Yukon, in: Esmond, D.S., Weston, L.H., Lewis, L.L. (Eds.), Yukon Exploration and Geology 2001. Exploration and Geological Services Division, Yukon Region, Indian and Northern Affairs, pp. 139-145.

Laughton, J.R., Thorkelson, D.J., Brideau, M.A., Hunt, J.A., Marshall, D.D., 2005. Early Proterozoic orogeny and exhumation of Wernecke Supergroup revealed by vent facies of Wernecke Breccia, Yukon, Canada. Canadian Journal of Earth Sciences 42, 1033–1044

Laznicka, P., Edwards, R.J., 1979. Dolores Creek, Yukon; a disseminated copper mineralization in sodic metasomatites. Economic Geology 74, 1352-1370.10.2113/gsecongeo.74.6.1352

LeMaitre, R.W., 2002. Igneous Rocks: A Classification and Glossary of Terms : Recommendations of International Union of Geological Sciences Subcommission on the Systematics of Igneous Rocks, 2nd ed. Cambridge University Press, Cambridge.

Li, Z.-X., Li, X.-H., Li, W.-X., Ding, S., 2008a. Was Cathaysia part of Proterozoic Laurentia? – new data from Hainan Island, south China. Terra Nova 20, 154-164.10.1111/j.1365-3121.2008.00802.x

Li, Z.X., Bogdanova, S.V., Collins, A.S., Davidson, A., De Waele, B., Ernst, R.E., Fitzsimons, I.C.W., Fuck, R.A., Gladkochub, D.P., Jacobs, J., Karlstrom, K.E., Lu, S., Natapov, L.M., Pease, V., Pisarevsky, S.A., Thrane, K., Vernikovsky, V., 2008b. Assembly, configuration, and break-up history of Rodinia: A synthesis. Precambrian Research 160, 179-210.10.1016/j.precamres.2007.04.021

MacLean, B.C., Cook, D.G., 2004. Revisions to the Paleoproterozoic Sequence A, based on reflection seismic data across the western plains of the Northwest Territories, Canada. Precambrian Research 129, 271-289.DOI: 10.1016/j.precamres.2003.10.008

Marshak, R.S., Karig, D.E., 1977. Triple junctions as a cause for anomalously near-trench igneous activity between the trench and volcanic arc. Geology 5, 233-236.10.1130/0091-7613(1977)5<233:tjaacf>2.0.co;2

Masuda, A., 1967. An estimation of lanthanide partition coefficient for the [`]calcium effect'. Earth and Planetary Science Letters 2, 277-279.Doi: 10.1016/0012-821x(67)90141-0

Medig, K.P.R., Thorkelson, D.J., Dunlop, R.L., 2010. The Proterozoic Pinguicula Group: Stratigraphy, contact relationships and possible correlations, in: MacFarlane, K.E., Weston, L.H., Blackburn, L.R. (Eds.), Yukon Exploration and Geology 2009. Yukon Geological Survey, pp. 265-278.

Meschede, M., 1986. A method of discriminating between different types of mid-ocean ridge basalts and continental tholeiites with the Nb瑎1bZr瑎1bY diagram. Chemical Geology 56, 207-218.10.1016/0009-2541(86)90004-5

Michel-Lévy, A., 1894. Étude sur la détermination des feldspaths dans les plaques minces, au point de vue de la classification des roches. Librairie Polytechnique, Baudry, Paris.

Milidragovic, D., Thorkelson, D.J., Davis, W.J., Marshall, D.D., Gibson, H.D., 2011. Evidence for late Mesoproterozoic tectonism in northern Yukon and the identification of a Grenville-age tectonothermal belt in western Laurentia. Terra Nova 23, 307-313.10.1111/j.1365-3121.2011.01015.x

Mitchelmore, M.D., Cook, F.A., 1994. Inversion of the Proterozoic Wernecke basin during tectonic development of the Racklan Orogen, northwest Canada. Canadian Journal of Earth Sciences 31, 447-457.10.1139/e94-041

Miyashiro, A., 1974. Volcanic rock series in island arcs and active continental margins. Am J Sci 274, 321-355.10.2475/ajs.274.4.321

Mullen, E.D., 1983. MnO/TiO2/P2O5: a minor element discriminant for basaltic rocks of oceanic environments and its implications for petrogenesis. Earth and Planetary Science Letters 62, 53-62.10.1016/0012-821x(83)90070-5

Nägler, T.F., Kramers, J.D., 1998. Nd isotopic evolution of the upper mantle during the Precambrian: models, data and the uncertainty of both. Precambrian Research 91, 233-252.Doi: 10.1016/s0301-9268(98)00051-5

Nesse, W.D., 2003. Introduction to Optical Mineralogy, 3rd ed. Oxford University Press, New York, Oxford.

Norris, D.K., 1997. Geology and mineral and hydrocarbon potential of northern Yukon Territory and northwestern district of Mackenzie, Geological Survey of Canada Bulletin, p. 401.

Pearce, J.A., Parkinson, I.J., 1993. Trace element models for mantle melting: application to volcanic arc petrogenesis, in: Prichard, H.M., Alabaster, T., Harris, N.B.W., Neary, C.R. (Eds.), Magmatic Processes and Plate Tectonics. Geological Society of London, Special Publications.

Pearce, T.H., 1968. A contribution to the theory ofvariation diagrams. Contributions to Mineralogy and Petrology 19, 142-157

Pecerillo, A., Taylor, S.R., 1976. Geochemistry of Eocene calc-alkaline volcanic rocks from the Kastamonu area, Northern Turkey. Contributions to Mineralogy and Petrology 58, 63-81

Peters, T.J., Thorkelson, D.J., 2011. Volcano-sedimentary megaclast in Wernecke breccia, Yukon, and its bearing on the Proterozoic evolution of northwestern Laurentia, in: McFarlane, K.E., Weston, L.H., Relf, C. (Eds.), Yukon Exploration and Geology 2010, pp. 197-206.

Plank, T., Langmuir, C., 1988. An evaluation of the global variations in the major element chemistry of arc basalts. Earth and Planetary Science Letters 90, 349-370

Project, B.V.S., 1981. Basaltic Volcanism on the Terrestrial Planets. Pergamon Press, Inc, New York.

Rogers, J.J.W., Santosh, M., 2002. Configuration of Columbia, a Mesoproterozoic Supercontinent. Gondwana Research 5, 5-22.10.1016/s1342-937x(05)70883-2

Rollinson, 1993. Using geochemical data: evaluation, presentation, interpretation. Longman Scientific and Technical, London, UK.

Rosing, M.T., 1990. The theoretical effect of metasomatism on Sm-Nd isotopic systems. Geochimica et Cosmochimica Acta 54, 1337-1341.Doi: 10.1016/0016-7037(90)90158-h

Rudnick, R.L., 1995. Making Continental-Crust. Nature 378, 571-578.citeulike-article-id:7832384

Schwab, D.L., Thorkelson, D.J., Mortensen, J.K., Creaser, R.A., Abbott, J.G., 2004. The Bear River dykes (1265-1269 Ma): westward continuation of the Mackenzie dyke swarm into Yukon, Canada. Precambrian Research 133, 175-186

Sears, J.W., Price, R.A., 2000. New look at the Siberian connection: No SWEAT. Geology 28, 423-426.10.1130/0091-7613(2000)28<423:nlatsc>2.0.co;2

Shaw, C.A., Karlstrom, K.E., 1999. The Yavapai-Mazatzal crustal boundary in the Southern Rocky Mountains. Rocky Mountain Geology 34, 37-52.10.2113/34.1.37

Shervais, J.W., 2001. Birth, death, and resurrection: The life cycle of suprasubduction zone ophiolites. Geochemistry, Geophysics, Geosystems 2, 2000GC000080

Sillitoe, R.H., 2010. Porphyry Copper Systems. Economic Geology 105, 3-41.10.2113/gsecongeo.105.1.3

Sun, S.S., McDonough, W.F., 1989. Chemical and isotopic systematics of oceanic basalts; implications for mantle composition and processes. Geological Society Special Publications 42, 313-345

Templeman-Kluit, D.J., 1981. Nor, summary of assessment work and description of mineral properties, Yukon Geology and Exploration, 1979-1980. Exploration and Geological Services Division, Yukon Region, Indian and Northern Affairs Canada, pp. 300-301.

Terry, M., Nicos, T., Rae, C., 2006. 2006 KRL Drillhole Locations and Prospect Geology. International KRL, Vancouver.

Thompson, R.N., Morrison, M.A., Dickin, A.P., Hendry, G.L., 1983. Continental Flood Basalts.....Arachnids rule OK?, in: Hawkesworth, C.J., Norry, M.J. (Eds.), Continental Flood Basalts and Mantle Xenoliths. Shiva Press, Nantwich, pp. 158-185.

Thorkelson, D.J., 2000. Geology and mineral occurrences of the Slats Creek, Fairchild Lake and "Dolores Creek" areas, Wernecke Mountains (106D/16, 106C/13, 106C/14), Yukon Territory, Bulletin. Exploration and Geological Services Division, Yukon, Indian and Northern Affairs Canada, Whitehorse, p. 10.

Thorkelson, D.J., Abbott, J.G., Mortensen, J.K., Creaser, R.A., Villeneuve, M.E., McNicoll, V.J., Layer, P.W., 2005. Early and Middle Proterozoic evolution of Yukon, Canada. Canadian Journal of Earth Sciences 42, 26.10.1139/e04-075

Thorkelson, D.J., Cook, D.G., MacLean, B.C., 2003. The Early Proterozoic Racklan and Forward orogenies of northwestern Laurentia: geological and seismic evidence, abstract #4633, AGU-EUG Joint Assembly, Nice, France.

Thorkelson, D.J., Madsen, J.K., Slugget, C.L., 2011. Mantle flow through the Northern Cordilleran slab window revealed by volcanic geochemistry. Geology 39, 267-270.10.1130/G31522.1

Thorkelson, D.J., Mortensen, J.K., Creaser, R.A., Davidson, G.J., Abbott, J.G., 2001a. Early Proterozoic magmatism in Yukon, Canada: constraints on the evolution of northwestern Laurentia. Canadian Journal of Earth Sciences 38, 1479 - 1494

Thorkelson, D.J., Mortensen, J.K., Davidson, G.J., Creaser, R.A., Perez, W.A., Abbott, J.G., 2001b. Early Mesoproterozoic intrusive breccias in Yukon, Canada: the role of hydrothermal systems in reconstructions of North America and Australia. Precambrian Research 111, 31-55

Thorkelson, D.J., Wallace, C.A., 1998. Geological map of Fairchild Lake area, Wernecke Mountains, Yukon (106C/13). Exploration and Geological Services Division, Yukon, Indian and Northern Affairs Canada, Whitehorse, Canada.

Turner, F.J., 1951. Observations on twinning of plagioclase in metamorphic rocks. American Mineralogist 36, 581-589

Walther, J.V., Orville, P.M., 1982. Volatile production and transport in regional metamorphism. Contributions to Mineralogy and Petrology 79, 252-257.10.1007/bf00371516

Weis, D., Kieffer, B., Maerschalk, C., Pretorius, W., Barling, J., 2005. High-precision Pb-Sr-Nd-Hf isotopic characterization of USGS BHVO-1 and BHVO-2 reference materials. Geochemistry, Geophysics, Geosystems 6.10.1029/2004GC000852

Whitmeyer, S.J., Karlstrom, K.E., 2007. Tectonic model for the Proterozoic growth of North America. Geosphere 3, 220-259.10.1130/ges00055.1

Williams, P.J., Barton, M.D., Johnson, D.A., Fontboté, L., de Haller, A., Mark, G., Oliver, N.H.S., Marschik, R., 2005. Iron oxide copper-gold deposits: Geology, Space-time distribution, and possible modes of origin, Economic Geology 100th Anniversary Volume, pp. 371-405.

Winchester, J.A., Floyd, P.A., 1977. Geochemical discrimination of different magma series and their differentiation products using immobile elements. Chemical Geology 20, 325-343

Windley, B., 1992. Chapter 11 Proterozoic Collisional and Accretionary Orogens, in: Condie, K.C. (Ed.), Developments in Precambrian Geology. Elsevier, pp. 419-446.

Windley, B.F., 1993. Uniformitarianism today: plate tectonics is the key to the past. Journal of the Geological Society 150, 7-19.10.1144/gsjgs.150.1.0007

Windley, B.F., Alexeiev, D., Xiao, W., Kroner, A., Badarch, G., 2007. Tectonic models for accretion of the Central Asian Orogenic Belt. Journal of the Geological Society 164, 31-47.10.1144/0016-76492006-022

Winter, J.D., 2001. An Introduction to Igneous and Metamorphic Petrology. Prentice-Hall, Upper Saddle River.

Wood, D., 1980a. The Application of a Th-Hf-Ta Diagram to Problems of Tectonomagmatic Classification and to Establishing the Nature of Crustal Contamination of Basaltic Lavas of the British Teritary Volcanic Province. Earth and Planetary Science Letters 50, 11-30

Wood, D.A., 1980b. The application of a ThHfTa diagram to problems of tectonomagmatic classification and to establishing the nature of crustal contamination of basaltic lavas of the British Tertiary Volcanic Province. Earth and Planetary Science Letters 50, 11-30

Wyman, D., Kerrich, R., 2010. Mantle plume – volcanic arc interaction: consequences for magmatism, metallogeny, and cratonization in the Abitibi and Wawa subprovinces, CanadaThis article is one of a series of papers published in this Special Issue on the theme Lithoprobe — parameters, processes, and the evolution of a continent. Canadian Journal of Earth Sciences 47, 565-589.10.1139/e09-049

YGS, 2011. Yukon MINFILE. Yukon Geological Survey, <http://servlet.gov.yk.ca/ygsmin/index.do>

Appendices

Appendix A: Sample Collection and Mapping

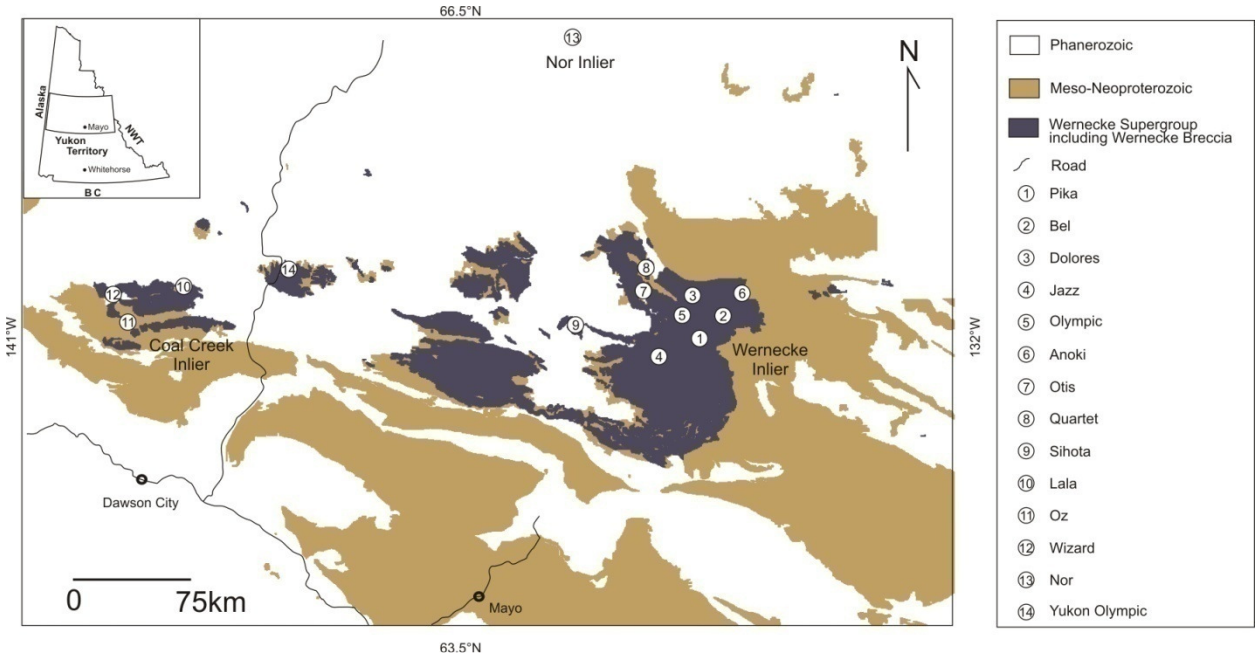

Fig. 23 Map of central-northern Yukon Territory showing the location of all the Wernecke igneous clast locations investigated

Pika

This location is near the Pika Mineral occurrence, in the Wernecke inlier at location 1 in Fig. 23 within the Quartet and Gillespie Lake Groups. Stratigraphically overlying the WBX body, separated by a paleosol horizon, is the basal conglomerate of the Pinguicula Group. Ten to hundred metre scale clasts of Bonnet Plume River Intrusions dominate the exposed breccia zone. Wernecke Supergroup clasts represent the rest of the clast material. These clasts are separated by small areas of hydrothermal breccia which themselves contain small clasts of both Bonnet Plume River Intrusions and Wernecke Supergroup (e.g. Fig. 4). Bonnet Plume River Intrusions clasts at Pika are primarily medium grained with pervasive chlorite alteration and ubiquitous disseminated hematite. Veins of epidote and alkali feldspar are common. Sulphide occurrences are located on the boundaries between large clasts and areas that are breccia-dominated. A map

was created at the Pika occurrence in the exposed bedrock of the creek bed that runs through the occurrence (Fig. 11).

Bel

This location is near the Bel Mineral occurrence, in the Wernecke inlier at location 2 in Fig. 23 within the Fairchild Lake Group. The breccia zone is dominated by one metre and smaller sedimentary clasts, most likely derived from the Wernecke Supergroup with one hundred metre scale megaclast of unaltered grey mudstone, likely from the Gillespie Lake Group. Bonnet Plume River Intrusions clasts at Bel are generally tens of metres in scale and sparsely scattered throughout the breccia zone. They are chloritized and with disseminated hematite throughout and often epidotized. Potassic alteration may be present, associated with epidotization. Quartz carbonate veins are common throughout the breccias zone with no relationship to the clasts. Major sulphide concentrations are found in these quartz-carbonate veins. A map was made of the Bel breccia zone based on talus relationships and bedrock, where exposed (Fig. 24).

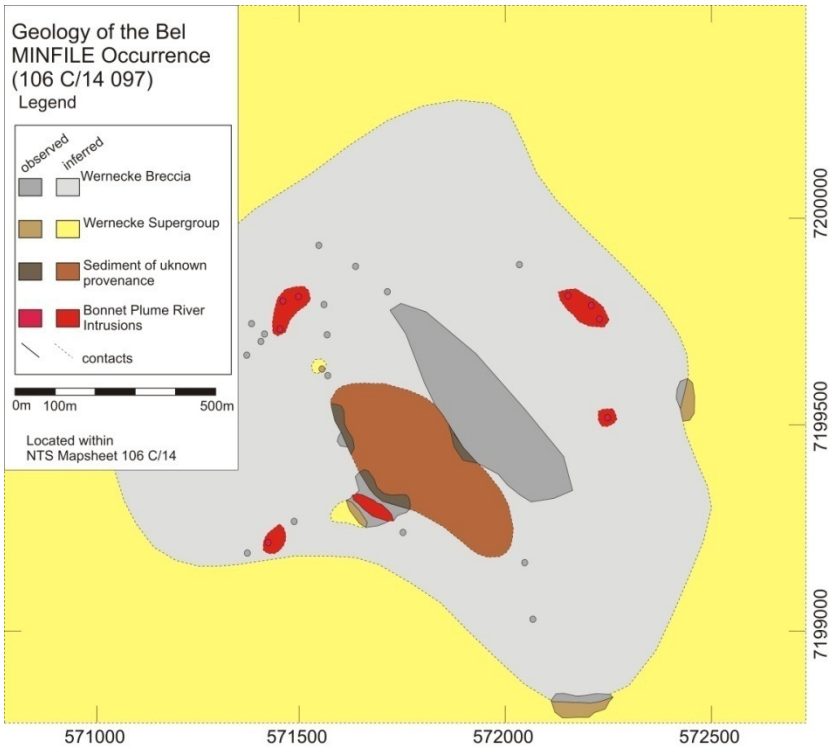

Fig. 24: Geological map of a portion of the Bel mineral occurrence. MINFILE is the Yukon mineral occurrence database (YGS, 2011)

Dolores

This location is near the Dolores Mineral occurrence, in the Wernecke inlier at location 3 in Fig. 23 within the Fairchild Lake Group. Despite two traverses of the area, no in-place Bonnet Plume River Intrusion clasts were located. The area that was investigated was primarily metasomatized crackle breccia within the FLG with minor zones of more developed mosaic to chaotic breccia. Two talus blocks of medium grained, chlorite-epidote altered gabbro-diorite were sampled however, because these blocks were not in place, there is no evidence that they were derived from Bonnet Plume River Intrusions and not from some other mafic intrusive suite in the area, such as the Bear River dykes (Schwab et al., 2004).

Jazz

This location is near the Jazz Mineral occurrence, in the Wernecke inlier at location 4 in Fig. 23within the Fairchild Lake Group. Clasts that had been mapped as Bonnet Plume River Intrusions on mineral exploration maps, upon closer inspection were found to be intensely altered chlorite and muscovite-phyric siltstones. Two samples were taken for geochemical analysis however; the breccia zone was not investigated extensively.

Olympic

This location is near the Olympic Mineral occurrence, in the Wernecke inlier at location 5 in Fig. 23within the Gillespie Lake Group. The breccia zone is dominated by clasts of the surrounding GLG. Bonnet Plume River Intrusion clasts make up a small minority of clasts. They are predominantly one to ten metres in scale. In addition to the altered gabbro-diorites, which are typical of the Bonnet Plume River Intrusions, clasts that resemble medium-grained anorthosites are present. Petrographic and microprobe inspection has revealed these to be albitites and therefore likely metasomatites.

Anoki

This location is near the Anoki Mineral occurrence, in the Wernecke inlier at location 6 in Fig. 23 predominantly within the Fairchild Lake Group but in fault contact with the Quartet and Gillespie Lake Groups. A sample of medium to coarse-grained diorite with clots of potassic alteration was taken at this location however, due to time constraints no further investigation was undertaken.

Otis

This location is near the Otis Mineral occurrence, in the Wernecke inlier at location 7 in Fig. 23 within the Quartet Group. A sample of fine-grained green rock with clots of potassic alteration and quartz veins was taken at this location however, due to time constraints no further investigation was undertaken.

Quartet

This location is near the Quartet Mineral occurrence, in the Wernecke inlier at location 8 in Fig. 23 within the Fairchild Lake Group. A sample of medium to coarse-grained diorite with pervasive potassic alteration was taken at this location however, due to time constraints no further investigation was undertaken.

Sihota

This location is near the Sihota Mineral occurrence, in the Royal Creek inlier at location 9 in Fig. 23 within the Quartet Group. A sample of medium to coarse-grained diorite with intense pervasive potassic alteration was taken at this location however, due to time constraints no further investigation was undertaken.

Lala

This location is near the Lala Mineral occurrence, in the Coal Creek inlier at location 10 in Fig. 23 within the Quartet and Gillespie Lake Groups. Despite the distance between this location and those in the Wernecke inlier, the field relations are identical. Megaclasts of Bonnet Plume River Intrusions and Wernecke Supergroup are surrounded by smaller clasts and a hydrothermally precipitated hematite, carbonate, and chlorite. The igneous clasts within the hematitic breccia occurrences are fine to medium-grained diorites, indistinguishable from the

Bonnet Plume River Intrusions. All igneous clasts have been pervasively chlorite altered with veins of epidote and alkali feldspar. At Lala, a knob of exposed bedrock including a Bonnet Plume River Intrusion megaclast was mapped in detail.

Oz

This location is near the Wernecke breccia near the Oz Mineral occurrence, in the Coal Creek inlier at 564906E location 11 in Fig. 23 within the Gillespie Lake Group. No Bonnet Plume River Intrusions were found at this location. Clasts comprise predominantly bedded siltstone, sometimes metasomatized with pervasive chlorite alteration and large chlorite porphyroblasts.

Wizard/Id

This location is near the Wizard mineral occurrence, located in the Coal Creek inlier at location 12 in Fig. 23 within the Quartet and Gillespie Lake Groups. One to ten metre scale clasts of Bonnet Plume River Intrusion are common on the exposed mountainside. These Bonnet Plume River Intrusions are predominantly fine to medium-grained potassically altered chlorite-rich diorite.

Nor

The Nor mineral occurrence is located in the Nor inlier at location 13 in Fig. 23 within the Fairchild Lake Group. Field relations were not discernable in detail because nearly the entire area is under cover. Igneous megaclasts seem to be less prevalent here than in other breccia locations; however, 1-10cm igneous clasts are common in drill core. Some igneous clasts are pervasively chlorite-biotite altered while others are potassically altered.

Yukon Olympic

This location is near the Yukon Olympic MINFILE occurrence, located in the Blackstone River inlier at location 14 in Fig. 23 within the Quartet Group. Within the hematitic breccia bodies exposed, megaclasts of fine-grained amygdaloidal basalt are common. Unlike the volcanic megaclast at Slab, these are more likely submarine basalt, not subaerial pahoehoe basalt. In addition to basaltic clasts, there are also megaclasts of medium-grained diorite. The diorite megaclasts are pervasively chlorite altered and host veins of epidote and alkali feldspar.

Table 2: Sample locations and descriptions

Year	Camp Name	Sample Number	NTS Sheet	Easting	Northing	Sample Type	Rock Description	Field Relations
2009	Pika	ABN 09 01-01-01a	106C/14	537069	7190797	Hand	Wbx with clast of gabbro (?) included	Talus
2009	Pika	ABN 09 02-01-01a	106C/14	573603	7191458	Hand	Brown Metasediment	In contact with WBX
2009	Pika	ABN 09 03-01-01a	106C/14	537295	7190837	Hand	Coarse grained gabbro-diorite w/ earth hematite, chl/ep altered	Wbx clast
2009	Pika	ABN 09 03-01-01c	106C/14	537295	7190837	Geochron		
2009	Pika	ABN 09 03-02-01a	106C/14	573190	7190760	Hand	Coarse BPRI, little alteration, minor calcite veins and wkly disseminated pyrite	Wbx clast
2009	Pika	ABN 09 03-02-01b	106C/14	573190	7190760	Chemistry		
2009	Pika	ABN 09 03-02-01c	106C/14	573190	7190760	Geochron		
2009	Pika	ABN 09 03-03-01a	106C/14	573145	7190645	Hand	Brown Metasediment	Wbx clast
2009	Pika	ABN 09 03-06-01a	106C/14	573161	7190695	Hand	sedimentary clast in wbx	Wbx clast
2009	Pika	ABN 09 03-06-01c	106C/14	573161	7190695	Geochron		
2009	Pika	ABN 09 03-10--1a	106C/14	573245	7190805	Hand	Medium grained diorite with disseminated earthy and specular hematite, magnetite, and malachite. Epidote and chlorite common.	Wbx clast
2009	Pika	ABN 09 03-10--1b	106C/14	573245	7190805	Chemistry		
2009	Pika	ABN 09 04-08-01a	106C/14	573561	7191417	Hand	Specularite/quartz/carbonate vein	Float
2009	Pika	ABN 09 04-10-01a	106C/14	573530	7191305	Hand	BPRI clast cut by small qtz-kfeld veins, calcite veins, relatively unaltered	Wbx clast
2009	Pika	ABN 09 04-10-01b	106C/14	573530	7191305	Chemistry		
2009	Pika	ABN 09 04-11-01a	106C/14	573530	7191305	Hand	BPRI/WBX contact, taken to thin section	BPRI/WBX contact

2009	Bel	ABN 09 05-08-01a	106C/14	571650	7199289	Hand	highly altered BPRI, strong specularite, epidote alteration, plag altered to K-feld	Isolated outcrop
2009	Bel	ABN 09 05-08-01b	106C/14	571650	7199289	Chemistry		
2009	Bel	ABN 09 05-10-01a	106C/14	571746	7199304	Hand	Indurated fine grained white quartzite	Clast in wbx
2009	Bel	ABN 09 05-10-01c	106C/14	571746	7199304	Geochron		
2009	Bel	ABN 09 06-08-01a	106C/14	571417	7199231	Hand	BPRI with mod. Chl alt., patchy ep. Alt, qtz carb veinlets	Wbx clast
2009	Bel	ABN 09 06-08-01b	106C/14	571417	7199231	Chemistry		
2009	Bel	ABN 09 07-03-01a	106C/14	572150	7199800	Hand	Chlorite breccia	BPRI margin in WBX
2009	Bel	ABN 09 07-03-01b	106C/14	572150	7199800	Chemistry		
2009	Bel	ABN 09 07-04-01a	106C/14	572222	7199751	Hand	Coarse BPRI, veins and vugs of bladed specularite, mod. Chl. Alt., qtz-carb veinlets	Wbx clast
2009	Bel	ABN 09 07-04-01b	106C/14	572222	7199751	Chemistry		
2009	Bel	ABN 09 07-04-01c	106C/14	572222	7199751	Geochron		
2009	Dolores	ABN 09 08-01-01a	106C/13	570515	7198030	Hand	Coarse BPRI	Stream float
2009	Dolores	ABN 09 08-01-01b	106C/13	570515	7198030	Chemistry		
2009	Dolores	ABN 09 09-02-01a	106C/13	570340	7197710	Hand	Coarse BPRI	Talus
2009	Dolores	ABN 09 09-02-01b	106C/13	570340	7197710	Chemistry		
2009	Dolores	ABN 09 09-02-01c	106C/13	570340	7197710	Geochron		
2009	Jazz	ABN 09 10-01-01a	106D/09	541053	7170608	Hand	Strongly metasomatized green siltstone with muscovite metasomoblasts	In contact with WBX
2009	Jazz	ABN 09 10-01-01b	106D/09	541053	7170608	Chemistry		
2009	Olympic	ABN 09 11-01-01a	106C/13	554824	7195328	Hand	BPRI with abundant specularite, and Potassic alteration	Wbx clast
2009	Olympic	ABN 09 11-01-01b	106C/13	554824	7195328	Chemistry		
2009	Olympic	ABN 09 11-02-01a	106C/13	554300	7194750	Hand	Microanorthosite, relatively unaltered	Wbx clast
2009	Olympic	ABN 09 11-02-01b	106C/13	554300	7194750	Chemistry		
2009	Olympic	ABN 09 11-02-01c	106C/13	554300	7194750	Geochron		

2009	Olympic	ABN 09 11-02-02a	106C/13	554300	7194750	Hand	Microanorthosite, Potassically altered	Wbx clast
2009	Olympic	ABN 09 11-03-01a	106C/13	554713	7194570	Hand	medium grained diorite, mapped as Bear River Dyke	Cutting Gillespie Lake Group
2009	Olympic	ABN 09 11-03-01b	106C/13	554713	7194570	Chemistry		
2009	Olympic	ABN 09 11-03-01c	106C/13	554713	7194570	Geochron		
2009	Anoki	ABN 09 12-01-01a	106C/14	582111	7207538	Hand	Coarse Diorite, clots of K-alteration	Wbx clast
2009	Anoki	ABN 09 12-01-01b	106C/14	582111	7207538	Chemistry		
2009	Anoki	ABN 09 12-01-01c	106C/14	582111	7207538	Geochron		
2009	Otis	ABN 09 12-02-01a	106E/01	529010	7213378	Hand	Taken in case it is BPRI, but more likely to be a metamorphosed siltstone	Wbx clast
2009	Otis	ABN 09 12-02-01b	106E/01	529010	7213378	Chemistry		
2009	Otis	ABN 09 12-02-01c	106E/01	529010	7213378	Geochron		
2009	Quartet	ABN 09 12-03-01a	106E/01	528760	7220320	Hand	BPRI (?) large K-spar grains, scattered hbl/pyx, looks igneous	Wbx clast
2009	Quartet	ABN 09 12-03-01b	106E/01	528760	7220320	Chemistry		
2009	Quartet	ABN 09 12-03-01c	106E/01	528760	7220320	Geochron		
2009	Quartet	ABN 09 12-03-02a	106E/01	528750	7220451	Hand	Medium grained diorite, relatively unaltered	Talus
2009	Quartet	ABN 09 12-03-02b	106E/01	528750	7220451	Chemistry		
2009	Quartet	ABN 09 12-03-02c	106E/01	528750	7220451	Geochron		
2009	Sihota	ABN 09 12-04-01a	106D/14	479133	7188642	Hand	Coarse Diorite, heavily K-altered	Wbx clast
2009	Sihota	ABN 09 12-04-01b	106D/14	479133	7188642	Chemistry		

2009	Sihota	ABN 09 12-04-01c	106D/14	479133	7188642	Geochron		
2009	Lala	ABN 09 14-01-01a	116B/14	585984	7197940	Hand	Wbx, pebble to boulder sized clasts, silica rich matrix with0.8mm biotite books	Breccia outcrop
2009	Lala	ABN 09 14-02-01a	116B/14	585997	7198006	Hand	Medium grained (1-3mm grains) diorite with minor qtz-carb veins and pyrite	Wbx clast
2009	Lala	ABN 09 14-02-01b	116B/14	585997	7198006	Chemistry		
2009	Lala	ABN 09 14-02-01c	116B/14	585997	7198006	Geochron		
2009	Lala	ABN 09 15-04-01a	116B/14	586220	7197442	Hand	Chloritic Breccia	Breccia outcrop
2009	Lala	ABN 09 15-04-02a	116B/14	586220	7197442	Hand	Diorite from within 15cm of the Chlorite Breccia/Diorite Contact	Wbx clast
2009	Lala	ABN 09 15-05-01a	116B/14	586157	7197759	Hand	Coarse Grained Potassically altered Diorite	Wbx clast
2009	Lala	ABN 09 15-05-01b	116B/14	586157	7197759	Chemistry		
2009	Lala	ABN 09 15-05-01c	116B/14	586157	7197759	Geochron		
2009	Lala	ABN 09 15-05-02a	116B/14	586157	7197759	Hand	Coarse Grained Diorite, relatively unaltered	Wbx clast
2009	Lala	ABN 09 15-05-02b	116B/14	586157	7197759	Geochron		
2009	Oz	ABN 09 16-06-01a	116B/12	564906	7175030	Hand	Crystalline grit (?) with clasts of material that looks igneous within a chlorite breccia	Talus
2009	Oz	ABN 09 16-06-01c	116B/12	564906	7175030	Geochron		

2009	Wizard	ABN 09 17-01-01a	116B/13	556150	7189003	Hand	Medium grained diorite, moderate-strong K-alteration, fracture surfaces coated in specularite, no epidote alteration.	Clast in wbx, cut by brown recessive weathering qtz-carb vein
2009	Wizard	ABN 09 17-01-01b	116B/13	556150	7189003	Chemistry		
2009	Wizard	ABN 09 17-01-01c	116B/13	556150	7189003	Geochron		
2009	Wizard	ABN 09 17-02-01a	116B/13	555155	7189101	Hand	Medium grained diorite, moderate K-alteration, specularite veins	Wbx clast
2009	Wizard	ABN 09 17-02-01b	116B/13	555155	7189101	Chemistry		
2009	Wizard	ABN 09 17-02-01c	116B/13	555155	7189101	Geochron		
2009	Wizard	ABN 09 17-02-02a	116B/13	555155	7189101	Hand	Wernecke breccia with clasts of Medium grained diorite	Breccia outcrop
2009	Wizard	ABN 09 18 (17.5)-01-01a	116B/13	557916	7189631	Hand	Med. Grained diorite, green fresh, brown weathering, well fractured, specularite wkly diss. Throughout and in small veins, wk. Pinkification	Wbx clast
2009	Wizard	ABN 09 18 (17.5)-01-01b	116B/13	557916	7189631	Chemistry		
2009	Wizard	ABN 09 18 (17.5)-01-01c	116B/13	557916	7189631	Geochron		

2009	Wizard	ABN 09 18 (17.5)-02-01a	116B/13	558164	7189829	Hand	fine grained diorite, wk-mod k-alteration, carbonate veins throughout	Wbx clast
2009	Wizard	ABN 09 18 (17.5)-02-01b	116B/13	558164	7189829	Chemistry		
2009	Nor	ABN 09 18-01-01a	106L/06	483041	7349004	Hand	Breccia with specularite/minor chlorite matrix with an unidentified green mineral	Breccia outcrop
2009	Nor	ABN 09 18-02-01a	106L/06	483061	7348984	Hand	Matrix dominated grey breccia	Talus
2009	Nor	ABN 09 18-02-01b	106L/06	483061	7348984	Chemistry		
2009	Nor	ABN 09 18-02-01c	106L/06	483061	7348984	Geochron		
2009	Nor	ABN 09 18-03-01a	106L/06	483450	7348550	Hand	dark green, fine grained mafic rock with v. Strong K-alteration (hence "syenite")	local blocks, most likely a clast in WBX
2009	Nor	ABN 09 18-03-01b	106L/06	483450	7348550	Chemistry		
2009	Nor	ABN 09 18-03-01c	106L/06	483450	7348550	Geochron		
2009	Yukon Olympic	ABN 09 19-01-01a	116G/01	635989	7217449	Hand	fine grained diorite, round qtz-carb filled ole, may be amygdules	Stream float
2009	Yukon Olympic	ABN 09 19-02-01a	116G/01	636153	7217391	Hand	fine grained diorite, possible amygdules and phenocrysts	In contact with WBX
2009	Yukon Olympic	ABN 09 19-02-02a	116G/01	636153	7217391	Hand	very fine grained rock, no round qtz-carb pockets, pervasive K-alteration, hematite throughout	In contact with WBX
2009	Yukon Olympic	ABN 09 19-02-02b	116G/01	636153	7217391	Chemistry		
2009	Yukon Olympic	ABN 09 19-02-03a	116G/01	636153	7217391	Hand	fine grained "amygdaloidal" diorite	In contact with WBX

2009	Yukon Olympic	ABN 09 19-03-01 a	116G/01	636123	7217420	Hand	possible hyaloclastite	Stream float
2009	Yukon Olympic	ABN 09 20-01-01a	116G/01	637532	7215683	Hand	fine grained green Diorite with phenocrysts of a black mineral	surrounded by breccia scree
2009	Yukon Olympic	ABN 09 20-01-01b	116G/01	637532	7215683	Chemistry		
2009	Yukon Olympic	ABN 09 20-02-01a	116G/01	636737	7216994	Hand	fine-medium grained diorite, blue-green weathering, green fresh with patches of moderate pinkification	Wbx clast
2009	Yukon Olympic	ABN 09 20-02-01b	116G/01	636737	7216994	Chemistry		
2009	Yukon Olympic	ABN 09 20-02-01c	116G/01	636737	7216994	Geochron		

Appendix B: Photomicrographs

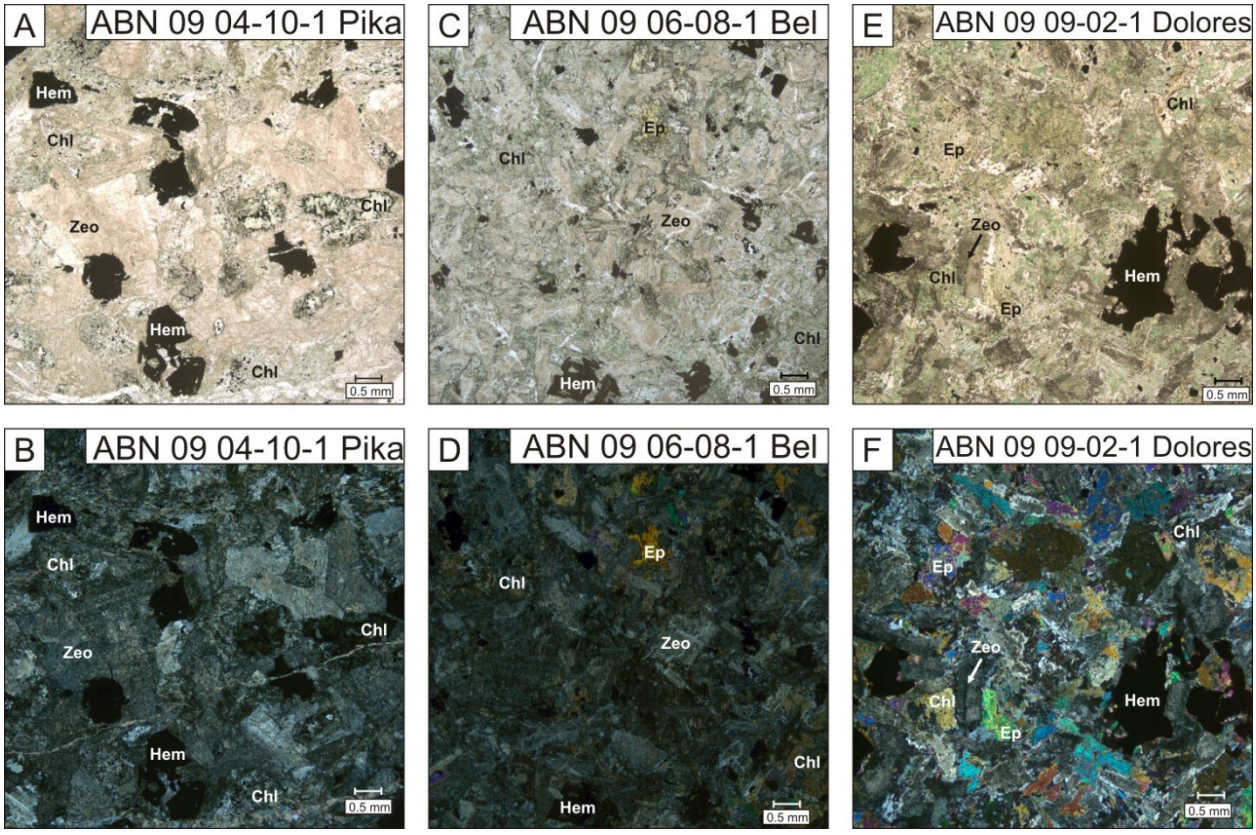

Fig. 25 Photomicrographs of Wernecke igneous clasts 1 of 4

A, B: ABN 09 04-10-1 in plane-polarized light and cross-polarized light respectively; identical fields of view. Zeolites (zeo) have partially pseudomorphed lath-shaped crystals, which may display a relict “twinning” indicating that the original mineral is likely plagioclase. Large composite hematite (hem) grains may display shapes that suggest that they have pseudomorphed ilmenite or magnetite. Chlorite (chl) mats are intergrown with smaller hematite grains. C, D: ABN 09 06-08-1 in plane-polarized light and cross-polarized light respectively; identical fields of view. Zeolites (zeo) have partially pseudomorphed lath-shaped crystals, which may display a relict “twinning” indicating that the original mineral is likely plagioclase. Large composite hematite (hem) grains may display shapes that suggest that they have pseudomorphed ilmenite or magnetite. Epidote (ep) metasomatic porphyroblasts are associated with chlorite mats, interstitial to hematite and zeolite grains. E, F: ABN 09 09-02-1 in plane-polarized light and cross-polarized light respectively; identical fields of view. Zeolites (zeo) have partially pseudomorphed lath-shaped crystals that may display a relict “twinning” indicating that the original mineral is likely plagioclase. Large composite hematite (hem) grains may display shapes that suggest that they have pseudomorphed ilmenite or magnetite. Chlorite (chl) mats are associated with epidote (ep) metasomatic porphyroblasts in the interstices between large hematite and zeolite grains.

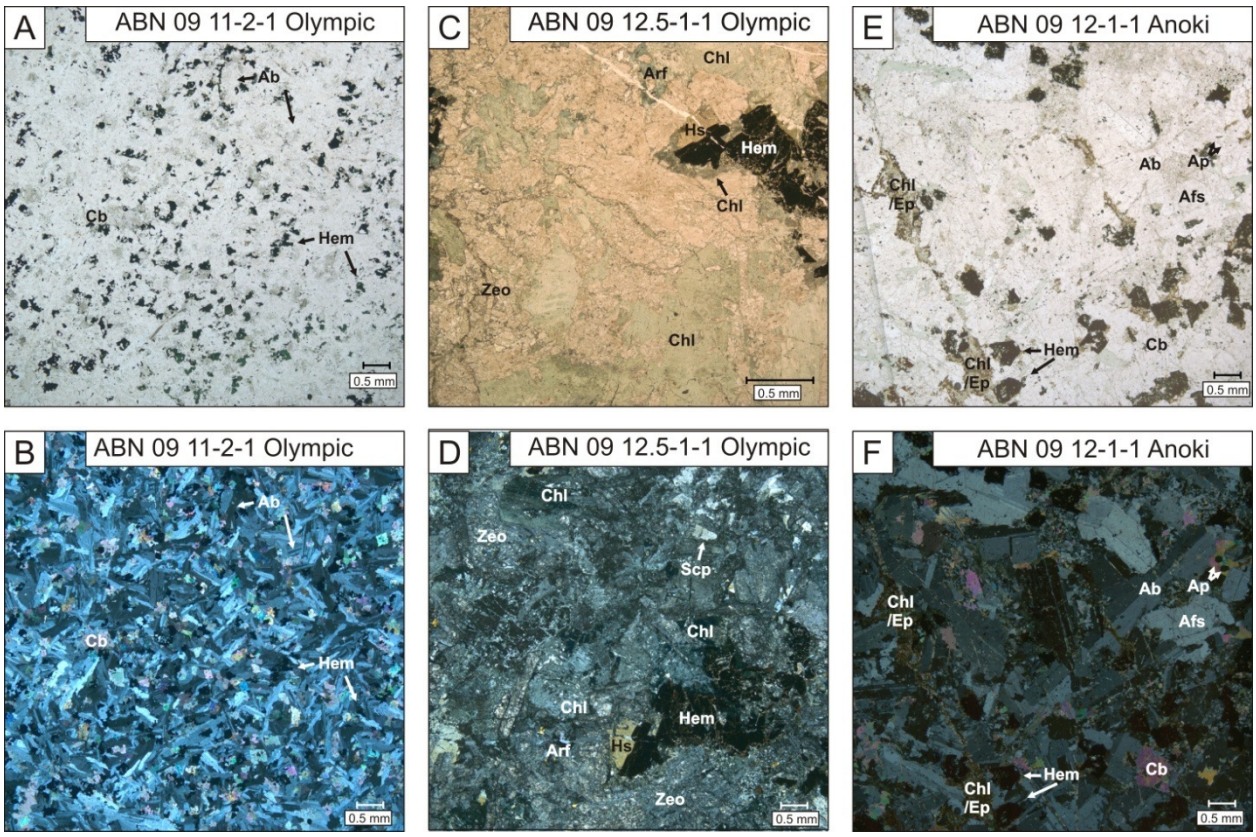

Fig. 26 Photomicrographs of Wernecke igneous clasts 2 of 4

A, B: ABN 09 11-2-1 in plane-polarized light and cross-polarized light respectively; identical fields of view. Plagioclase (ab) has a composition of an0, or end-member albite, determined by Michael-Lévy method (Michel-Lévy, 1894; Nesse, 2003). Hematite (hem) and carbonate (cb) grains are not interstitial to the albite and therefore are likely metasomatic porphyroblasts. C, D: ABN 09 12.5-1-1 in plane-polarized light and cross-polarized light respectively; fields of view are **not identical**. The amphiboles hastingsite (hst) and arfvedonite (arf), as determined by SEM, are visible as the olive green and navy blue minerals respectively. Chlorite (chl) is present both associated with (likely consuming) amphiboles and as isolated mats. Hematite (hem) is present as large glomeroporphyroblasts. E, F: ABN 09 12-1-1 in plane-polarized light and cross-polarized light respectively; identical fields of view. Large laths of albite (ab) (an0, determined by SEM) with ragged edged are present with minor alkali feldspar (afs). Euhedral crystals of hematite (hem) are present with associated chlorite (chl) overprinting the feldspars. Anhedral carbonate (cb) crystals are present overprinting the feldspars. Euhedral apatite (ap) metasomatic porphyroblasts are associated with carbonate.

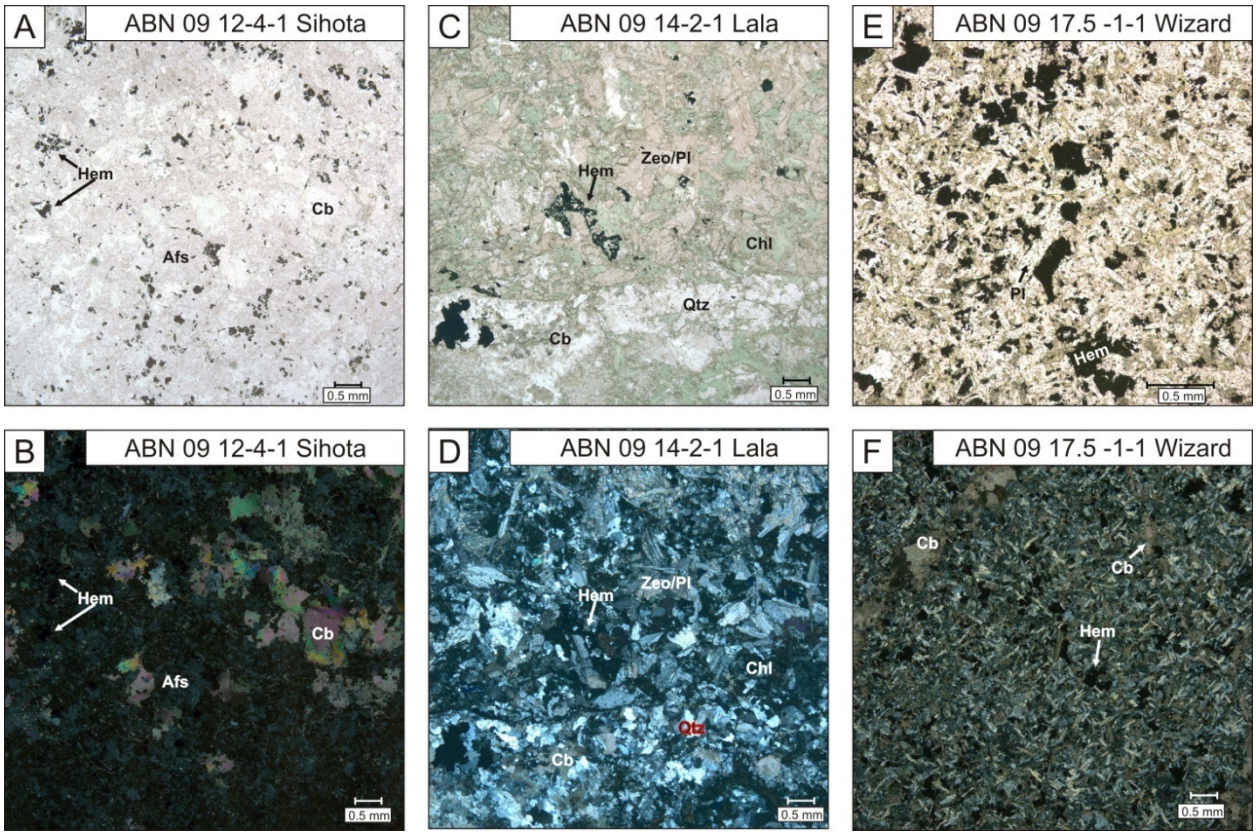

Fig. 27 Photomicrographs of Wernecke igneous clasts 3 of 4

A, B: ABN 09 12-4-1 in plane-polarized light and cross-polarized light respectively; identical fields of view. Anhedral, untwined, alkali feldspar (afs) is present as the dominant mineral. Hematite (hem) is present as disseminated crystals. Large carbonate (cb) metasomatic porphyroblasts overprint alkali feldspar. C, D: ABN 09 14-2-1 in plane-polarized light and cross-polarized light respectively; identical fields of view. A quartz (qtz)-carbonate (cb)-hematite (hem) vein cuts across the lower third of the slide. Zeolitic (zeo) plagioclase (pl) laths become less zeolitic with increasing proximity to the vein. Large chlorite mats are interstitial to the plagioclase/plagioclase pseudomorphs. Hematite is present as fine disseminated crystals and in one location mantling a plagioclase/zeolite lath. E, F: ABN 09 17.5-1-1 in plane-polarized light and cross-polarized light respectively; fields of view are **not identical**. Plagioclase (pl) is present as fine microlites. Chlorite (chl) is interstitial to the plagioclase microlites. Hematite (hem) crystals are disseminated throughout. A carbonate (cb) vein cuts across the upper left-hand corner. Carbonate is also present overprinting plagioclase and chlorite.

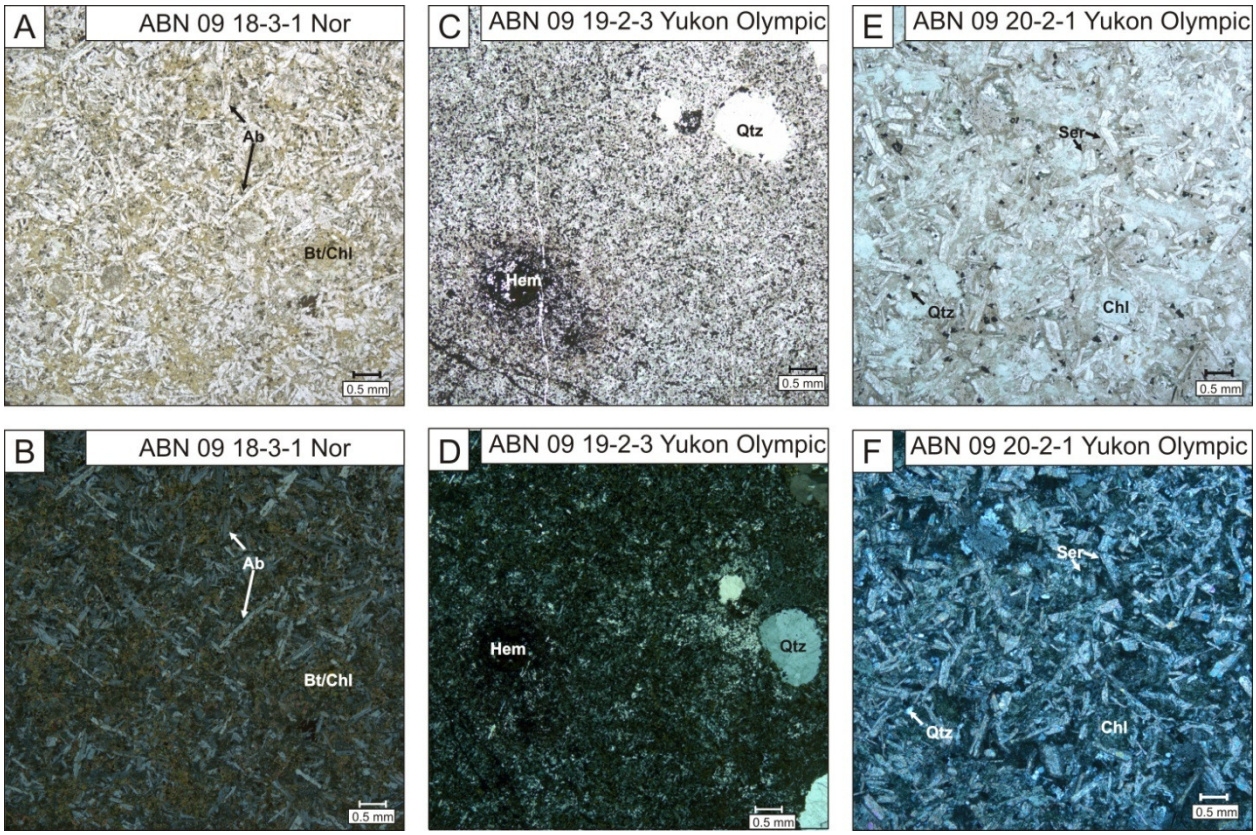

Fig. 28 Photomicrographs of Wernecke igneous clasts 4 of4

A, B: ABN 09 18-3-11 in plane-polarized light and cross-polarized light respectively; identical fields of view. Albite (an0, determined by SEM) crystals are elongate and have ragged edges. Biotite is present, associated with (likely consuming) chlorite. Hematite is finely disseminated throughout. C, D: ABN 09 19-02-03 in plane-polarized and cross-polarized light respectively, fields of view are **not identical**. Plagioclase is present as very fine microlites. Chlorite is present in mats throughout the groundmass. A small amount of alkali feldspar is present in the groundmass. Quartz is present in thin veins and amygdules. Hematite is ubiquitous in the groundmass and in some cases has a shape suggesting that it has pseudomorphed magnetite. E, F: ABN 09 20-2-1 in plane-polarized light and cross-polarized light, fields of view are identical. Sericite has partially pseudomorphed lath-shaped crystals, which may display a relict "twinning" indicating that the original mineral is likely plagioclase. Chlorite has grown in the interstices between the plagioclase laths suggesting that the chlorite may have pseudomorphed anhedral mafic crystals. Quartz is present in subhedral grains; it appears to be primary. Hematite and magnetite form overgrowths and are present with the chlorite in the interstices between the plagioclase laths.

Appendix C: Whole Rock Geochemistry

During the field season of 2009, forty-three samples were collected for whole rock geochemical analysis. These samples included Wernecke igneous clasts, Wernecke Breccia, metasediments from within the Wernecke Breccias, and one sample of a Bear River dyke.

C1: Sample processing method

Samples were field cleaned in order to remove large areas of weathered material, then crushed in a jaw crusher with steel plates to sub-1cm sized fragments. A portion of the crushed sample was picked to remove vein material and weathered material that was missed during field cleaning. The picked sample was then milled with a disk mill with ceramic rings, in order to minimize contamination. An approximately 50g fraction of this milled powder was sent to Activation Laboratories Ltd. in Ancaster, Ontario for analysis.

C2: Geochemical analysis

The samples were analyzed with research package 4E at Activation Laboratories Ltd of Ancaster, Ontario. Major elements were analyzed by fusion-inductively coupled plasma optical emission spectroscopy, while trace elements were analyzed by instrumental neutron activation analysis, total dissolution inductively coupled plasma optical emission spectroscopy, fusion inductively coupled plasma optical emission spectroscopy, and/or fusion inductively coupled plasma mass spectrometry.

Samples analyzed by fusion inductively coupled plasma optical emission spectroscopy were fused with a lithium metaborate/tetraborate mixture in a graphite crucible and dissolved in a 5% solution of nitric acid. This solution was analyzed with a combination simultaneous/sequential Thermo Jarrell-Ash Enviro II ICP.

Samples analyzed by instrumental neutron activation analysis were enclosed in a polyethylene vial and irradiated at a neutron flux of $7x10^{12}$ n $cm^{-1}s^{-1}$ along with flux wires and a reference material internal to Activation Laboratories Ltd. After a 7-day period allowing ^{24}Na to decay, the samples were counted on a high purity Ge detector with resolution of better than 1.7 KeV for the 1332 KeV Co-60 photopeak and compared with the reference material.

Total dissolution inductively coupled optical emission spectroscopy was performed by dissolving the sample in hydrofluoric acid, and a mixture of nitric acid and perchloric acid followed by heating to dryness and dissolution in hydrochloric acid. The sample was then analyzed using a Perkin Elmer Optima 3000 ICP.

Fusion inductively coupled plasma mass spectrometry was performed by fusing the sample with lithium metaborate/tetraborate. The sample was ten diluted and analyzed with a Perkin Elmer Sciex ELAN 6000, 6100 or 9000 ICP/MS.

Further details can be found at: (http://www.actlabs.com/page.aspx?page=518&app=226&cat1=549&tp=12&lk=no&menu=64), accessed Feb. 2nd 2011.

C3: Whole Rock Geochemical Data

Table 3: Whole rock geochemical data for the Bonnet Plume River Intrusions and Devil volcanics. FUS-ICP: fusion-inductively coupled plasma optical emission spectroscopy. INAA: instrumental neutron activation analysis. TD-ICP: total dissolution-inductively coupled plasma optical emission spectroscopy. FUS-MS: fusion inductively coupled plasma mass spectrometry.

Analyte Symbol	SiO2	Al2O3	Fe2O3	MnO	MgO	CaO	Na2O	K2O	TiO2	P2O5	LOI	Total
Unit Symbol	%	%	%	%	%	%	%	%	%	%	%	%
Analysis Method	FUS-ICP	FUS-ICP	FUS-ICP	FUS-ICP	FUS-ICP	FUS-ICP	FUS-ICP	FUS-ICP	FUS-ICP	FUS-ICP	FUS-ICP	FUS-ICP
ABN 09-03-02-01b	40.86	14.52	12.02	0.412	4.26	7.86	2.96	4.21	2.289	0.15	9.69	99.23
ABN 09-03-10-1b	41.63	15.26	18.37	0.206	4.46	2.98	1.93	5.72	2.868	0.08	6.08	99.58
ABN 09-04-10-01b	45.96	12.38	16.72	0.112	6.53	4.14	2.41	1.48	2.819	0.13	6.75	99.42
ABN 09-04-11-01b	43.66	15.01	13.93	0.211	8.51	2.9	0.03	3.82	1.834	0.12	9.97	99.99
ABN 09-05-08-01b	51.27	14.56	8.42	0.15	5.42	7.01	5.13	1.3	1.588	0.07	4.73	99.66
ABN 09-06-01-01b	48.88	15.28	11.45	0.145	8.1	6.36	3.25	1.71	1.053	0.08	4.04	100.3
ABN 09-06-08-01b	48.86	14.19	10.62	0.153	5.83	5.57	2.13	6.12	1.4	0.13	5.11	100.1
ABN 09-07-03-01b	53.66	12.7	10.44	0.124	2.83	5.81	3.11	4.94	0.529	0.2	6.13	100.5
ABN 09-07-04-01b	45.12	11.79	16.06	0.221	8.74	4.87	1.8	1.01	1.605	0.12	8.62	99.96
ABN 09-07-2-1b	51.95	14.66	8.53	0.15	5.47	7.08	5.2	1.32	1.591	0.07	4.74	100.8
ABN 09-08-01-01b	48.54	12.26	14.91	0.149	4.83	7.5	4.7	0.97	1.955	0.17	3.58	99.56
ABN 09-09-02-01b	48.29	13.64	14.25	0.217	5.86	9.27	3.39	0.58	1.726	0.17	2.83	100.2
ABN 09-10-01-01b	53.22	14.04	15.45	0.08	3.24	0.33	0.08	4.94	0.588	0.24	5.82	98.03
ABN 09-10-02-01b	51.6	17.52	12.17	0.05	2.93	0.73	0.07	6.62	0.753	0.19	6.3	98.93
ABN 09-11-01-01b	53.18	11.07	14.53	0.227	6.29	1.88	1.81	2.01	1.775	0.18	6.19	99.15
ABN 09-11-02-01b	47.5	13.44	10.88	0.342	2.63	5.84	7.62	0.11	2.068	0.41	8.54	99.38
ABN 09-11-03-01b	38.33	8.45	12.65	0.389	14.34	8.99	0.73	0.79	1.04	0.11	13.3	99.13
ABN 09-12-01-01b	50.98	12.37	8.01	0.139	3.19	8.44	5.39	0.14	2.81	0.39	8.66	100.5
ABN 09-12-02-01b	43.83	13.75	18.09	0.17	6.83	2.93	0.77	6.02	1.834	0.11	4.89	99.24
ABN 09-12-03-01b	52.28	14.76	10.12	0.082	1.39	4.98	1.15	7.85	0.652	0.2	5.98	99.45
ABN 09-12-03-02b	47.8	12.39	15.27	0.098	5.38	7.67	4.11	1.09	1.999	0.21	2.98	99.01
ABN 09-12-04-01b	48.79	12.22	12.32	0.19	6.91	3.46	0.1	4.96	1.613	0.17	8.3	99.02
ABN 09-12-7-1b	39.07	8.09	17.26	0.166	13.21	14.52	0.7	0.18	3.582	0.06		96.84
ABN 09-12.5-01-01b	49.76	14.41	12.19	0.385	5.93	8.41	2.38	1.67	0.771	0.06	2.75	98.71
ABN 09-13-2-1b	46.92	15.12	11.18	0.154	11.79	1.24	1.58	1.91	0.937	0.06	8.55	99.43
ABN 09-14-01-01b	65.46	8.22	3.62	0.125	3.55	4.64	1.75	3.49	0.305	0.11	8.24	99.52
ABN 09-14-02-01b	44.77	15.52	11.71	0.175	6.62	3.29	1.65	3.07	1.601	0.13	9.97	98.5
ABN 09-15-04-02a	49.23	12.85	12.39	0.243	6.61	3.1	3.64	0.71	2.099	0.19	8.06	99.11
ABN 09-15-05-01b	63.61	12.32	6.8	0.134	3.13	1.93	4	1.63	0.749	0.16	4.72	99.18
ABN 09-15-05-02b	47.44	12.1	15.24	0.211	7.43	3.66	1.65	0.92	1.58	0.32	8.74	99.29
ABN 09-16-5-1b	56.96	14.84	8.22	0.148	3.49	0.28	0.29	9.17	1.809	0.21	3.67	99.08
ABN 09-17-01-01b	57.51	14.64	8.13	0.148	3.54	0.26	0.19	9.25	1.77	0.19		95.64
ABN 09-17-02-01b	40.1	14.52	14.31	0.24	10	3.04	0.1	5.56	1.659	0.15	10.05	99.73
ABN 09-18(17.5)-02-01b	44.24	13.03	16.21	0.134	4.89	4.62	4.61	0.91	1.574	0.13	9.33	99.68
ABN 09-18-02-01b	56.1	13.44	5.65	0.075	0.16	9.1	7.72	0.14	0.536	0.17	7.62	100.7
ABN 09-18-03-01b	49.33	13.99	7.27	0.113	6.99	7.35	5.48	1.72	1.346	0.1	7.01	100.7
ABN 09-19-02-02b	48.12	12.23	17.16	0.142	10.8	0.28	0.04	1.96	1.896	0.18	7.29	100.1
ABN 09-19-02-03b	43.21	12.4	25.76	0.118	5.5	0.26	0.1	6.33	1.85	0.19	3.58	99.3
ABN 09-19-6-1b	64.18	12.76	6.65	0.134	3.18	1.97	4.2	1.71	0.782	0.17	4.71	100.5
ABN 09-20-01-01b	47.37	14.76	11.22	0.155	11.96	1.26	1.55	1.93	0.892	0.07	8.45	99.61
ABN 09-20-02-01b	55.63	15	8.39	0.119	9.08	0.17	0.57	3.76	0.613	0.09	6.27	99.69
ABN 09-21-1-1b	52.56	13.89	15.93	0.08	3.22	0.34	0.08	5.09	0.593	0.26	5.51	97.55
ABN 09-21-2-1b	60.22	11.95	6.12	0.311	2.58	8.04	4.2	4.63	0.137	0.45		98.64
DT 07-10-1-1b	49.33	11.75	10.79	0.444	4.49	7	5.31	0.44	0.373	0.15	10.18	100.2
DT 07-8-2-1b	47.72	9.49	6.58	0.724	5.78	9.02	0.7	5.34	0.431	0.15	14.01	99.93
DT 07-8-3-1b	44.78	15.01	7.6	0.403	5.55	6.23	0.16	9.12	0.586	0.19	9.98	99.61
DT 07-8-4-1b	56.65	12.99	10.04	0.372	2.03	3.42	6.41	0.55	0.52	0.18	5.4	98.56
DT 07-8-4-2b	65.06	19.36	1.81	0.063	0.85	0.85	5.85	3.23	0.677	0.12	2.3	100.2
DT 07-8-4-3b	44.92	13.92	13.25	0.356	9.57	7.41	2.21	1.86	0.997	0.08		94.58
DT 07-9-1-1b	42.83	9.37	6.51	0.9	7.8	10.83	0.18	4.38	0.382	0.13	16.35	99.67
DT 07-9-2-1b	46.94	14.36	8.89	0.22	4.33	7.72	2.21	6.87	1.122	0.11	7.29	100.1

Table 3 continued

Analyte Symbol	Au	Ag	As	Ba	Be	Bi	Br	Cd	Co	Cr	Cs	Cu
Unit Symbol	ppb	ppm	ppm	ppm	ppm	ppm	ppm	ppm	ppm	ppm	ppm	ppm
Analysis Method	INAA	MULT INAA / TD-ICP	INAA	FUS-ICP	FUS-ICP	FUS-MS	INAA	TD-ICP	INAA	INAA	FUS-MS	TD-ICP
ABN 09-03-02-01b	< 1	< 0.5	< 1	827	< 1	< 0.1	< 0.5	< 0.5	45.1	< 0.5	0.3	20
ABN 09-03-10-1b	< 1	< 0.5	3	342	< 1	0.1	< 0.5	0.7	33.2	< 0.5	0.5	119
ABN 09-04-10-01b	< 1	< 0.5	3	574	< 1	0.1	< 0.5	0.6	40.9	< 0.5	1.2	10
ABN 09-04-11-01b	< 1	< 0.5	3	350	2	< 0.1	< 0.5	0.5	70.7	44.7	2.6	8
ABN 09-05-08-01b	< 1	< 0.5	5	140	< 1	0.2	< 0.5	< 0.5	43.2	168	0.2	4
ABN 09-06-01-01b	< 1	< 0.5	5	306	< 1	0.2	3.2	< 0.5	54.5	227	1.3	30
ABN 09-06-08-01b	< 1	< 0.5	< 1	857	< 1	0.2	< 0.5	< 0.5	39.1	73	0.8	5
ABN 09-07-03-01b	< 1	< 0.5	10	856	< 1	0.1	< 0.5	0.5	18.6	57	0.8	8
ABN 09-07-04-01b	< 1	< 0.5	5	208	< 1	0.5	< 0.5	0.8	49.1	35.9	1	3
ABN 09-07-2-1b	< 1	< 0.5	6	142	< 1	0.2	< 0.5	< 0.5	39.7	170	0.2	4
ABN 09-08-01-01b	< 1	< 0.5	9	145	< 1	0.2	< 0.5	0.6	53.3	21.4	0.4	11
ABN 09-09-02-01b	5	< 0.5	6	98	< 1	0.5	< 0.5	0.7	54.3	55.7	0.1	82
ABN 09-10-01-01b	87	7.3	36	813	2	1.9	< 0.5	0.8	57.3	140	1.6	> 10000
ABN 09-10-02-01b	< 1	< 0.5	62	596	3	1.7	< 0.5	0.9	82.2	90.9	7.7	3
ABN 09-11-01-01b	< 1	< 0.5	22	353	< 1	< 0.1	< 0.5	0.6	34	44.5	1.3	145
ABN 09-11-02-01b	< 1	< 0.5	16	23	< 1	0.1	3.4	0.6	38.7	< 0.5	< 0.1	16
ABN 09-11-03-01b	< 1	< 0.5	5	114	< 1	< 0.1	< 0.5	0.9	69.1	1490	2.8	42
ABN 09-12-01-01b	< 1	< 0.5	9	30	< 1	0.2	< 0.5	< 0.5	23.7	< 0.5	0.2	19
ABN 09-12-02-01b	< 1	< 0.5	5	1747	< 1	0.2	< 0.5	0.9	60.8	81.3	1.9	75
ABN 09-12-03-01b	7	< 0.5	12	642	4	0.5	< 0.5	0.5	9.2	117	2.1	22
ABN 09-12-03-02b	< 1	< 0.5	8	139	< 1	< 0.1	< 0.5	0.7	40.4	54.5	< 0.1	143
ABN 09-12-04-01b	7	< 0.5	6	233	< 1	2.1	4.7	0.6	30.9	86.8	2	3
ABN 09-12-7-1b	16	< 0.5	< 1	49	< 1	0.1	7.4	0.8	89.5	491	0.5	102
ABN 09-12.5-01-01b	< 1	< 0.5	5	521	< 1	0.3	< 0.5	0.6	37.8	38.3	0.7	106
ABN 09-13-2-1b	< 1	< 0.5	< 1	1159	< 1	< 0.1	2.1	0.6	38	308	2.6	9
ABN 09-14-01-01b	< 1	< 0.5	2	275	< 1	< 0.1	1.9	< 0.5	4.6	35.6	0.9	1
ABN 09-14-02-01b	< 1	< 0.5	< 1	275	< 1	0.2	22.1	0.6	58.8	200	1.3	223
ABN 09-15-04-02a	< 1	< 0.5	5	420	< 1	0.2	3	< 0.5	44.2	23.2	0.4	3
ABN 09-15-05-01b	< 1	< 0.5	< 1	956	< 1	0.3	< 0.5	< 0.5	27.5	42.2	2.1	5
ABN 09-15-05-02b	< 1	< 0.5	3	282	< 1	0.2	< 0.5	0.8	50.3	164	1.2	103
ABN 09-16-5-1b	< 1	< 0.5	< 1	3116	< 1	0.4	19.3	0.6	52	93.2	1.2	129
ABN 09-17-01-01b	< 1	< 0.5	3	3159	< 1	0.4	< 0.5	< 0.5	43.4	64.2	1	128
ABN 09-17-02-01b	< 1	< 0.5	2	1127	< 1	0.8	3.2	0.7	57.7	138	0.5	11
ABN 09-18(17.5)-02-01b	< 1	< 0.5	6	136	< 1	0.1	2.3	0.7	43.3	40.1	1.5	1
ABN 09-18-02-01b	3	< 0.5	2	33	1	< 0.1	< 0.5	< 0.5	2	56.3	< 0.1	< 1
ABN 09-18-03-01b	15	< 0.5	3	98	< 1	0.1	< 0.5	< 0.5	79.3	120	6.1	< 1
ABN 09-19-02-02b	< 1	< 0.5	8	178	1	0.4	< 0.5	1.1	60.7	48.1	1.2	2
ABN 09-19-02-03b	< 1	0.5	6	1654	< 1	0.3	3	1.4	61.1	49.2	< 0.1	43
ABN 09-19-6-1b	4	< 0.5	5	996	1	0.3	3.5	0.7	24.5	44.5	2.1	5
ABN 09-20-01-01b	< 1	< 0.5	2	1150	< 1	< 0.1	< 0.5	0.5	36.1	327	2.7	10
ABN 09-20-02-01b	< 1	< 0.5	5	319	1	0.2	< 0.5	0.5	44	398	1.1	9
ABN 09-21-1-1b	13	6.9	45	804	2	2.1	4.5	0.6	58	82.7	1.6	> 10000
ABN 09-21-2-1b	< 1	< 0.5	28	454	25	0.2	< 0.5	0.7	17.2	37.6	2.9	3
DT 07-10-1-1b	< 1	< 0.5	3	253	1	0.3	1.7	< 0.5	9.1	41.8	0.3	< 1
DT 07-8-2-1b	2	< 0.5	2	1458	< 1	0.8	3.8	< 0.5	11.4	54.5	1	< 1
DT 07-8-3-1b	< 1	< 0.5	2	352	2	2.6	4.5	< 0.5	15.5	75.8	2	< 1
DT 07-8-4-1b	< 1	< 0.5	5	6206	1	2.5	3.6	0.6	5.1	72	0.5	< 1
DT 07-8-4-2b	< 1	< 0.5	12	774	3	1.8	14.9	< 0.5	17.6	172	3	< 1
DT 07-8-4-3b	< 1	< 0.5	11	615	< 1	0.5	5.4	1.1	85.1	295	0.4	30
DT 07-9-1-1b	5	< 0.5	3	791	< 1	0.4	3	< 0.5	20.1	37.2	1.4	3
DT 07-9-2-1b	< 1	< 0.5	5	958	< 1	0.9	2.1	0.8	74.6	153	0.9	596

Table 3 continued

Analyte Symbol	Ga	Ge	Hf	Hg	In	Ir	Mo	Nb	Ni	Pb	Rb	S	Sb
Unit Symbol	ppm	ppm	ppm	ppm	ppm	ppb	ppm	ppm	ppm	ppm	ppm	%	ppm
Analysis Method	FUS-MS	FUS-MS	FUS-MS	INAA	FUS-MS	INAA	FUS-MS	FUS-MS	TD-ICP	TD-ICP	FUS-MS	TD-ICP	INAA
ABN 09-03-02-01b	20	0.9	3	< 1	< 0.1	< 1	< 2	8.9	35	< 5	61	0.07	1.2
ABN 09-03-10-1b	19	1.4	1.9	< 1	< 0.1	< 1	< 2	4.5	53	5	96	0.023	2.7
ABN 09-04-10-01b	20	1.8	2.9	< 1	< 0.1	< 1	< 2	7.1	38	< 5	35	0.005	1.8
ABN 09-04-11-01b	24	2.9	2.8	< 1	< 0.1	< 1	< 2	7.7	96	< 5	129	0.159	4.1
ABN 09-05-08-01b	16	2.1	2.7	< 1	< 0.1	< 1	< 2	8.2	59	< 5	14	0.002	2.6
ABN 09-06-01-01b	16	1.4	1.6	< 1	< 0.1	< 1	< 2	3.7	106	< 5	85	0.017	1.3
ABN 09-06-08-01b	16	1.4	2.4	< 1	< 0.1	< 1	< 2	7.2	91	< 5	93	0.008	1.4
ABN 09-07-03-01b	18	1.6	3.7	< 1	< 0.1	< 1	< 2	11.3	44	< 5	75	0.002	0.7
ABN 09-07-04-01b	19	2	2.8	< 1	< 0.1	< 1	< 2	7.8	150	< 5	20	0.004	2.7
ABN 09-07-2-1b	16	2	2.6	< 1	< 0.1	< 1	< 2	7.2	56	< 5	13	0.001	2.2
ABN 09-08-01-01b	19	1.8	3.6	< 1	< 0.1	< 1	< 2	9.6	34	< 5	8	0.16	1.1
ABN 09-09-02-01b	19	1.8	3.1	< 1	< 0.1	< 1	< 2	9	62	7	8	0.162	1.7
ABN 09-10-01-01b	18	2.3	3.6	< 1	0.1	34	13	15.5	110	< 5	148	1.91	2.7
ABN 09-10-02-01b	30	2.8	3.6	< 1	< 0.1	< 1	< 2	9.1	314	< 5	327	1.34	5.7
ABN 09-11-01-01b	25	4.6	3.6	< 1	< 0.1	< 1	< 2	11.5	51	< 5	28	0.115	6.6
ABN 09-11-02-01b	15	0.7	6.5	< 1	< 0.1	< 1	< 2	25	11	< 5	< 1	0.22	5
ABN 09-11-03-01b	14	1.7	2.1	< 1	< 0.1	< 1	< 2	4.3	707	< 5	18	0.09	2.1
ABN 09-12-01-01b	22	1.4	7.8	< 1	< 0.1	< 1	3	21.5	34	6	< 1	0.002	2.1
ABN 09-12-02-01b	20	1.9	2.6	< 1	< 0.1	< 1	< 2	5.1	69	< 5	236	0.003	1
ABN 09-12-03-01b	15	1.6	3.1	< 1	< 0.1	< 1	< 2	12.7	30	< 5	177	0.007	1.2
ABN 09-12-03-02b	21	2.1	3.8	< 1	< 0.1	< 1	< 2	11.7	48	< 5	28	0.005	0.8
ABN 09-12-04-01b	24	2.6	3.2	< 1	< 0.1	< 1	3	11.1	98	< 5	104	0.002	0.6
ABN 09-12-7-1b	18	1.6	3.5	< 1	< 0.1	< 1	< 2	18.2	168	< 5	< 1	0.054	< 0.1
ABN 09-12.5-01-01b	17	1.7	1.5	< 1	< 0.1	< 1	< 2	2	58	< 5	61	0.004	4.4
ABN 09-13-2-1b	13	2.1	1.1	< 1	< 0.1	< 1	< 2	1.6	80	< 5	32	0.009	1.2
ABN 09-14-01-01b	5	1.2	3.5	< 1	< 0.1	< 1	< 2	6.1	7	< 5	61	< 0.001	0.5
ABN 09-14-02-01b	19	1.5	2.3	< 1	< 0.1	< 1	< 2	5.5	81	< 5	75	0.12	1.9
ABN 09-15-04-02a	19	2.1	3.8	< 1	< 0.1	< 1	< 2	10.1	47	< 5	6	0.006	2.7
ABN 09-15-05-01b	17	1	12.3	< 1	< 0.1	< 1	< 2	21.5	34	13	25	0.017	1
ABN 09-15-05-02b	19	1.6	4.6	< 1	< 0.1	< 1	< 2	10.5	86	21	14	0.084	1.2
ABN 09-16-5-1b	17	1.3	3.8	< 1	< 0.1	< 1	3	10	71	< 5	176	0.012	1.9
ABN 09-17-01-01b	14	1.1	3.6	< 1	< 0.1	< 1	< 2	9	73	7	158	0.013	0.5
ABN 09-17-02-01b	22	1	2.8	< 1	< 0.1	< 1	< 2	8	255	< 5	98	0.002	0.7
ABN 09-18(17.5)-02-01b	18	1.6	2.8	< 1	< 0.1	< 1	< 2	7.9	70	< 5	8	0.004	2.2
ABN 09-18-02-01b	12	1	3.3	< 1	< 0.1	< 1	< 2	9.1	3	< 5	< 1	0.002	0.7
ABN 09-18-03-01b	23	2.1	1.9	< 1	< 0.1	< 1	< 2	4.1	91	< 5	179	0.002	0.9
ABN 09-19-02-02b	21	2.5	4	< 1	< 0.1	< 1	< 2	11.7	44	< 5	25	0.004	2.6
ABN 09-19-02-03b	17	1.1	3.8	< 1	< 0.1	< 1	< 2	11.4	44	< 5	60	0.019	1.7
ABN 09-19-6-1b	18	1.1	12.2	< 1	< 0.1	< 1	< 2	21.1	32	13	25	0.017	1.3
ABN 09-20-01-01b	14	2.2	1.2	< 1	< 0.1	< 1	< 2	2.1	80	< 5	34	0.011	1.2
ABN 09-20-02-01b	14	1.8	1.8	< 1	< 0.1	< 1	< 2	3.4	145	< 5	62	0.004	2.1
ABN 09-21-1-1b	18	2.4	3.5	< 1	0.1	< 1	13	17.3	105	< 5	148	1.83	2.5
ABN 09-21-2-1b	28	1.9	8.2	< 1	< 0.1	< 1	< 2	28	7	80	222	0.013	< 0.1
DT 07-10-1-1b	13	1.1	2.5	< 1	< 0.1	< 1	< 2	8.2	16	< 5	8	0.007	0.3
DT 07-8-2-1b	10	1.2	3.4	< 1	< 0.1	< 1	< 2	8.4	22	< 5	102	0.026	1.1
DT 07-8-3-1b	17	1.7	3.5	< 1	< 0.1	< 1	< 2	12.4	36	< 5	201	0.004	1.1
DT 07-8-4-1b	15	1.3	3.2	< 1	< 0.1	< 1	< 2	12.6	12	< 5	17	0.149	0.6
DT 07-8-4-2b	22	2.4	6.4	< 1	< 0.1	< 1	2	16.3	16	< 5	127	0.004	5.6
DT 07-8-4-3b	19	2.1	1.5	< 1	< 0.1	< 1	< 2	3.1	96	9	29	0.07	2.4
DT 07-9-1-1b	11	1.3	2.8	< 1	< 0.1	< 1	41	9.2	29	< 5	82	0.017	1.2
DT 07-9-2-1b	13	1.3	1.6	< 1	< 0.1	< 1	< 2	4.1	57	46	128	0.255	0.6

Table 3 continued

Analyte Symbol	Sc	Se	Sn	Sr	Ta	Th	U	V	W	Y	Zn	Zr
Unit Symbol	ppm	ppm	ppm	ppm	ppm	ppm	ppm	ppm	ppm	ppm	ppm	ppm
Analysis Method	INAA	INAA	FUS-MS	FUS-ICP	FUS-MS	FUS-MS	FUS-MS	FUS-ICP	INAA	FUS-ICP	MULT INAA / TD-ICP	FUS-MS
ABN 09-03-02-01b	45	< 0.5	2	100	0.59	3.75	1.25	616	< 1	26	91	117
ABN 09-03-10-1b	55.8	< 0.5	1	53	0.32	1.7	0.75	1118	< 1	8	111	63
ABN 09-04-10-01b	45.8	< 0.5	1	57	0.53	3.07	0.91	782	< 1	27	66	107
ABN 09-04-11-01b	48.3	< 0.5	4	9	0.54	3.9	2.12	379	< 1	36	52	110
ABN 09-05-08-01b	38.1	< 0.5	2	211	0.46	1.88	1.77	258	< 1	25	92	97
ABN 09-06-01-01b	40.2	< 0.5	< 1	225	0.26	1.12	0.37	250	< 1	16	69	58
ABN 09-06-08-01b	31.8	< 0.5	1	57	0.5	3.67	1.08	324	< 1	21	77	95
ABN 09-07-03-01b	14.4	< 0.5	4	38	0.88	13.6	5.35	96	< 1	18	51	143
ABN 09-07-04-01b	27.9	< 0.5	2	38	0.57	3.83	1.76	372	< 1	24	114	111
ABN 09-07-2-1b	37.4	< 0.5	2	209	0.45	2.36	1.8	263	< 1	24	93	96
ABN 09-08-01-01b	36.7	< 0.5	2	208	0.72	5.31	1.57	457	< 1	33	93	142
ABN 09-09-02-01b	35.7	< 0.5	1	260	0.65	4.14	1.05	348	< 1	28	113	119
ABN 09-10-01-01b	12.6	< 0.5	5	9	1.19	18.3	15.2	81	< 1	13	25	140
ABN 09-10-02-01b	27.1	< 0.5	12	8	0.91	23.2	2.45	292	< 1	35	34	141
ABN 09-11-01-01b	27.6	< 0.5	2	13	0.86	4.68	2.3	330	< 1	27	97	142
ABN 09-11-02-01b	18.6	< 0.5	3	73	1.83	16.7	4.84	241	< 1	36	7	280
ABN 09-11-03-01b	26.2	< 0.5	1	85	0.29	2.96	1.24	241	< 1	15	271	86
ABN 09-12-01-01b	33.3	< 0.5	4	60	1.7	12.8	4.37	382	< 1	38	26	316
ABN 09-12-02-01b	38.5	< 0.5	2	53	0.43	1.76	2.28	476	< 1	27	60	94
ABN 09-12-03-01b	6.38	< 0.5	11	26	1.25	20	2.35	129	15	21	19	115
ABN 09-12-03-02b	37.7	< 0.5	2	267	0.87	6.44	1.66	470	< 1	36	12	150
ABN 09-12-04-01b	25.9	< 0.5	4	28	0.71	6.61	1.72	325	< 1	11	32	127
ABN 09-12-7-1b	55.1	< 0.5	4	262	0.79	0.84	0.27	561	< 1	12	138	104
ABN 09-12.5-01-01b	36.9	< 0.5	< 1	179	0.14	0.92	0.23	293	< 1	19	221	56
ABN 09-13-2-1b	32.7	< 0.5	< 1	44	0.11	0.33	0.44	230	< 1	10	56	39
ABN 09-14-01-01b	5.62	0.7	2	19	0.48	9.04	1.2	57	< 1	13	9	142
ABN 09-14-02-01b	48.9	< 0.5	< 1	15	0.38	0.68	0.39	424	< 1	15	92	93
ABN 09-15-04-02a	31.7	< 0.5	2	30	0.67	3.31	3.07	526	< 1	34	36	149
ABN 09-15-05-01b	22	< 0.5	< 1	61	1.6	5.53	2.07	146	< 1	41	106	512
ABN 09-15-05-02b	44.3	< 0.5	1	88	0.74	1.81	0.63	358	< 1	41	205	178
ABN 09-16-5-1b	27.2	< 0.5	< 1	25	0.76	6.13	2.45	313	< 1	8	88	162
ABN 09-17-01-01b	23.2	< 0.5	< 1	24	0.68	5.8	2.29	331	< 1	8	88	140
ABN 09-17-02-01b	26.3	< 0.5	4	37	0.54	3.05	2.72	270	< 1	8	59	108
ABN 09-18(17.5)-02-01b	41.1	< 0.5	< 1	41	0.53	3.49	2.11	480	< 1	26	40	113
ABN 09-18-02-01b	7.43	< 0.5	3	56	0.85	14.4	2.43	65	10	16	2	129
ABN 09-18-03-01b	43.6	< 0.5	2	60	0.3	1.31	2.44	397	< 1	26	35	70
ABN 09-19-02-02b	41.1	< 0.5	2	4	0.82	5.22	1.71	499	< 1	43	78	159
ABN 09-19-02-03b	30.1	< 0.5	2	15	0.78	5.36	3.28	419	< 1	19	39	152
ABN 09-19-6-1b	23.2	< 0.5	< 1	62	1.57	5.54	2.08	140	< 1	41	105	516
ABN 09-20-01-01b	33.8	< 0.5	< 1	44	0.12	0.35	0.46	237	< 1	10	56	42
ABN 09-20-02-01b	42.4	< 0.5	< 1	13	0.24	2.97	0.92	213	< 1	13	80	71
ABN 09-21-1-1b	10.1	< 0.5	6	9	1.19	18.1	15.3	80	11	14	23	140
ABN 09-21-2-1b	8.5	< 0.5	7	271	1.74	373	280	49	< 1	123	219	301
DT 07-10-1-1b	11.5	< 0.5	3	52	0.65	12	3.1	75	< 1	14	17	98
DT 07-8-2-1b	12.5	< 0.5	3	71	0.77	12.8	1.83	59	5	22	21	135
DT 07-8-3-1b	16.4	< 0.5	3	34	1.07	16.1	4.1	120	< 1	38	22	134
DT 07-8-4-1b	11.8	< 0.5	4	296	0.99	16.1	2.69	79	< 1	12	9	122
DT 07-8-4-2b	19.5	< 0.5	4	59	1.12	20	2.02	71	< 1	43	7	271
DT 07-8-4-3b	50.3	< 0.5	< 1	615	0.21	1.37	0.53	317	< 1	18	148	52
DT 07-9-1-1b	20.9	< 0.5	2	82	0.78	12.4	5.59	67	10	14	29	104
DT 07-9-2-1b	39.3	< 0.5	< 1	97	0.27	1.43	0.47	284	< 1	18	126	60

Table 3 continued

Analyte Symbol	La	Ce	Pr	Nd	Sm	Eu	Gd	Tb	Dy	Ho	Er	Tl
Unit Symbol	ppm	ppm	ppm	ppm	ppm	ppm	ppm	ppm	ppm	ppm	ppm	ppm
Analysis Method	FUS-MS	FUS-MS	FUS-MS	FUS-MS	FUS-MS	FUS-MS	FUS-MS	FUS-MS	FUS-MS	FUS-MS	FUS-MS	FUS-MS
ABN 09-03-02-01b	8.85	20.4	2.62	12.2	4.02	1.92	5.28	0.82	4.85	1.01	3.03	0.25
ABN 09-03-10-1b	4.51	10.5	1.27	5.12	1.3	0.451	1.5	0.25	1.63	0.37	1.2	0.36
ABN 09-04-10-01b	14.4	29	3.53	15.1	3.96	1.34	4.54	0.79	4.99	1.05	3.18	0.12
ABN 09-04-11-01b	16.8	31.5	3.37	13	3	0.923	4.26	0.85	5.75	1.33	4.1	0.25
ABN 09-05-08-01b	11.5	26.1	3.1	12.7	3.37	1.06	3.92	0.7	4.53	0.96	2.83	0.09
ABN 09-06-01-01b	5.34	13.5	1.78	8.24	2.35	0.772	2.74	0.48	2.92	0.6	1.73	0.18
ABN 09-06-08-01b	12.3	23.6	2.57	10.2	2.67	0.756	3.14	0.57	3.7	0.81	2.48	0.32
ABN 09-07-03-01b	37.3	67.7	6.86	24.2	4.26	1.02	3.66	0.58	3.56	0.77	2.35	0.21
ABN 09-07-04-01b	12.5	28.6	3.61	15.8	4.21	1.56	4.42	0.74	4.53	0.93	2.87	0.09
ABN 09-07-2-1b	12.6	28.4	3.35	13.3	3.48	1.12	4.02	0.71	4.49	0.92	2.72	0.08
ABN 09-08-01-01b	20.9	47.8	5.38	21.7	5.03	1.72	5.72	1	6.41	1.36	4.06	0.06
ABN 09-09-02-01b	16.8	35	4.15	17.5	4.41	1.12	4.9	0.84	5.26	1.07	3.11	0.06
ABN 09-10-01-01b	106	174	17	58.4	9.28	2.48	5.84	0.67	2.93	0.51	1.47	0.23
ABN 09-10-02-01b	95.4	166	16.9	59	9.91	2.87	7.52	1.11	6.37	1.32	3.81	0.58
ABN 09-11-01-01b	31	66.1	7.82	31.4	6.73	1.66	5.79	0.88	5.17	1.08	3.28	0.12
ABN 09-11-02-01b	25.8	51.9	5.8	22.4	4.92	1.32	5.45	1.03	6.76	1.6	5.29	< 0.05
ABN 09-11-03-01b	10.9	22.4	2.66	11.3	2.98	0.88	3.24	0.54	3	0.61	1.82	0.11
ABN 09-12-01-01b	42	92.4	10.9	43.7	9.15	2.29	8.51	1.32	7.56	1.54	4.6	< 0.05
ABN 09-12-02-01b	11.8	27	3.57	16	4.31	2.18	4.75	0.82	4.99	1.05	3.17	0.48
ABN 09-12-03-01b	9.41	18.2	2.31	11.2	4.04	1.1	4.93	0.82	4.71	0.87	2.27	0.49
ABN 09-12-03-02b	26.3	55.2	6.38	25.9	6.04	1.73	6.26	1.08	6.7	1.39	4.12	0.06
ABN 09-12-04-01b	11	22.8	2.58	9.9	2.28	0.662	2.23	0.37	2.06	0.41	1.33	0.34
ABN 09-12-7-1b	8.93	26.1	3.64	17.4	4.28	1.43	3.93	0.56	2.88	0.51	1.21	< 0.05
ABN 09-12.5-01-01b	4.05	10.4	1.38	6.31	1.96	0.795	2.63	0.5	3.29	0.73	2.19	0.14
ABN 09-13-2-1b	1.71	3.44	0.4	1.66	0.66	0.328	1.37	0.28	1.84	0.39	1.23	0.13
ABN 09-14-01-01b	9.71	21.3	2.43	9.43	2.14	0.704	2.3	0.39	2.25	0.43	1.23	0.12
ABN 09-14-02-01b	6.93	14.8	1.81	8.02	2.18	0.768	2.61	0.46	2.91	0.63	1.92	0.11
ABN 09-15-04-02a	26.6	54.2	6.34	24.9	5.51	2.03	6.28	1.16	7.62	1.69	5.03	< 0.05
ABN 09-15-05-01b	9.44	25.9	3.45	15.7	4.39	1.31	5.37	1.06	7.36	1.73	5.72	0.08
ABN 09-15-05-02b	11	27.8	3.82	17.7	5.27	1.89	6.67	1.22	7.76	1.64	5.02	0.13
ABN 09-16-5-1b	33.3	66.9	6.89	24.4	4.04	0.764	2.32	0.33	1.94	0.41	1.4	0.51
ABN 09-17-01-01b	29.3	60.6	6.48	22.9	3.68	0.751	2.24	0.34	1.87	0.4	1.35	0.46
ABN 09-17-02-01b	8.5	18.3	2.01	7.4	1.56	0.605	1.54	0.26	1.65	0.36	1.16	0.24
ABN 09-18(17.5)-02-01b	7.15	15.4	1.87	8.33	2.59	1.02	3.61	0.69	4.67	1.03	3.14	0.06
ABN 09-18-02-01b	5.16	11.5	1.36	5.53	1.61	0.547	2.22	0.42	2.78	0.6	1.81	< 0.05
ABN 09-18-03-01b	11.7	22.9	2.89	12.9	3.85	1.33	4.45	0.74	4.55	0.96	2.79	0.2
ABN 09-19-02-02b	16	37.2	4.65	19.7	5.11	1.64	6.66	1.26	7.98	1.68	4.81	0.06
ABN 09-19-02-03b	14.1	31.2	3.6	14.4	3.09	0.876	2.75	0.48	3.17	0.73	2.52	0.09
ABN 09-19-6-1b	9.71	26.6	3.54	16.1	4.46	1.31	5.6	1.08	7.49	1.74	5.71	0.09
ABN 09-20-01-01b	1.61	3.35	0.39	1.68	0.73	0.346	1.41	0.29	1.97	0.42	1.27	0.13
ABN 09-20-02-01b	5.54	13.2	1.48	5.74	1.33	0.406	1.72	0.33	2.1	0.44	1.39	0.11
ABN 09-21-1-1b	107	176	17	57.5	9.14	2.5	5.87	0.68	3.01	0.53	1.46	0.23
ABN 09-21-2-1b	68.8	166	19.7	75.2	15.9	2.41	15.8	3.06	20.1	4.45	14.7	1.26
DT 07-10-1-1b	6.82	14	1.58	6.3	1.64	0.505	2.02	0.36	2.23	0.47	1.43	0.1
DT 07-8-2-1b	50.7	97.6	10.2	35.7	6.05	1.23	4.38	0.69	4.05	0.83	2.61	0.38
DT 07-8-3-1b	19.6	40.5	4.63	18.1	4.14	1.25	4.81	0.94	6.06	1.28	3.65	0.55
DT 07-8-4-1b	18.2	35.5	3.95	14.9	3.21	0.724	3.08	0.5	2.62	0.48	1.37	0.12
DT 07-8-4-2b	40.8	76.4	8.16	29.5	5.34	1.38	5.83	1.14	7.73	1.66	4.8	0.15
DT 07-8-4-3b	7.13	16.2	2.03	8.53	2.32	0.861	2.77	0.51	3.21	0.67	2.03	0.17
DT 07-9-1-1b	2.93	6.84	0.84	3.43	1.18	0.377	1.73	0.34	2.21	0.47	1.45	0.38
DT 07-9-2-1b	5.47	12.8	1.56	6.65	2.04	0.593	2.54	0.49	3.11	0.64	1.89	0.5

Table 3 continued

Analyte Symbol	Tm	Yb	Lu
Unit Symbol	ppm	ppm	ppm
Analysis Method	FUS-MS	FUS-MS	FUS-MS
ABN 09-03-02-01b	0.439	2.66	0.395
ABN 09-03-10-1b	0.185	1.19	0.179
ABN 09-04-10-01b	0.455	2.73	0.386
ABN 09-04-11-01b	0.57	3.24	0.434
ABN 09-05-08-01b	0.397	2.33	0.318
ABN 09-06-01-01b	0.246	1.53	0.225
ABN 09-06-08-01b	0.371	2.35	0.355
ABN 09-07-03-01b	0.339	2.02	0.283
ABN 09-07-04-01b	0.417	2.62	0.373
ABN 09-07-2-1b	0.39	2.25	0.315
ABN 09-08-01-01b	0.595	3.77	0.557
ABN 09-09-02-01b	0.457	2.85	0.407
ABN 09-10-01-01b	0.213	1.35	0.205
ABN 09-10-02-01b	0.525	3.06	0.412
ABN 09-11-01-01b	0.484	3.06	0.471
ABN 09-11-02-01b	0.839	5.61	0.85
ABN 09-11-03-01b	0.255	1.47	0.199
ABN 09-12-01-01b	0.667	4.41	0.683
ABN 09-12-02-01b	0.471	2.93	0.44
ABN 09-12-03-01b	0.311	1.85	0.266
ABN 09-12-03-02b	0.6	3.81	0.565
ABN 09-12-04-01b	0.235	1.72	0.297
ABN 09-12-7-1b	0.151	0.86	0.115
ABN 09-12.5-01-01b	0.323	2.07	0.307
ABN 09-13-2-1b	0.184	1.19	0.179
ABN 09-14-01-01b	0.176	1.08	0.161
ABN 09-14-02-01b	0.287	1.8	0.271
ABN 09-15-04-02a	0.705	4.11	0.584
ABN 09-15-05-01b	0.919	6.37	1.01
ABN 09-15-05-02b	0.745	4.63	0.665
ABN 09-16-5-1b	0.252	1.87	0.316
ABN 09-17-01-01b	0.244	1.83	0.308
ABN 09-17-02-01b	0.193	1.46	0.243
ABN 09-18(17.5)-02-01b	0.463	2.92	0.432
ABN 09-18-02-01b	0.266	1.75	0.262
ABN 09-18-03-01b	0.399	2.56	0.383
ABN 09-19-02-02b	0.67	4.06	0.575
ABN 09-19-02-03b	0.461	3.3	0.504
ABN 09-19-6-1b	0.924	6.4	1.04
ABN 09-20-01-01b	0.193	1.25	0.189
ABN 09-20-02-01b	0.223	1.5	0.228
ABN 09-21-1-1b	0.209	1.38	0.215
ABN 09-21-2-1b	2.56	18.2	2.91
DT 07-10-1-1b	0.24	1.74	0.285
DT 07-8-2-1b	0.44	3.08	0.479
DT 07-8-3-1b	0.518	3.12	0.44
DT 07-8-4-1b	0.206	1.47	0.235
DT 07-8-4-2b	0.671	3.93	0.547
DT 07-8-4-3b	0.301	1.93	0.293
DT 07-9-1-1b	0.235	1.64	0.259
DT 07-9-2-1b	0.279	1.81	0.276

C4: CIPW Normative Mineralogy

The CIPW norm (Cross et al., 1903) of Bonnet Plume River Intrusion samples was calculated using an excel spreadsheet program created and provided by Dr. D. Thorkelson, of Simon Fraser University. The normative mineral abundances of the Bonnet Plume River Intrusions do not reflect their igneous mineral abundances due to extensive metasomatism.

Table 4: CIPW normative mineralogy of the Bonnet Plume River Intrusions and Devil volcanics. W.R.: whole rock.

Sample	*ABN 09 03-02-01*	*ABN 09 03-10-01*	*ABN 09 4-10-01*	*ABN 09 4-11-01*	*ABN 09 5-8-1*	*ABN 09 06-01-01*	*ABN 09 06-08-01*	*ABN 09 07-02-01*	*ABN 09 07-03-01*	*ABN 09 07-04-01*
Location	Pika	Pika	Pika	Pika	Bel	Bel	Bel	Bel	Bel	Bel
Fe_2O_3/FeO	0.2	0.2	0.2	0.2	0.2	0.2	0.2	0.2	0.2	0.2
Apatite	0.40	0.20	0.33	0.31	0.17	0.20	0.32	0.17	0.50	0.31
Ilmenite	4.95	5.97	5.90	3.95	3.22	2.11	2.84	3.19	1.08	3.41
Orthoclase	19.59	36.92	9.62	25.53	8.17	10.63	38.53	8.20	31.31	6.67
Albite	0.00	1.61	22.43	0.29	40.00	28.92	8.41	40.20	28.23	17.01
Anorthite	15.79	15.59	20.44	15.40	13.68	23.19	11.80	13.42	6.54	23.57
Corundum	0.00	0.72	0.00	6.61	0.00	0.00	0.00	0.00	0.00	0.00
Titanite	0.00	0.00	0.00	0.00	0.00	0.00	0.00	0.00	0.00	0.00
Rutile	0.00	0.00	0.00	0.00	0.00	0.00	0.00	0.00	0.00	0.00
Acmite	0.00	0.00	0.00	0.00	0.00	0.00	0.00	0.00	0.00	0.00
Na-metasilicate	0.00	0.00	0.00	0.00	0.00	0.00	0.00	0.00	0.00	0.00
Magnetite	0.00	0.00	0.00	0.00	0.00	0.00	0.00	0.00	0.00	0.00
Hematite	0.00	0.00	0.00	0.00	0.00	0.00	0.00	0.00	0.00	0.00
Diopside	23.06	0.00	1.03	0.00	18.83	7.80	13.91	19.01	19.59	2.12
Wollastonite	0.00	0.00	0.00	0.00	0.00	0.00	0.00	0.00	0.00	0.00
Hypersthene	0.00	0.00	33.30	46.55	0.00	4.14	0.00	0.00	5.39	38.28
Olivine	13.99	30.19	6.95	0.00	12.59	23.03	18.35	12.53	7.36	8.61
Quartz	0.00	0.00	0.00	1.36	0.00	0.00	0.00	0.00	0.00	0.00
Perovskite	0.00	0.00	0.00	0.00	0.00	0.00	0.00	0.00	0.00	0.00
Nepheline	15.42	8.80	0.00	0.00	3.35	0.00	5.85	3.29	0.00	0.00
Leucite	6.80	0.00	0.00	0.00	0.00	0.00	0.00	0.00	0.00	0.00
class	Metalum	Peralum	Metalum	Peralum	Metalum	Metalum	Metalum	Metalum	Metalum	Metalum
W.R. Mg#	42.20	32.75	43.81	55.18	56.54	58.71	52.50	56.45	35.24	52.27
Silicate Mg#	46.44	36.30	48.20	58.22	61.11	60.68	55.60	60.96	36.13	54.50
Ab%	78.80	84.28	52.64	99.57	44.38	48.77	100.00	44.45	93.94	50.38
An%	21.20	15.72	47.36	0.43	55.62	51.23	0.00	55.55	6.06	49.62

Table 3 continued, Ab: albite content of plagioclase, An, anorthite continent of plagioclase. Mg number calculated using Fe_2O_3/FeO of 0.2,

Sample	*ABN 09 08-01-01*	*ABN 09 09-02-01*	*ABN 09 11-01-01*	*ABN 09 11-02-01*	*ABN 09 12-01-01*	*ABN 09 12-02-01*	*ABN 09 12-03-01*	*ABN 09 12-03-02*	*ABN 09 12-04-01*	*ABN 09 12.5-01-01*
Location	Glacier Lake	Glacier Lake	Olympic	Olympic	Anoki	Otis	Quartet	Quartet	Sihota	Olympic
Fe2O3/FeO	0.2	0.2	0.2	0.2	0.2	0.2	0.2	0.2	0.2	0.2
Apatite	0.42	0.41	0.46	1.06	0.99	0.28	0.50	0.52	0.44	0.15
Ilmenite	3.94	3.43	3.70	4.40	5.88	3.78	1.34	4.03	3.44	1.56
Orthoclase	6.07	3.58	13.01	0.73	0.91	38.48	50.20	6.82	32.82	10.45
Albite	33.55	29.93	16.78	44.58	50.12	5.00	10.53	31.09	0.95	21.33
Anorthite	10.05	21.17	8.94	2.39	10.05	14.96	12.90	12.84	17.99	25.11
Corundum	0.00	0.00	3.21	0.00	0.00	0.97	0.00	0.00	0.89	0.00
Titanite	0.00	0.00	0.00	0.00	0.00	0.00	0.00	0.00	0.00	0.00
Rutile	0.00	0.00	0.00	0.00	0.00	0.00	0.00	0.00	0.00	0.00
Acmite	0.00	0.00	0.00	0.00	0.00	0.00	0.00	0.00	0.00	0.00
Na-metasiicate	0.00	0.00	0.00	0.00	0.00	0.00	0.00	0.00	0.00	0.00
Magnetite	0.00	0.00	0.00	0.00	0.00	0.00	0.00	0.00	0.00	0.00
Hematite	0.00	0.00	0.00	0.00	0.00	0.00	0.00	0.00	0.00	0.00
Diopside	23.82	21.54	0.00	22.98	27.59	0.00	10.79	21.90	0.00	15.63
Wollastonite	0.00	0.00	0.00	0.00	0.00	0.00	0.00	0.00	0.00	0.00
Hypersthene	0.00	2.19	40.24	0.00	4.33	0.00	9.35	0.00	39.06	19.85
Olivine	17.51	17.76	0.00	8.97	0.12	35.43	4.38	19.70	0.00	5.93
Quartz	0.00	0.00	13.67	0.00	0.00	0.00	0.00	0.00	4.40	0.00
Perovskite	0.00	0.00	0.00	0.00	0.00	0.00	0.00	0.00	0.00	0.00
Nepheline	4.64	0.00	0.00	14.89	0.00	1.11	0.00	3.10	0.00	0.00
Leucite	0.00	0.00	0.00	0.00	0.00	0.00	0.00	0.00	0.00	0.00
class	Metalum	Metalum	Peralum	Metalum	Metalum	Peralum	Metalum	Metalum	Peralum	Metalum
W.R. Mg#	39.36	45.32	46.61	33.17	44.59	43.05	21.54	41.28	53.07	49.98
Silicate Mg#	42.48	48.10	49.41	37.15	54.85	45.42	22.53	44.54	56.11	50.71
Ab%	27.19	23.64	66.77	3.80	6.57	93.40	100.00	32.43	98.90	55.94
An%	72.81	76.36	33.23	96.20	93.43	6.60	0.00	67.57	1.10	44.06

Table 4 continued

Sample	*ABN 09 14-02-01*	*ABN 09 15-04-02*	*ABN 09 15-05-01*	*ABN 09 15-05-02*	*ABN 09 17-02-01*	*ABN 09 17.5-02-01*	*ABN 09 18-03-01*	*ABN 09 19-02-02*	*ABN 09 19-02-03*	*ABN 09 20-01-01*
Location	Lala	Lala	Lala	Lala	Wizard	Wizard	Nor	Yukon Olympic	Yukon Olympic	Yukon Olympic
Fe2O3/FeO	0.2	0.2	0.2	0.2	0.2	0.2	0.2	0.2	0.2	0.2
Apatite	0.35	0.49	0.40	0.84	0.39	0.34	0.25	0.46	0.47	0.18
Ilmenite	3.50	4.46	1.52	3.39	3.59	3.38	2.76	3.97	3.78	1.89
Orthoclase	20.81	4.68	10.28	6.12	37.29	6.06	10.93	12.73	40.18	12.69
Albite	16.01	34.38	36.13	15.72	0.79	34.95	28.56	0.37	0.91	14.60
Anorthite	17.76	15.80	9.11	18.10	16.02	13.72	9.14	0.24	0.05	6.45
Corundum	4.37	1.01	0.90	2.81	3.59	0.00	0.00	10.97	5.77	8.91
Titanite	0.00	0.00	0.00	0.00	0.00	0.00	0.00	0.00	0.00	0.00
Rutile	0.00	0.00	0.00	0.00	0.00	0.00	0.00	0.00	0.00	0.00
Acmite	0.00	0.00	0.00	0.00	0.00	0.00	0.00	0.00	0.00	0.00
Na-metasiicate	0.00	0.00	0.00	0.00	0.00	0.00	0.00	0.00	0.00	0.00
Magnetite	0.00	0.00	0.00	0.00	0.00	0.00	0.00	0.00	0.00	0.00
Hematite	0.00	0.00	0.00	0.00	0.00	0.00	0.00	0.00	0.00	0.00
Diopside	0.00	0.00	0.00	0.00	0.00	9.48	23.95	0.00	0.00	0.00
Wollastonite	0.00	0.00	0.00	0.00	0.00	0.00	0.00	0.00	0.00	0.00
Hypersthene	34.83	37.34	18.99	46.23	0.00	0.00	0.00	57.27	23.07	52.08
Olivine	2.37	0.00	0.00	0.00	38.24	27.16	12.86	0.00	25.77	0.00
Quartz	0.00	1.83	22.67	6.79	0.00	0.00	0.00	13.99	0.00	3.19
Perovskite	0.00	0.00	0.00	0.00	0.00	0.00	0.00	0.00	0.00	0.00
Nepheline	0.00	0.00	0.00	0.00	0.09	4.90	11.56	0.00	0.00	0.00
Leucite	0.00	0.00	0.00	0.00	0.00	0.00	0.00	0.00	0.00	0.00
class	Peralum	Peralum	Peralum	Peralum	Peralum	Metalum	Metalum	Peralum	Peralum	Peralum
W.R. Mg#	53.25	51.94	48.25	49.52	58.52	37.62	65.97	55.72	29.83	68.20
Silicate Mg#	56.47	55.99	50.61	51.86	61.02	39.82	70.03	58.36	31.30	69.64
Ab%	77.10	26.09	62.17	50.22	99.02	26.32	61.10	98.88	99.13	69.26
An%	22.90	73.91	37.83	49.78	0.98	73.68	38.90	1.12	0.87	30.74

Table 3 continued

Sample	*ABN 09 20-02-01*	*DT 07 08-04-03*
Location	Yukon Olympic	Sihota
Fe2O3/FeO	0.2	0.2
Apatite	0.23	0.20
Ilmenite	1.26	2.04
Orthoclase	24.03	11.82
Albite	5.22	17.82
Anorthite	0.28	24.26
Corundum	10.72	0.00
Titanite	0.00	0.00
Rutile	0.00	0.00
Acmite	0.00	0.00
Na-metasiicate	0.00	0.00
Magnetite	0.00	0.00
Hematite	0.00	0.00
Diopside	0.00	12.14
Wollastonite	0.00	0.00
Hypersthene	38.31	0.00
Olivine	0.00	30.48
Quartz	19.96	0.00
Perovskite	0.00	0.00
Nepheline	0.00	1.24
Leucite	0.00	0.00
class	Peralum	Metalum
W.R. Mg#	68.54	59.60
Silicate Mg#	69.81	60.74
Ab%	92.27	60.37
An%	7.73	39.63

C5: Geochemical Error Analyses

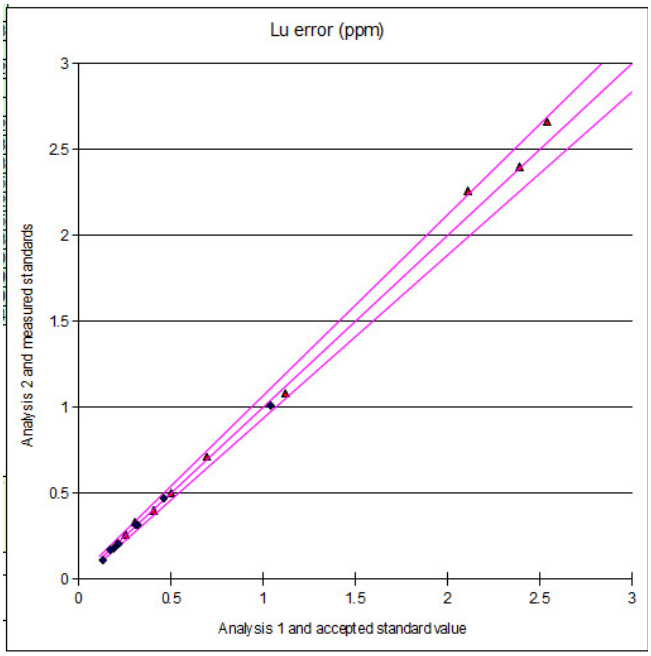

Fig. 29: An example of iterative error calculation (using lutetium) for geochemical results. Standards are plotted against their known concentrations; duplicate analyses are plotted against each other. When the results are contained within the error envelope line (y=mx+b), the absolute (b) and relative error (m) is known. Pink triangles are standards, blue diamonds are duplicates.

Geochemical error analysis was performed empirically, comparing the results of the analyses of duplicate samples and standards. The excel program used for determining geochemical error was provided by Dr. D. Thorkelson of Simon Fraser University. The program plots the corresponding analyses on the x and y-axes; the more similar the analyses, the closer to unity the point will be situated. An error envelope is plotted to surround the data. The equation that defines this envelope's deviation from unity is the equation that defines the error of the analyses (Fig. 29).Results are presented in Fig. 30Standards SY-2 and MRG-1 (Govindaraju, 1994) were included by the authors, and standards GXR-1, WMG-1, NIST 694, DNC-1, GBW 07113, GXR-4, SDC-1, SCO-

1, GXR-6, LKSD-3, NIST 1633b, NOD-A-1, NOD-P-1, W-2a, SY-4, CTA-AC-1, BIR-1a, NSC-DC70014, NSC-DC70009, OREAS 100a, OREAS 101a, OREAS 13b, JR-1, FER-1, and DNC-1a were included by Activation Labs. Five duplicates were included by the authors, and five duplicates were included by Activation Labs.

	Average concentration, % or ppm	Average error % or ppm	Average percent error
SiO2	53.16	3.49	6.56
Al2O3	14.86	0.40	2.67
Feo*	12.35	0.42	3.40
MnO	0.20	0.00	1.49
MgO	6.90	0.09	1.29
CaO	4.62	0.07	1.43
Na2O	2.73	0.15	5.57
K2O	3.24	0.10	3.04
TiO2	1.76	0.05	2.64
P2O5	0.17	0.02	8.90
Ba	666.20	40.97	6.15
Co	45.85	6.13	13.36
Cr	119.09	18.12	15.22
Cu	45.18	1.22	2.70
Ga	18.49	2.17	11.74
Hf	3.57	0.14	3.80
Nb	9.21	1.14	12.35
Ni	71.66	3.79	5.29
Rb	66.73	5.15	7.71
Sb	2.00	1.00	50.00
Sc	35.13	3.61	10.27
Sr	94.40	2.00	2.12
Ta	0.67	0.08	11.47
Th	4.48	0.59	13.15
U	1.76	0.09	4.83
V	374.66	16.24	4.33
Y	24.11	1.24	5.15
Zn	78.74	3.36	4.27
Zr	141.46	14.32	10.12
La	14.22	1.19	8.35
Ce	30.75	2.05	6.66
Pr	3.63	0.23	6.38
Nd	14.91	0.65	4.34
Sm	3.66	0.23	6.37
Eu	1.16	0.03	2.93
Gd	4.07	0.15	3.73
Tb	0.72	0.09	11.98
Dy	4.53	0.19	4.10
Ho	0.97	0.05	5.12
Er	2.97	0.16	5.34
Tl	0.19	0.05	27.33
Tm	0.45	0.02	4.79
Yb	2.86	0.14	4.75
Lu	0.43	0.03	6.49

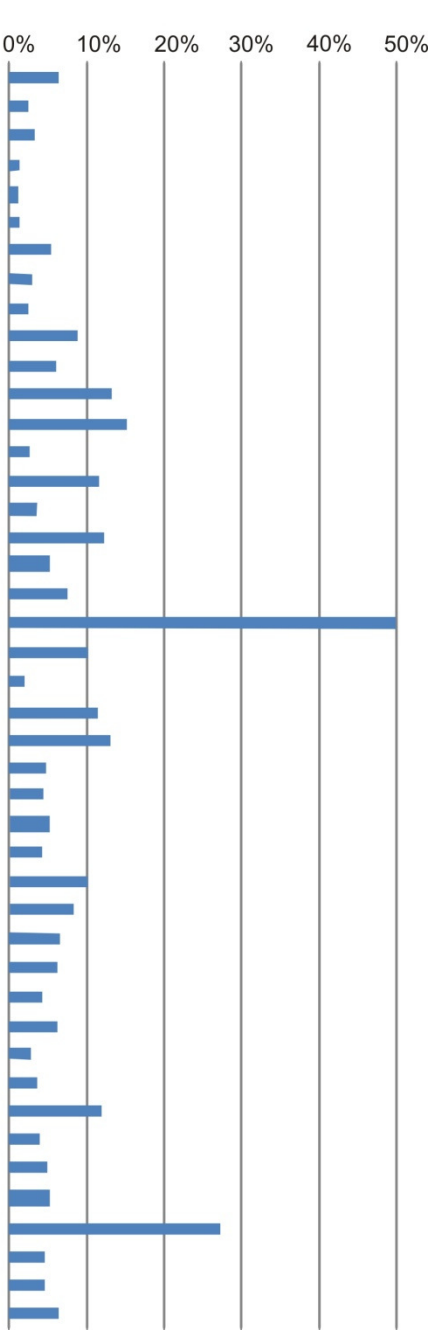

Fig. 30: Numeric and graphic display of geochemical error for each element analyzed.

Appendix D: Fravect Geochemical Modelling

Model description

The FRAVECT modelling system is based on a pure fractional crystallization model of trace element behaviour. Its purpose is to determine which mineral or combination of minerals could be involved in closed system fractionation of the sample suite. Ultimately, this modelling was inconclusive because not only is it improbable that the Bonne Plume River Intrusions were derived from a single magma system fractionating in a closed-system environment, but additionally, their chemistry has been altered by metasomatism.

FRAVECT models closed-system fractionation by allowing the user to compare the spread of sample composition within a suite against idealized evolution paths in which only one mineral is fractionating.

Mineral fractionation evolution paths are defined by the equation

$$C_L = C_O \times F^{(D-1)}$$

Where C_L is the concentration of the element in the evolved sample, C_O is the concentration of the element in the parental sample, F is the fraction of the rock that has been removed by fractional crystallization, and D is the distribution coefficient.

Any point in geochemical space can be chosen as the parental composition (C_O) however, choosing the composition of one of the least geochemically evolved samples in a given suite is well justified. Values for D were taken from various literature sources aggregated in Rollinson (1993) (Table 4.1, page 108) for melts of basalt and basaltic andesite composition.

FRAVECT also allows for multi-mineral geochemical evolution paths by creating a synthetic bulk partition coefficient from a weighted average of the partition coefficients of individual minerals. Crystallization assemblages that may represent the igneous system from which the samples are taken will have evolution paths that follow a trend defined by the sample points. It is important to note that a candidate crystallization assemblage is not a unique solution, merely a possible solution.

The FRAVECT model is based upon the assumption that samples are related purely by closed system fractional crystallization. This is certainly not the case with the Wernecke igneous clasts.

Results

At face value, this trace element geochemical modelling indicates that the Wernecke igneous clasts range widely in composition and have no consistent fractionation trends. The full range of fractionation appears to be greater than 90%. However, this range cannot be explained by closed-system fractional crystallization alone. Across various trace element systems, the minerals that consistently define the best trends were orthopyroxene, clinopyroxene, olivine and plagioclase. Metasomatism, crustal assimilation, and differences in primary magmas provide alternative and more plausible explanations for the large range of trace element compositions.

Appendix E: Stonergram Geochemical Modelling

Major and minor element geochemical modelling was performed using the Stonergram program. This program models geochemical evolution by fractional crystallization and metasomatism. Melt evolution was modelled by the removal of stoichiometrically appropriate quantities of major oxides for the minerals thought to have crystallized and subsequently been removed from the magma system. Metasomatism was modelled by the addition or removal of quantities of major oxides. Similarly to PER diagrams (Pearce, 1968) and isocon plots (Grant, 1986), the Stonergram program normalizes geochemical changes to a conserved element. The results of the modelling were inconclusive because it was not possible to determine what chemical change could be attributed to primary igneous processes, and what was the product of metasomatism.

Parental Sample Selection

In order to use the Stonergram program, an initial geochemical composition is needed. This provides a reference point for both the major oxides and the conserved element. Ideally, this would be chosen from within the sample suite however, it could also be fabricated if no suitable candidates were sampled.

Several geochemical criteria were used in order to determine the most suitable sample from within the sampled Bonnet Plume River Intrusions. High concentrations of scandium and low concentrations of hafnium, niobium, lanthanum, and lutetium indicated samples that are more primitive. These elements were chosen due to their immobility under most crustal conditions (Floyd and Winchester, 1978; Rollinson, 1993; Gifkins et al., 2005). All samples were ranked based on concentrations of these elements,

and the sample with the highest cumulative rank (ABN 09 03-10-1b) was chosen as the most primitive sample.

An Idealization of the Parental Sample

Almost all samples of the Bonnet Plume River Intrusions have undergone extensive metasomatism, likely a result of interaction with the WBX (Thorkelson et al., 2001a). As a result of this alteration, sample ABN 09 03-10-01b has a major element geochemical pattern that does not represent the original igneous composition. In order to use this sample, changes were made to its composition where it seemed to be highly unusual. These changes are detailed in Table 5:

Table 5: Major element composition for the source parental sample and modified parental sample used in the Stonergram geochemical models, bold values are modified.

	SiO_2	Al_2O_3	FeO*	MgO	CaO	Na_2O	K2O	TiO_2	P_2O_5
ABN 09 03-10-01b	45.42	16.65	**18.03**	**4.87**	**3.3**	2.1	**6.24**	3.13	0.087
Modified Parental Sample	45.42	16.65	**15**	**8**	**7**	2.1	**1**	3.13	0.087

The new composition reflects the elemental ratios of the least altered samples, the average absolute concentrations of the least evolved samples, and the igneous compositions of typical diorites and gabbros from island arcs (Gill, 1981; Plank and Langmuir, 1988; Winter, 2001).

Choice of "Conserved" Element (Sc)

The choice of scandium as an element against which to measure igneous differentiation and metasomatism seems odd at first however; it is the most suitable element in this instance. Firstly, it is immobile during metamorphism and metasomatism (see Fig. 17: Selected elements showing enrichments and depletions due to alkali

metasomatism, normalized to the average elemental concentration of samples with "normal" K/Na values (0.5-2).). Secondly, its abundance in the upper crust is low, therefore open system processes such as wall rock assimilation and metasomatism that may have occurred during the residence of the Bonnet Plume River Intrusions in the upper crust would have little effect on the absolute abundance of scandium. The issue of the non-conservative behaviour of scandium during magma crystallization is handled in the Stonergram program by making a reasonable estimate of the phases crystallizing from the melt and assigning a corresponding bulk partition coefficient ($K_{d)}$ to the scandium system. The Stonergram program then uses this partition coefficient to determine the percent fractionation between the parental sample and the evolved sample based on the difference in concentration of the conserved element in each based on the equation $C_L = C_O \times F^{(D-1)}$. In this equation, C_L is the concentration of the element in the evolved sample, C_O is the concentration of the element in the parental sample, F is the fraction of the rock that has been removed, and D is the distribution coefficient, which is equivalent to the bulk partition coefficient. Given that the partition coefficient can be reasonably estimated therefore, the non-conservative behaviour of scandium does not present an issue.

Calculation of Forsterite, Enstatite, and Diopside Content in Olivine, Orthopyroxene, and Clinopyroxene

The composition of olivine and the pyroxenes was calculated in order to simplify the choices within the modelling system and to create well-justified values. The equation for calculating this for individual samples is based on the Fe/Mg ratio of the sample. It is:

$$X = 100 \times \left(\frac{1}{\left(\left((1 - Fe_r) \times {}^{FeO}/_{MgO} \times n \right) + 1 \right)} \right)$$

(Baker and Eggler, 1987)

Where X is the mineral composition, Fe_r is the Fe^{3+}/Fe^{2+} of the model, and n is the empirically determined constant for the mineral being calculated. In this case, n was:

- Forsterite→ 0.29
- Enstatite→ 0.26
- Diopside→ 0.25

These values are valid at 2kbar (Baker and Eggler, 1987), which was deemed appropriate as it corresponds to approximately 7km depth in the modern Aleutian arc (Baker, 1987), where, given their basaltic to andesitic composition, the Bonnet Plume River Intrusions might roughly be expected to lie within the crust (Fliedner and Klemperer, 1999; Holbrook et al., 1999)

An average value of the parental and evolved compositions of is then used for the modelling.

Iron loss through crystallization and metasomatism

The maximum allowed magnetite crystallization was set at 5% after which remaining Fe loss was modelled by metasomatic Fe removal, which is chemically equivalent. This was done because it is unreasonable to expect much greater than 5% magnetite crystallization as was being modelled before this limit was set.

Operation of the Stonergram Program

After the initial set-up f the modelling system (choosing a parental and an evolved sample, choosing a conserved element, and determining a suitable K_D), the following steps must be taken for modelling:

A suitable Fe^{3+}/Fe^{2+} must be entered. This is based on the likely oxidation conditions during crystallization. In the case of this modelling, 0.1 was chosen.

Input the An content of plagioclase and the Ti content of magnetite crystallizing in the magmatic system

Input values for the suspected crystals mineralizing in the magmatic system and elements varying in subsequent metasomatism until a match with the evolved sample has been found

*Note: this is not a unique solution, but given well-justified inputs, it is a probable solution

Results

No strong conclusions could be drawn from Stonergram geochemical modelling, however it suggests that geochemical variations were produced mainly by augite, orthopyroxene and plagioclase fractionation, and only minor removal of magnetite, rutile, titanite and apatite. The total amount of fractionation is modelled at nearly 50%. Despite using the least altered samples in the major element modelling, it was necessary to invoke open-system processes such as metasomatism, crustal assimilation, or variable primary magma systems in order to model the calculated bulk composition differentiation trend. Specifically, concentrations of K_2O, Na_2O, TiO_2 and P_2O_5 could not be modelled by

mineral fractionation alone, and required elemental additions or subtractions. The alkali elements showed the greatest divergence from closed-system processes, and the high level of potassium in the rock was modelled with an open-system gain of 3.33 mol%, and Na_2O modelled with a loss of 2.6 mol% (Fig. 11). Most of the open-system variability that was found was most likely the effect of Wernecke Breccia fluid metasomatism.

Appendix F: Statistical Testing for Geochemical Mobility

The effect of geochemical mobility, combined with metasomatic variability can be seen when comparing the standard deviation of elemental concentration normalized to the average elemental concentration for each element among the whole suite of Bonnet Plume River Intrusions and Devil volcanics (Fig. 31). This technique reveals the high variability of the elements identified using the sodic-potassic technique detailed in section 2.5.3. The LILE have the widest ranges of concentrations, consistent with the idea that they were highly mobile during Wernecke Breccia metasomatism. The HFSE have concentration ranges similar to that of the least mobile LILE, with the exception of yttrium, which has the smallest range of all the elements tested. The REE show decreasing concentration ranges from lanthanum to lutetium, with a dip at europium. The transition metals show both wide and narrow ranges, with copper being one of the most mobile elements and scandium one of the least mobile elements.

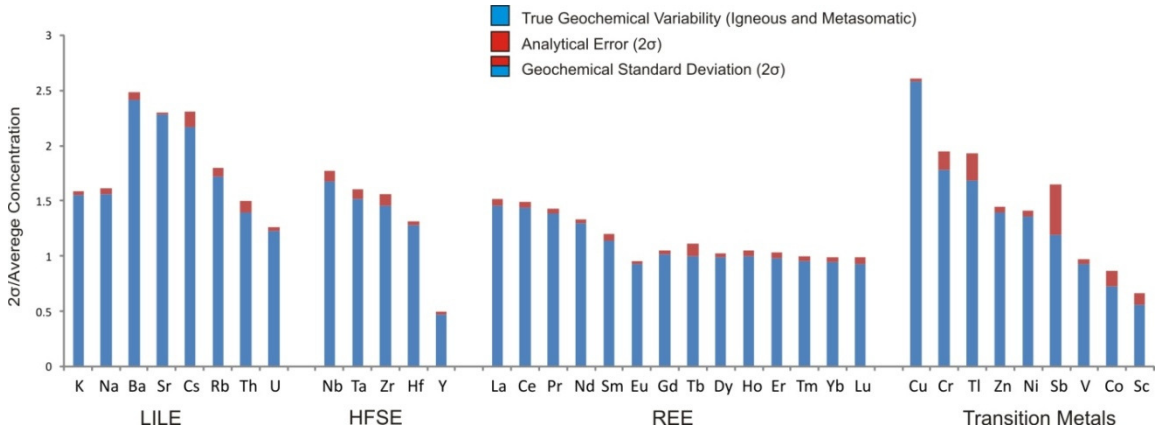

Fig. 31: 2 Standard deviation geochemical variability relative to average elemental concentration of selected elements. LILE – large ion lithophile elements. HFSE – high field strength elements. REE – rare earth elements.

Appendix G: Samarium - Neodymium Isotope Analysis Methods and Calculations

From among the forty samples that were geochemically analysed, ten samples were chosen for additional neodymium isotope analysis. These samples were chosen for their geographic location or their likelihood of representing a primary igneous composition. Powdered aliquots of these samples were sent to the PCIGR for analysis following the method of Weis et al. (2005). Results are presented in Table 1. These results were used, in conjunction with previous geochemical results to determine εNd values and TDM values for the samples. The methods are detailed in this appendix.

Throughout this appendix, all time dependant values will be noted with a subscript indicating the time for which they apply, "0" for the present, "t" for any time before present or for the time of extraction, 1.71 Ga, and T_s for the time of secondary disturbance (metasomatism), 1.60 Ga.

Table 6: Sm-Nd analysis variables and constants.

	description	unit	value
$\left(^{143}Nd/_{144}Nd\right)_0$	Measured atomic ratio	N/A	Measured
$\left(^{143}Nd/_{144}Nd\right)_{0\_CHUR}$	Atomic ratio	N/A	0.512638[1]
$\left(^{147}Sm/_{144}Nd\right)_{0\_CHUR}$	Atomic ratio	N/A	0.1966[2]
Nd	Measured concentration	ppm	Measured
Sm	Measured concentration	ppm	Measured
$A_r Nd$	Relative	g/mol	144.2397

	atomic mass		
$A_r Sm$	Relative atomic mass	g/mol	150.3656
$^{144}Nd/_{Nd}$	Fraction of total Sm which is ^{144}Nd	N/A	$1/\left(\left(\sum {}^{XXX}Nd/{}^{144}Nd\right) + {}^{143}Nd/{}^{144}Nd\right)$
$^{147}Sm/_{Sm}$	Fraction of total Sm which is ^{147}Sm	N/A	0.149957
λ	$^{147}Sm \rightarrow {}^{143}Nd$ α-decay constant	year^{-1}	6.54×10^{-12}

[1](Jacobsen and Wasserburg, 1980)
[2](Amelin and Rotenberg, 2004)

Based on the measured concentrations of *Sm* and *Nd*; the measured ratio of $^{143}Nd/^{144}Nd$; and known relative atomic masses and isotope abundances, the $^{147}Sm/_{144}Nd$ value can be calculated as follows:

$$^{147}Sm/_{144}Nd = \left(\frac{^{147}Sm/_{Sm} \cdot Sm}{A_r Sm}\right) \Big/ \left(\frac{^{144}Nd/_{Nd} \cdot Nd}{A_r Nd}\right)$$

In this equation, $^{144}Nd/_{Nd}$ is calculated as follows:

$$^{144}Nd/_{Nd} = 1/\left(\left(\sum {}^{XXX}Nd/{}^{144}Nd\right) + {}^{143}Nd/{}^{144}Nd\right)$$

$$\left(\sum {}^{XXX}Nd/{}^{144}Nd\right) = 3.69014$$

The evolution of $^{143}Nd/^{144}Nd$ is modelled by the following equation:

$$^{143}Nd/_{144}Nd_{t} = {}^{143}Nd/_{144}Nd_{0} - {}^{147}Sm/_{144}Nd_{0} \cdot \left(e^{\lambda t} - 1\right)$$

The evolution of CHUR (**CH**ondritic **U**niform **R**eservoir) is modelled by the same equation, substituting CHUR specific values for measured values.

εNd as defined by DePaolo and Wasserburg (1976) is defined as the per mil deviation of a sample from CHUR. It is calculated as follows:

$$\varepsilon Nd_t = 10^4 \cdot \left(\frac{^{143}Nd/_{144}Nd_{t\_sample}}{^{143}Nd/_{144}Nd_{t\_CHUR}} \right)$$

The rate at which εNd evolves away from CHUR is defined as follows:

$$f_{Sm/Nd} = \left(\frac{^{147}Sm/_{144}Nd_{0}}{^{147}Sm/_{144}Nd_{0\_CHUR}} \right) - 1$$

The Depleted Mantle

The depleted mantle is a theoretical construct that represents mantle from which melts have been previously extracted. It consists of the residuum of melt extraction, which, due to differences in melt-residuum distribution coefficients during partial melting is depleted in Nd relative to Sm therefore; it has a higher $^{147}Sm/^{144}Nd$ value than CHUR and will evolve away from CHUR positively in εNd space.

The depleted mantle was first put forward in order to account for the poor fit of neodymium model ages with other geochronologic data when using CHUR as a mantle

source, as well as discrepancies between the εNd of some modern rocks and CHUR (DePaolo, 1981a). It was found that when melts were extracted from a reservoir that had evolved positively in εNd away from CHUR, the model age was consistent with other geochemical data. DePaolo's (1981a)equation modelling the evolution of the depleted mantle in εNd-time space is :

$$\varepsilon Nd_{DM}^{D81} = \frac{0.25}{10^{18}}t^2 - \frac{-3}{10^9}t + 8.5$$

An alternative model was put forward by Nägler and Kramers (1998) in order to correct a deficiency in previous models (DePaolo, 1981a; Goldstein et al., 1984); they indicate that the depleted mantle has evolved away from CHUR since the formation of the earth while data show that the depleted mantle did not begin evolving away from CHUR until ca. 3Ga (Nägler and Kramers, 1998). Throughout this work, the model of Nägler and Kramers (1998) is used to calculate depleted mantle εNd values. This model's equation is shown below:

$$\varepsilon Nd_{DM}^{NK98} = \frac{0.164}{10^{27}}t^3 - \frac{0.566}{10^{18}}t^2 - \frac{2.79}{10^9}t + 10.4$$

The effects of metasomatism on Sm-Nd ratios, εNd, and TDM

When rocks are subjected to metasomatism, their chemical compositions change, they behave as an open system. Although metasomatism is more commonly thought of as affecting more mobile elements such as barium, potassium and strontium; samarium and neodymium may also be affected (Cullers et al., 1973).

Despite behaving very similarly in fractionating magma systems and many other geologic processes, they may behave quite differently depending on a number of factors, including fluid-rock interaction (Masuda, 1967; Burton and O'Nions, 1988; Kikawada et al., 2001).

Altering a rock may have two effects on the Sm-Nd isotope system and all derived values: altering the $^{143}Nd/^{144}Nd$ ratio and altering the Sm/Nd ratio. Altering the $^{143}Nd/^{144}Nd$ ratio has an immediate impact on the εNd value of the rock. Depending on the isotopic composition of the metasomatizing fluid, the εNd value may be increased or decreased. If the interaction between a sufficiently large fluid reservoir is long and vigorous, complete isotopic homogenization of the rock with the metasomatizing fluid may be achieved (Halama et al., 2011). The alteration of the Sm/Nd ratio of a rock will also affect its εNd value(Rosing, 1990). The Sm/Nd ratio is directly correlated with the $^{147}Sm/^{144}Nd$ ratio, which controls $f_{Sm/Nd}$. As the Sm/Nd ratio increases, the εNd evolution trend becomes more positive and conversely, as the Sm/Nd ratio decreases, the εNd evolution trend becomes more negative. This relationship is modelled by the following equation:

$$\delta f_{Sm/Nd} = \left(\frac{\left(\left({}^{1}/_{F} - 1 \right) {}^{147}Sm/_{144}Nd_{t_s} \right) - {}^{147}Sm/_{144}Nd_{0}}{{}^{147}Sm/_{144}Nd_{0\_CHUR}} \right) - 1$$

With time, the discrepancy between the measured $^{143}Nd/^{144}Nd$ and the hypothetical igneous (non-disturbed) $^{143}Nd/^{144}Nd$ increases (Rosing, 1990). This relationship is modelled by the equation below:

$$\left({}^{143}Nd/{}^{144}Nd\right)_0 = \left({}^{143}Nd/{}^{144}Nd\right)_t + \left(\left({}^{147}Sm/{}^{144}Nd\right)_0 \left(e^{\lambda t_s} - 1\right)\right) + \left(\left(1/F\right)\left({}^{147}Sm/{}^{144}Nd\right)_{t_s} \left(e^{\lambda(t-t_s)} - 1\right)\right)$$

The change in evolution trend is represented in an εNd graph as an inflection point at the time of disturbance (see Fig. 32). If the change is not accounted for, there is an apparent shift in the $^{143}Nd/^{144}Nd$ ratio at the time of the igneous event which produced the rock (Rosing, 1990). This shift is modelled by the following equation:

$$\delta\left({}^{143}Nd/{}^{144}Nd\right)_t = \left(1/F - 1\right)\left({}^{147}Sm/{}^{144}Nd\right)_0 \left(e^{\lambda t} - e^{\lambda t_s}\right)$$

The change in $\left({}^{143}Nd/{}^{144}Nd\right)_t$ also creates a change in the εNd at the time of the igneous event.

$$\delta\,\varepsilon Nd_t = \left(\left(1/F - 1\right)\left({}^{147}Sm/{}^{144}Nd\right)_0 \left(e^{\lambda t} - e^{\lambda t_s}\right)(10^4)\right) \Big/ \left({}^{143}Nd/{}^{144}Nd\right)_{t\_CHUR}$$

This change in εNd_t must be accounted for when determining the model age of the rock, otherwise it will be erroneous.

Hypothetical epsilon neodymium paths for the Wernecke igneous clasts

Three εNd paths from initial melt extraction from depleted mantle to present are shown in Fig. 32 showing the influences of crustal assimilation and metasomatism on hypothetical Wernecke igneous clasts and how this affects the T_{DM} of these clasts.

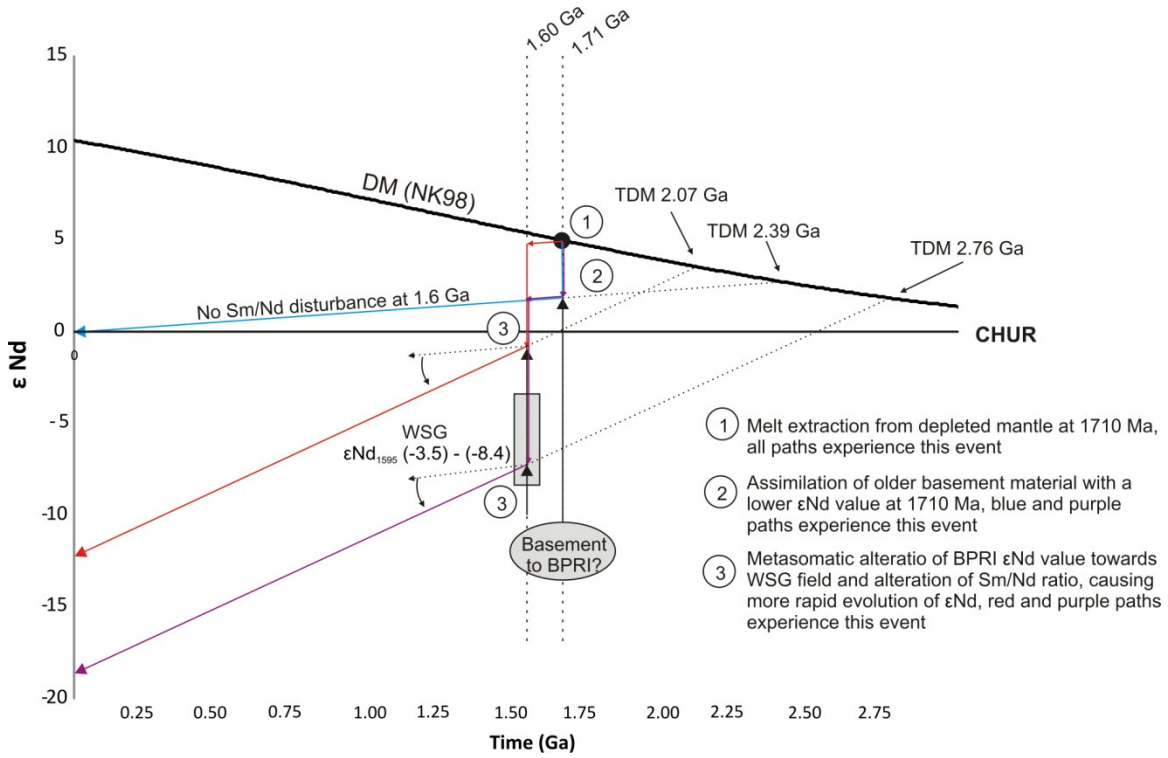

Fig. 32: εNd plot after DePaolo (1981a) showing the depleted mantle (DM) (model of Nägler and Kramers, 1998) showing three possible evolution paths from mantle derivation at 1710 Ma to the present. TDM – time of intersection with the depleted mantle curve. WSG – Wernecke Supergroup. CHUR – chondritic uniform reservoir. DM (NK98) – Depleted mantle model of Nägler and Kramers (1998)